

**DEVELOPMENT AND APPLICATION OF INHIBITORY
LUMINOPSINS FOR THE TREATMENT OF EPILEPSY**

A Thesis
Presented to
The Academic Faculty

by

Jack K. Tung

In Partial Fulfillment
of the Requirements for the Degree
Doctor of Philosophy in the
School of Engineering

Georgia Institute of Technology
May 2016

Copyright © 2016 by Jack K. Tung

DEVELOPMENT AND APPLICATION OF INHIBITORY LUMINOPIINS FOR THE TREATMENT OF EPILEPSY

Approved by:

Dr. Robert E. Gross, Advisor
Department of Biomedical Engineering
Georgia Institute of Technology

Dr. Shan Ping Yu
Department of Anesthesiology
Emory University

Dr. Shawn Hochman
Department of Biomedical Engineering
Georgia Institute of Technology

Dr. Ute Hochgeschwender
Department of Neuroscience
Central Michigan University

Dr. Nicholas Boulis
Department of Biomedical Engineering
Georgia Institute of Technology

Date Approved: December 16, 2015

To my parents

ACKNOWLEDGEMENTS

I would like to express my gratitude to my advisor, Dr. Robert Gross, for giving me a fascinating idea and letting me run with it. I am grateful that I was able to pursue my research interests and be involved in all aspects of this project from conception, designing and conducting experiments, data analysis, and grant writing. I know that these experiences have been invaluable in training me to be a future independent investigator.

I would also like to acknowledge my other mentors and committee members: Drs. Steve Potter, Ute Hochgeschwender, Ling Wei, Shan Ping Yu, Shawn Hochman, and Nicholas Boulis for their support and feedback. Special thanks to Drs. Hochgeschwender and Potter for guiding me from the beginning and always believing in me. Thank you Drs. Wei and Yu for including me in your group and always motivating me to work harder and do better.

I am also extremely grateful for the unconditional love and support I have received from my friends and family over the years. Although my parents have had their own share of problems to deal with over the past few years, they have always prioritized my trivial needs before their own and have always been there for me no matter what. Thank you mom and dad for everything you have done for me – I am motivated to become a better person and do good work because of you both. I would also like to thank my girlfriend Hyeyun for her support over the years; she has definitely spent way more time in the lab than anyone else I know in the forensics consulting industry. I would also like to thank my friends who have spent the extra effort to keep in touch and drag me out

of lab. Without you guys, I would surely forget how to interact with human beings normally in a social context.

I would like to thank my lab members, colleagues, and students that have helped me in the lab over the years. You have all contributed to my knowledge and understanding of my thesis in some way. Special thanks to Claire-Anne for keeping the lab running and going out of her way to make sure that I got everything I needed to do my experiments. Your advice and guidance over the years have also been extremely valuable. Special thanks to Ken as well for your guidance and making this luminopsin journey a little less daunting. I would also like to thank the individuals that have helped train me in various techniques in the lab: Mike and Dongdong in whole cell recordings, Neal for *in vivo* recordings, and Jon and Ming for *in vitro* MEA recordings. You all have been instrumental in teaching me how to do the experiments I wanted to do. I would also like to thank James, Michael, Alex, and the rest of my lab for their helpful discussion and feedback. In addition, I would like to thank my students Aida, Thomas, and Kevin for their help in the lab and thought provoking questions.

Lastly, I would like to thank my funding sources, which ultimately allowed the lab and I to begin to working on this project. I am extremely grateful to the National Institutes of Health for funding the Eureka R01 (NS079757), R01 (NS079268), and NRSA (NS086433) that currently supports this project.

TABLE OF CONTENTS

	Page
ACKNOWLEDGEMENTS	iv
LIST OF TABLES	viii
LIST OF FIGURES	ix
SUMMARY	xi
<u>CHAPTER</u>	
I. Introduction	1
1.1 Epilepsy background	2
1.2 Optogenetics background	5
1.3 Optogenetics and epilepsy	7
1.4 Translational challenges for optogenetics	16
II. Bioluminescence: what it is and how to measure it	18
2.1 Introduction	18
2.2 <i>In vitro</i> bioluminescence imaging	21
2.3 <i>In vivo</i> bioluminescence imaging	28
2.4 Conclusion	30
III. Inhibitory luminopsins	31
3.1 Introduction	31
3.2 iLMO constructs	33
3.3 <i>In vitro</i> characterization in HEK293 cells	35
3.4 <i>In vitro</i> characterization in cortical neurons	40
3.5 <i>In vivo</i> characterization in rats	47
3.6 Application in behaving animals	55

IV. Application of inhibitory luminopsins to epilepsy	65
4.1 Introduction	65
4.2 Optogenetic inhibition of acute focal seizures with iLMO2	67
4.3 Optogenetic inhibition of acute generalized seizures with iLMO2	73
V. Responsive luminopsins	79
5.1 Introduction	79
5.2 Development and characterization	80
VI. Conclusion and future directions	87
6.1 Conclusion	87
6.2 Future directions	89
Appendix A: iLMO1 development	91
Appendix B: Excitatory luminopsins	96
Appendix C: Methods of transgene expression	102
Appendix D: Targeted expression of GABAergic cells	106
Appendix E: Summary of constructs	108
REFERENCES	110

LIST OF TABLES

	Page
Table 1.3.1. Summary of optogenetic approaches used for epilepsy.	15
Table 2.1. Common luciferases used in neuroscience research.	19
Table 5.1. Summary of results when various calcium-dependent luciferases were co-expressed (either by fusion or co-transfection) with various opsins.	82

LIST OF FIGURES

	Page
Figure 1.1.1. Neuromodulation targets for epilepsy.	4
Figure 1.1.2. Optogenetic vs. electrical stimulation.	5
Figure 1.2.1. Channelrhodopsin and Halorhodopsin.	6
Figure 1.3.1. Optogenetic approaches to halting seizure activity.	14
Figure 2.2.1. Objective comparison.	22
Figure 2.2.2. Intermediate lens comparison.	23
Figure 2.2.3. Camera comparison.	25
Figure 2.3.1. <i>In vivo</i> bioluminescence imaging.	29
Figure 3.2.1. Schematic representation of the iLMO2 fusion protein.	34
Figure 3.3.1. Characterization of iLMO2 in HEK293 cells.	38
Figure 3.4.1. Bioluminescence and fluorescence images of cortical neurons expressing iLMO2	41
Figure 3.4.2. Whole cell recordings of cortical neurons expressing iLMO2.	42
Figure 3.4.3: iLMO2 is able to suppress synchronous bursting activity <i>in vitro</i> .	44
Figure 3.5.1. Cannula-electrode.	49
Figure 3.5.2. iLMO2 suppresses neural activity <i>in vivo</i> .	50
Figure 3.5.3. Average responses to CTZ and vehicle.	51
Figure 3.5.4. Effect of isoflurane anesthesia on iLMO activity.	52
Figure 3.6.1. Rotation testing.	57
Figure 3.6.2. <i>In vivo</i> bioluminescence imaging.	57
Figure 3.6.3. Post-mortem histology.	58
Figure 4.2.1. Example of bicuculline-induced discharges in the hippocampus.	68
Figure 4.2.2. Suppression of bicuculline-induced discharges by CTZ.	69

Figure 4.2.3. Changes in seizure activity when CTZ or vehicle is co-administered with bicuculline in anesthetized rats.	70
Figure 4.3.1. Effects of CTZ on PTZ-induced seizures.	74
Figure 4.3.2. Prophylactic treatment with CTZ reduces c-fos expression induced by PTZ.	75
Figure 5.2.1. GFP-Aequorin bioluminescence is reduced when co-expressed with Halorhodopsin and Arch	82
Figure 5.2.2. Dose-dependent bioluminescence over time.	83
Figure 5.2.3. ATP-dependent bioluminescence over time.	84
Figure 5.2.4. Responsive luminopsins utilizing calcium-dependent Nanolantern increase their bioluminescence after stimulation with ATP.	84
Figure 5.2.5. KCl induced bioluminescence in cortical neurons.	85

SUMMARY

Optogenetics has demonstrated great promise as a direct neuromodulatory tool for halting seizure activity in various animal models of epilepsy. However, light delivery into the brain is still a major practical challenge that needs to be addressed before future clinical translation is feasible. Not only does light delivery into the brain require surgically implanted hardware that can be both invasive and restrictive, but it is also difficult to illuminate large or complicated structures in the brain due to light scatter and attenuation. We have bypassed the challenges of external light delivery by directly coupling a bioluminescent light source (a genetically encoded *Renilla luciferase*) to an inhibitory opsin (*Natronomonas halorhodopsin*) as a single fusion protein, which we term an inhibitory luminopsin (iLMO).

iLMOs were developed, tested, and characterized *in vitro* and *in vivo* using intracellular recordings, multielectrode arrays, and behavioral testing. iLMO2 was shown to generate hyperpolarizing outward currents in response to both external light and luciferase substrate, which was sufficient to suppress action potential firing and synchronous bursting activity *in vitro*. iLMO2 was further shown to suppress single-unit firing rate and local field potentials in the hippocampus of anesthetized and awake animals. Finally, expression of iLMO was scaled up to multiple structures of the basal ganglia to modulate rotational behavior of freely moving animals in a hardware-independent fashion. iLMO2 was further utilized to acutely suppress focal epileptic discharges induced by intracerebral injection of bicuculline and generalized seizures resulting from system administration of pentylenetetrazol.

Several calcium-dependent luciferases have also been utilized as a means to report neural activity with bioluminescence. These have been coupled to inhibitory opsins as responsive luminopsins (rLMOs) that are capable of responding to neural activity.

Inhibitory luminopsins have enabled the possibility of optogenetic inhibition of neural activity in a non-invasive and hardware-independent fashion. This work increases the versatility, scalability, and practicality of utilizing optogenetic approaches for halting seizure activity in vivo.

CHAPTER I

INTRODUCTION

The human brain is comprised of billions of cells talking to one another in a complex network consisting of trillions of connections. Each cell is like a different instrument contributing to a vast symphony of activity that is intricately coordinated together to dictate the complex behaviors we see and exhibit every day. When this activity is not coordinated, it can lead to pathological conditions such as epilepsy.

To understand how the brain works and eventually correct the abnormal activity seen in diseases such as epilepsy, we need tools that can isolate each ‘instrument’ and measure its contribution to the entire behavior. For example, if the brass section is playing too fast or the cellos are joining in too loudly, we need to be able to selectively slow down brass instruments and quiet down the cellos in order to maintain the harmonic balance of the symphony. Our laboratory has been interested in using a revolutionary technique called optogenetics, which allows scientists to selectively modulate the activity of neurons in a cell-type specific manner with light. We aim to utilize this precise tool to correct the abnormal ‘cacophonous’ activity seen in epilepsy.

This introductory chapter will provide a brief overview of existing treatment options for patients with epilepsy as a framework for describing optogenetics, a powerful tool that has shown great potential as a future neuromodulatory therapy. I will then review the current progress made with optogenetic approaches to treat epilepsy and then describe the limitations that currently impede effective clinical translation of these techniques, which is the main challenge that this thesis aims to address.

1.1 Epilepsy is a disorder of abnormal neuronal activity

Epilepsy currently affects 3 million people in the U.S. and 65 million people worldwide, or roughly 1% of the population, accounting for a significant worldwide health burden. About 150,000 patients in the U.S. and 2.4 million worldwide are diagnosed with epilepsy every year. Annual epilepsy related medical expenditures are close to \$10 billion annually in the U.S. alone¹ and up to \$4748 in direct annual costs per patient in other countries².

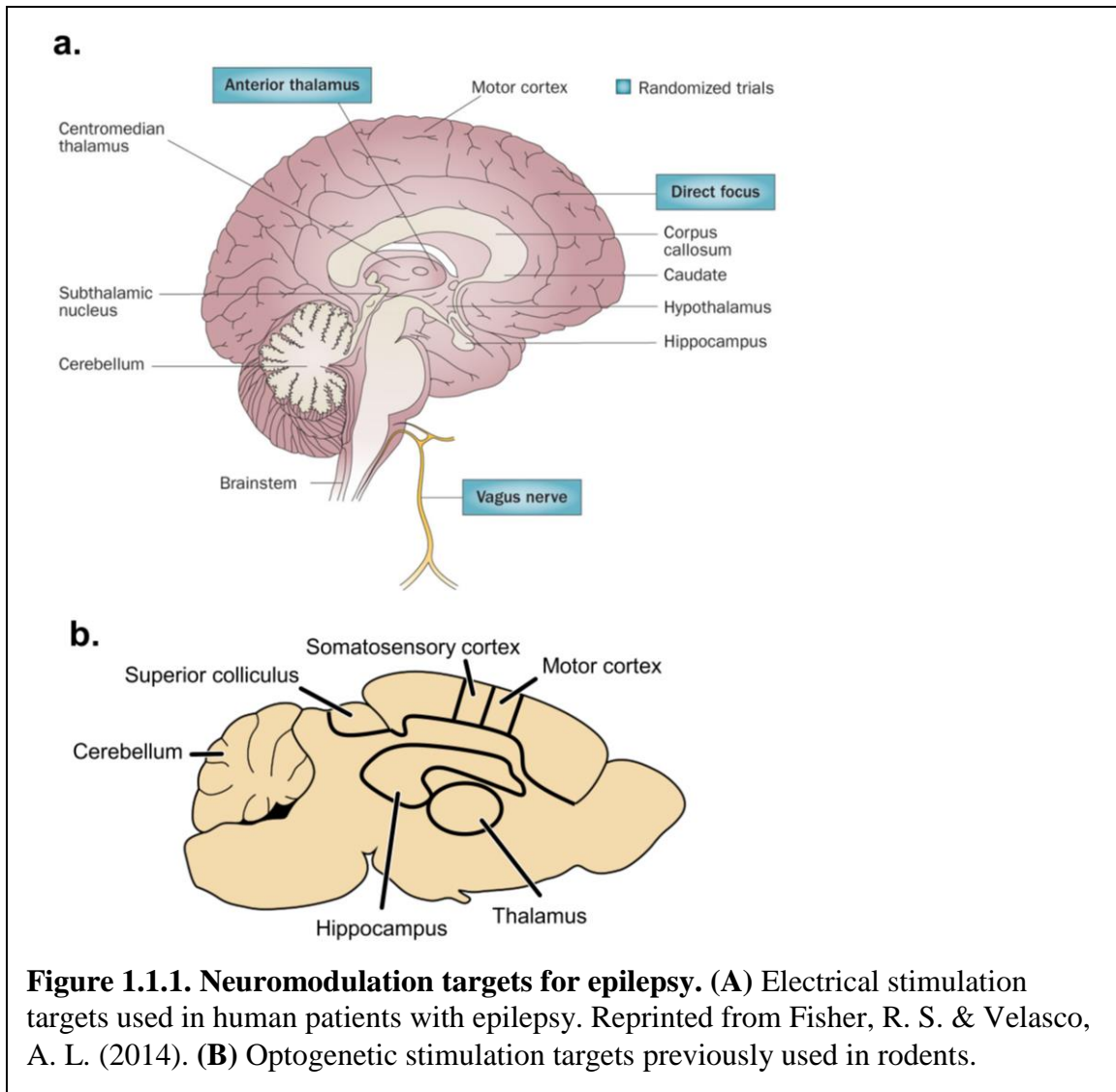
Epilepsy is a disease characterized by aberrant neural activity in the brain that ultimately leads to recurrent and spontaneous seizures. Seizures can manifest in a variety of ways due to multiple etiologies and their onsets are characteristically unpredictable. Epilepsy is therefore a very debilitating disease for both patients and their affected families because performance of daily life activities is often impaired, injuries and even death are not uncommon, cognitive decline is frequent, and socioeconomic decline prevalent. In fact, epilepsy was responsible for approximately 20.6 million disability-adjusted life years lost in 2012³.

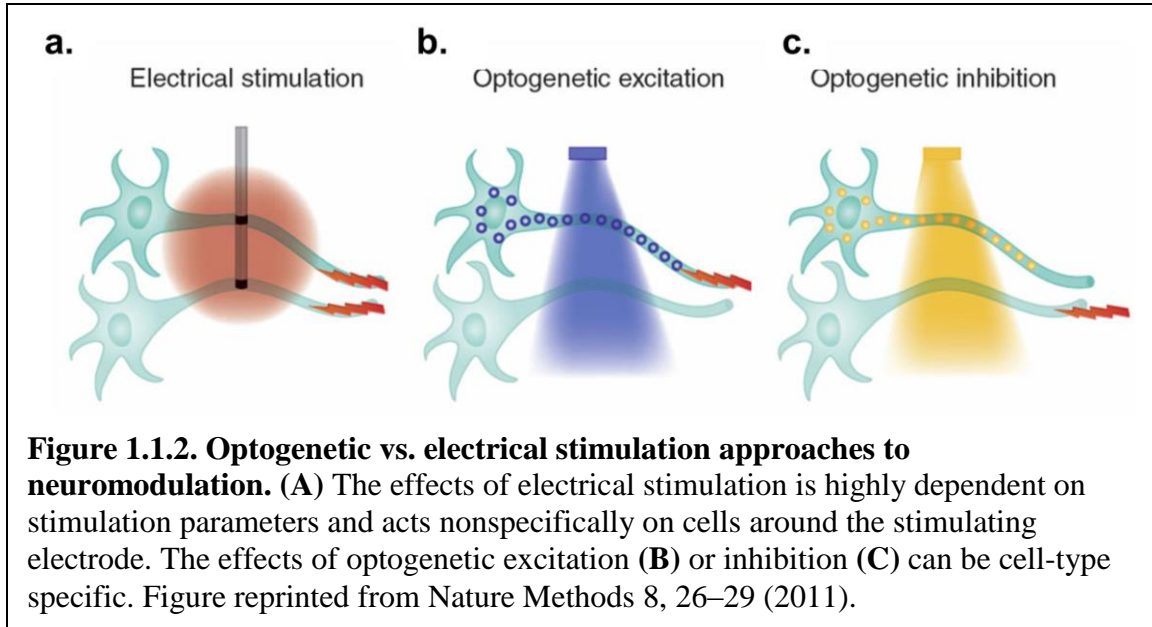
Pharmacotherapy is generally the first treatment choice option for patients with epilepsy. Fortunately, most patients are able to control their seizures with anti-epileptic drugs. However, these drugs are generally required for the lifetime of the patient and are also commonly associated with side effects that are poorly tolerated in some patients⁴. Moreover, 30% of patients with epilepsy do not become seizure free with anti-epileptic drugs⁵. These drug-resistant patients are generally limited to two other treatment options: resective surgery or neurostimulation.

Candidates who are deemed eligible and undergo resective surgery of the epileptic tissue are generally able to achieve complete seizure freedom 60-70% of the time⁶. As with any surgical procedure, there is risk for adverse events associated with

intracranial EEG monitoring (if needed), surgery, and recovery. These patients are also at risk for neurological deficits such as memory, speech and motor impairments, especially if the area of resection lies in eloquent brain areas. Because of these significant risks and stringent inclusion criteria, and for other reasons such as risk-aversion and lack of referrals or access to care, only about 3000 patients actually receive surgery each year⁷.

Neuromodulatory approaches to correcting abnormal brain activity have shown great promise in reducing seizures in patients with intractable epilepsy and the various approaches used in the past are illustrated in **Figure 1.1.1a**. The most successful therapies include vagus nerve stimulation⁸⁻¹⁰, stimulation of the anterior nucleus of the thalamus (SANTÉ)^{11,12}, and responsive neurostimulation (RNS) of epileptic foci^{13,14}. Clinical trials using these devices have demonstrated that 56-68% of patients were able to reduce their seizure frequency by more than 50% at their last visit (the average reduction of seizures in these patients was 48-76%)¹⁵. Although electrical stimulation allows more targeted and reversible therapy to the brain compared to pharmacotherapy or surgical resection, it is still a challenge to specifically and effectively target only pathological circuits while leaving healthy tissue undisturbed (**Figure 1.1.2a**). This is primarily due to the fact that the effects of electrical stimulation on the surrounding tissue are highly dependent on patient-specific neuroanatomy (e.g. it remains difficult to effectively reach seizure onset zones located in deep sulci) and parameters of stimulation, which can be hard to predict. Given the potential side effects, suboptimal response rates, and selective inclusion criteria for surgery, new therapies for epilepsy patients are in dire need.





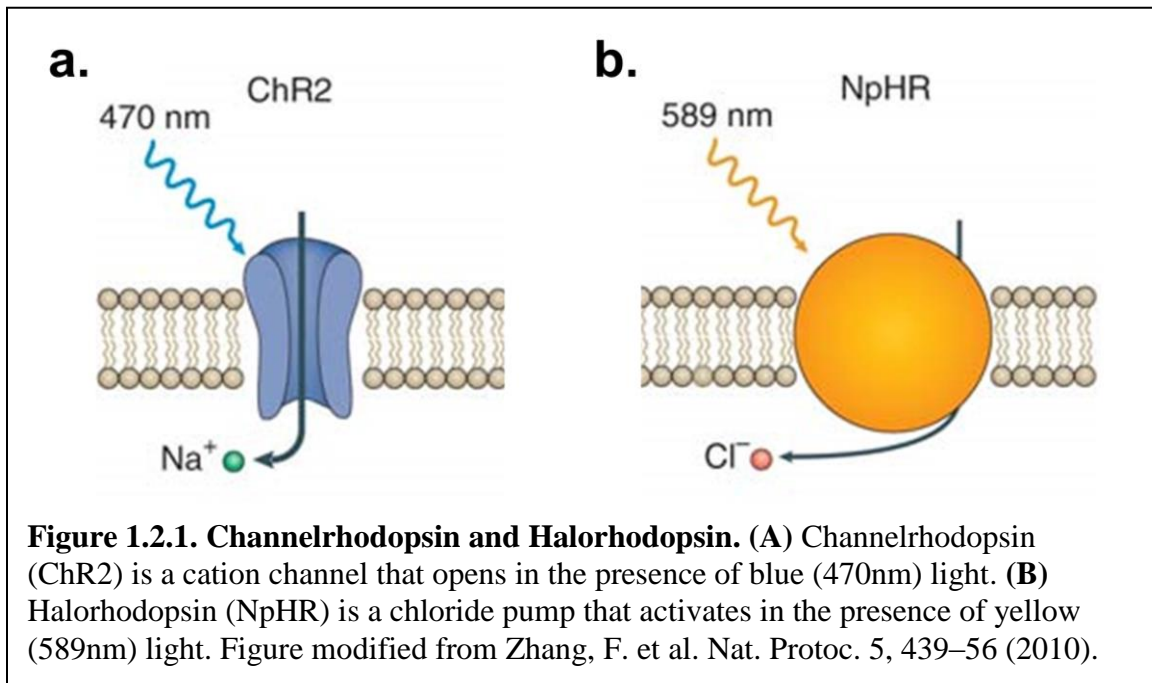
1.2 Optogenetics: a revolutionary method to control neuronal activity with light.

Optogenetics offers an unprecedented ability to alter neuronal activity with very high spatial and temporal accuracy. By utilizing cell-specific expression of light-sensitive ion channels and pumps (opsins) in the brain, scientists can selectively activate (**Figure 1.1.2b**) or inhibit (**Figure 1.1.2c**) specific cell populations in the context of complex neural circuitry. This unprecedented degree of control of cell-type specific physiology has proven to be an invaluable research tool enabling neuroscientists to study a wide variety of topics such as brain circuitry, learning, movement, and behavior like never before.

Two of the most widely used opsins in neuroscience research are channelrhodopsin (ChR) and halorhodopsin (NpHR). ChR is a non-selective cation channel that becomes activated in the presence of blue light (**Figure 1.2.1a**). Blue light is therefore capable of depolarizing the membrane potential of neurons expressing ChR and driving action potential firing¹⁶. In contrast, NpHR is a chloride pump that is activated in the presence of yellow light¹⁷. When neurons expressing NpHR are illuminated by yellow light, chloride is transported into the cytosol, hyperpolarizing the membrane potential and

decreasing the likelihood of action potential firing (**Figure 1.2.1b**). Both of these opsins have been utilized for seizure control in the studies outlined in this chapter.

There are several methods of expressing opsins in the rodent brain, each with advantages and disadvantages. One common method utilizes viral vectors, which allow for efficient long-term expression of transgenes. Viral vectors encoding opsin genes are produced *in vitro* and are subsequently injected into the brain where they can transduce target cells. Cell-type specific expression of opsins can be achieved by utilizing an appropriate promoter driving transgene expression. Another method used to achieve cell-type specific expression of opsins uses Cre-recombinase driver animals, in which floxed or double-inverted vectors containing opsin genes can be specifically expressed in Cre-recombinase positive cells, driven by cell-specific promoters^{18–20}. Cre-driver mouse lines are widely available, and rat lines are increasingly being produced as well. Various transgenic mouse lines endogenously expressing opsins have also been developed and are widely available.



1.3 Optogenetic approaches to treating epilepsy.

With the ability to selectively excite or inhibit neuronal activity in cell type-specific fashion with optogenetics, three major approaches have been taken to interrupt seizure activity in the rodent: nonspecific inhibition of neurons, inhibiting excitatory (e.g. glutamatergic) neurons, and exciting inhibitory (e.g. GABAergic) neurons. The structures that have been targeted and the experimental approaches utilized are illustrated in **Figure 1.1.1b** and **Figure 1.3.1**, respectively, and summarized in **Table 1.3**.

Nonspecific inhibition of neurons

Since seizures are generally thought to manifest from overexcitability of pathological circuits, researchers have naturally tried to decrease the excitability of these circuits using NpHR. Berglind et al.²¹ utilized an adeno-associated virus (AAV) encoding enhanced NpHR (eNpHR3.0) under control of the human synapsin promoter (hSyn) to express NpHR in ubiquitously in neurons of the mouse hippocampus. Epileptiform bursting was induced in these animals by compromising inhibitory drive with acute injection of bicuculline into the hippocampus. Upon illumination with yellow light, the authors were able to decrease epileptiform burst rate by 17%. Although the reduction in burst rate was significant, the rather modest decrease in epileptiform bursts was attributed to the diffusion of bicuculline being too widespread compared to the area of optogenetic inhibition.

It is often difficult to interpret effects of optogenetic manipulation if opsin expression is found in multiple cell types in the area of illumination (e.g. with a CMV, EF1 α , or hSyn promoter). For example, the hSyn promoter drives expression of NpHR not only in excitatory pyramidal cells, but also in interneurons, the inhibition of which could potentially offset the inhibitory effects of silencing principal cells as they become disinhibited by decreased inputs from interneurons. Although GABA_A transmission was blocked with bicuculline in these experiments, there still may have been other inhibitory

circuits that were not affected by bicuculline (such as GABA_B expressing or glycinergic neurons) that could have been subsequently turned off by optogenetic inhibition.

Inhibition of principal glutamatergic neurons

Tonnesen et al.²² first demonstrated that specific inhibition of principal cortical neurons via a lentivirus carrying NpHR under control of the calcium/calmodulin-dependent kinase II isoform α (CaMKII α) promoter was sufficient in reducing epileptiform activity in hippocampal organotypic brain slices. The same virus was used in a chronic tetanus toxin model of epilepsy in rats by Wykes et al.²³, where NpHR activation in the motor cortex of awake animals was shown to attenuate epileptic activity induced by tetanus toxin. In this study, rats were photostimulated 7-10 days after co-injection of tetanus toxin and a CaMKII α -NpHR2.0 lentivirus in the motor cortex. Although photostimulation was able to significantly reduce epileptic activity in the electroencephalogram (EEG), it was not sufficient to completely prevent all epileptic EEG events or produce any behavioral effects. This could be partially attributed to suboptimal expression levels of NpHR in the brain. For example, the copy number of NpHR delivered to neurons in the brain may be relatively small due to the fact that it is often difficult to obtain high-titer lentivirus compared to adeno-associated viral vectors (AAV). Furthermore, trafficking of NpHR to the cell membrane has been shown to be rather inefficient and may thus lead to suboptimal hyperpolarization of membrane potential upon photoactivation. Membrane trafficking of NpHR has been subsequently improved with addition of trafficking and endoplasmic reticulum-export sequences to eNpHR3.0, improving NpHR photocurrent dramatically²⁴.

Sukhotinsky et al.²⁵ utilized this improved eNpHR3.0 for delaying seizure activity in an acute model of epilepsy in rats. In this study, an AAV encoding CaMKII α -eNpHR3.0 was injected into the hippocampus. Photoactivation (both continuous and pulsed illumination) in these animals was able to significantly delay the onset of status

epilepticus (by 6 minutes) following systemic pilocarpine injection in awake behaving animals. Although both electrographic and behavioral manifestations of seizures were able to be delayed in these animals, they were not completely abolished. The modest scale of seizure attenuation was attributed to the fact that the seizure model they used was not focal, resulting in a large number of potentially epileptogenic neurons residing outside the range of light delivery and expression of opsin.

Excitation of interneurons

A high frequency stimulation approach (akin to DBS,) to optogenetic stimulation was taken by Chiang et al.²⁶ 50-Hz photostimulation of the hippocampus of transgenic mice expressing ChR2 under control of the Thy1 promoter was able to suppress seizures evoked by intracerebral injection of 4-aminopyridine by 82.4%. Although the Thy1 promoter is non-specifically expressed in neurons of the brain, the authors found that ChR2 expression was mostly localized to GABAergic interneurons in the hippocampus, suggesting that seizure suppression was achieved by enhancing inhibitory GABAergic inputs to overexcited circuits in the hippocampus.

Targeting interneurons with ChR2 seems especially appropriate for epilepsy models that result from a loss of inhibitory activity. The advantage of this approach is that GABAergic interneurons widely innervate multiple pyramidal cells in the hippocampus^{27,28} and could thus exert very strong effects on the epileptic network. However, GABAergic interneurons have also been directly implicated in synchronizing epileptic activity²⁹⁻³¹ and conceivably could potentiate seizure activity following photoactivation. Stimulation parameters must therefore be carefully determined to ensure that proper inhibitory drive is delivered to the circuit in question. Monitoring simultaneously the effects of optogenetic driving on the circuit using neural recording either by multielectrodes, voltage sensitive dyes or genetically encoded indicators may be advantageous in this context.

Modulation of structures remote from the epileptic origin

The studies described above have all focused on modulating seizure activity found directly at the epileptic focus or site of injury. Targeting remote structures projecting to different areas involved in seizure genesis and propagation can have unique advantages since seizures may arise from multiple structures or discrete networks in the brain³².

Indeed, electrical stimulation of structures remote from epileptic foci such as the cerebellum³³⁻³⁷, thalamus^{12,38-44}, subthalamic nucleus⁴⁵⁻⁴⁷, and caudate⁴⁸⁻⁵⁰ have shown to be beneficial in reducing seizures in human patients. Optogenetic control of some of these remote structures have also been utilized to suppress seizure activity in various rodent models.

Paz et al. targeted thalamocortical neurons with an optogenetic strategy that interrupted electrographic and behavioral seizures in a cortical seizure model in rats⁵¹. In this study, rats were given a focal cortical stroke that resulted in hyperexcitability of thalamocortical neurons. Optogenetic inhibition of glutamatergic thalamocortical neurons via an AAV encoding CaMKII α -eNphR3.0 was subsequently shown to interrupt electrographic and behavioral seizures when light illumination was manually switched on during seizure. By modulating the activity of thalamocortical neurons, the authors were able to demonstrate the potential benefits of targeting structures that lie upstream from areas of seizure activity.

Krook-Magnuson et al. investigated the role of the cerebellum in controlling spontaneous temporal lobe seizures by optogenetically targeting parvalbumin-expressing neurons (e.g. Purkinje cells) in the medial (vermis) and lateral (lobulus simplex) cerebellar cortex of mice⁵². They found that interruption of cerebellar activity (either by

excitation with ChR2 or inhibition with NpHR) in the lateral or medial cerebellum was able to reduce seizure duration. In contrast, only excitation of PV+ Purkinje cells in the medial cerebellum was able to reduce seizure frequency in addition to duration.

Soper et al. subsequently demonstrated that activation of the superior colliculus via ChR2 was able to attenuate seizure activity in various rat models of epilepsy⁵³. These effects were seen on seizures involving the forebrain and brainstem (induced by systemic pentylenetetrazol administration), complex partial seizures (induced by focal bicuculline injection in the area tempestas), absence seizures (induced by systemic gamma butyrolactone administration), and brainstem seizures (in genetically epilepsy prone rats). The fact that modulation of a single area in the brain could reduce seizure activity found in different models of epilepsy illustrates the potential of targeting remote structures that have broad influence on various networks. The cell-type specificity of optogenetic approaches can further refine the effects that these remote structures have on the areas they project to.

Seizure-responsive optogenetic intervention

A major clinical goal for neuromodulatory devices is to be able to deliver therapy only when it is needed (i.e. only in response to a seizure). The Responsive Neurostimulation System (RNS) by NeuroPace¹⁴ is a good example of an implantable device used in humans where electrical stimulation is delivered in response to detection of a seizure event (closed-loop) as opposed to delivering electrical stimulation either continuously or at pre-determined intervals (open-loop). Devices that are able to deliver therapy in a closed-loop fashion not only reduce side-effects related to stimulation, but also improve

the efficiency and longevity of these devices by conserving battery power. Development of similar devices which can deliver light in response to seizure activity in real time will be a necessary goal for optogenetic therapies to find a clinical application in humans, given the power required for light delivery, the possibly deleterious effects of continuous light delivery (e.g. by heating), and possible effects on continued channel function (e.g. habituation).

Optogenetic stimulation using detection approaches analogous to those used in the clinically-approved RNS system have been demonstrated by Paz et al. and Krook-Magnuson et al in rodents. Paz et al.⁵¹ expanded upon their open-loop approach for interrupting thalamocortical seizures, by developing a method to automatically trigger optical stimulation when the EEG line-length crossed a certain threshold that was indicative of a seizure event. Using this closed-loop approach, the authors were able to detect and silence seizures within 1s of seizure onsets. Krook-Magnuson et al.⁵⁴ took a more comprehensive approach of utilizing a closed-loop seizure detection algorithm to either silence excitatory principal cells or excite inhibitory interneurons in the mouse hippocampus. In this study, transgenic mice expressing NpHR in principal cells (CaMKII α -NpHR) or ChR in GABAergic interneurons (Parvalbumin-ChR) were generated. These mice were then injected with kainic acid into the dorsal hippocampus to generate a chronic model of temporal lobe epilepsy. The authors were able to detect subsequent spontaneous seizures using custom software that utilized features such as signal power, spike waveform, and frequency. Upon detection of seizures in CaMKII α -NpHR mice, optogenetic inhibition of principal cells ipsilateral to the kainate injection stopped 58% of seizures within 5s of light illumination and reduced the mean seizure

duration by 70%. Upon detection of seizures in PV-ChR mice, optogenetic excitation of PV-positive interneurons ipsilateral to the kainate injection stopped 59% of seizures within 5s of light illumination and reduced the mean seizure duration by 43%. Across all animals, optogenetic intervention reduced behavioral seizures by 29.6%. This same approach was utilized to specifically inhibit granule cells of the dentate gyrus of the hippocampus (with transgenic mice), which was shown to stop 75% of seizures within 5s of light delivery and reduce the seizure duration by 66%⁵⁵.

These studies have demonstrated the possibility of detecting and suppressing seizure activity with optogenetics in real time. Early detection and intervention of seizure activity has been particularly valuable for patients with epilepsy because epileptic foci could be targeted to limit seizure generalization and altered levels of consciousness. With the ability to modulate circuits with the cell type specificity of optogenetics, these closed-loop approaches to seizure suppression can potentially achieve even greater efficacy with reduced side effects.

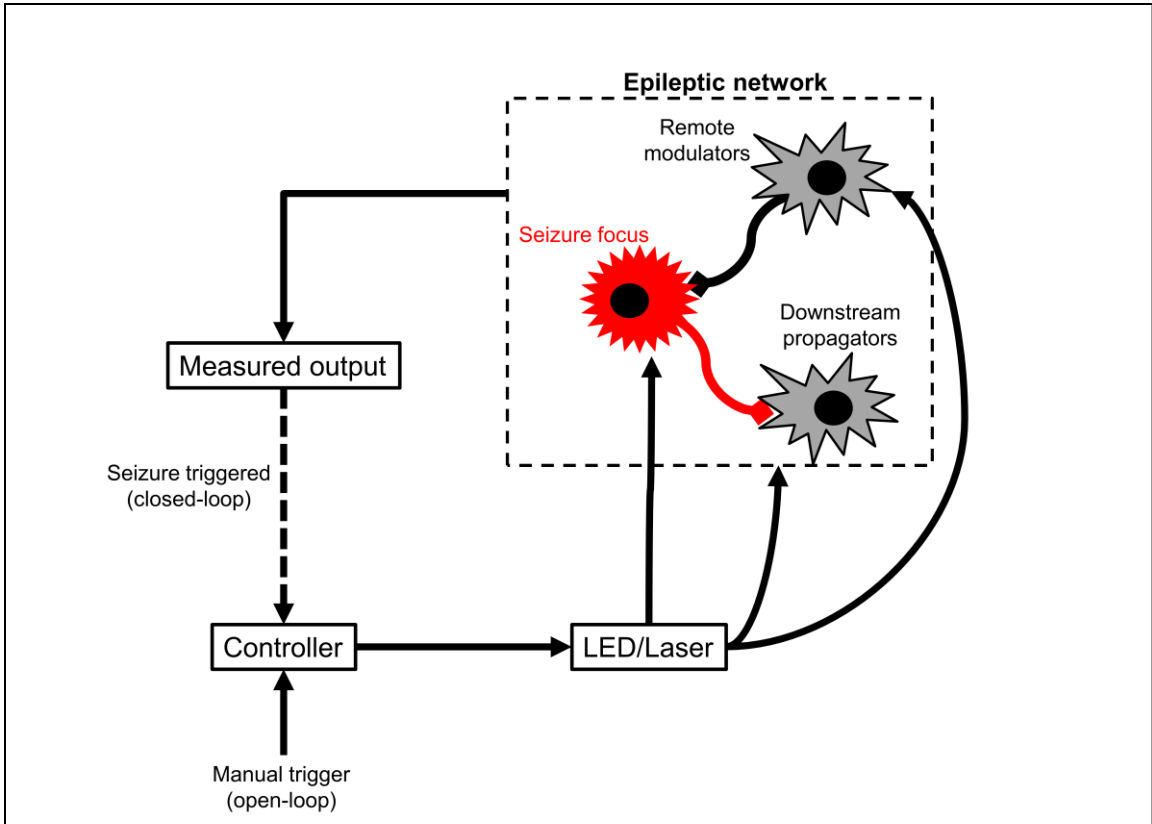


Figure 1.3.1. Optogenetic approaches to halting seizure activity. Optogenetics can be utilized to target specific cell types in the epileptic network directly at the seizure focus, remote modulators of the seizure focus, or downstream propagators of seizure activity. Light can either be delivered manually in an open-loop fashion, or automatically in response to a detected seizure (closed-loop).

Table 1.3.1. Summary of optogenetic approaches used for epilepsy.

	Reference	Opsin	Animal model	Seizure model	Stimulation location/ parameters	Electrographic response	Behavior response
Remote structures	Closed-loop optogenetic control of thalamus as a tool for interrupting seizures after cortical injury ⁵¹ .	CAMKII α -NpHR3.0	Rat	-Focal cortical seizures by photothrombotic stroke in somatosensory cortex (chronic)	-Ventrobasal thalamus. -On-demand continuous illumination.	-Interruption of epileptic activity. -Reduction of RMS power in cortex (bilateral) and thalamus	-Interruption of all behavioral seizures.
	Cerebellar directed optogenetic intervention inhibits spontaneous hippocampal seizures in a mouse model of temporal lobe epilepsy ⁵² .	Transgenics: -PV-ChR2 -PV-NpHR -Pcp-ChR2	Mouse	-Kainic acid injected to left dorsal hippocampus (chronic)	-Lateral cerebellar cortex, vermis -On-demand 3s short (50ms on/ 100ms off) and long (1000ms on/50ms off) pulses.	- <u>PV-ChR2</u> : <i>Vermis</i> : 39% duration reduction, 175% increase in time to next seizure. <i>Lateral</i> : 30-35% duration reduction - <u>PV-NpHR</u> : <i>Lateral</i> : 32-44% duration reduction - <u>Pcp-ChR2</u> : <i>Lateral</i> : 46-49% duration reduction <i>Vermis</i> : reduction in seizure frequency.	-N/A (not reported)
	Optogenetic activation of superior colliculus neurons suppresses seizures originating in diverse brain networks ⁵³ .	hSyn-ChR2	Rat	-Systemic PTZ -Focal BM injection -GEPRs -Systemic GB	-Superior colliculus (bilateral) -Continuous, 5Hz, 100Hz pulses with 50% duty cycle before seizure onset.	- <u>PTZ</u> : attenuation of seizures. - <u>BM</u> : attenuation of seizures. - <u>GB</u> : decrease frequency and duration of discharges	- <u>PTZ</u> : decrease in severity. - <u>BM</u> : decrease in severity and frequency - <u>GEPR</u> : decrease in severity and latency to onset. - <u>GB</u> : decrease in severity.
Neocortical	Optogenetic and Potassium Channel Gene Therapy in a Rodent Model of Focal Neocortical Epilepsy ²³ .	CAMKII α -NpHR2.0	Rat	-Tetanus toxin (chronic)	-Motor cortex -20s on/ 20-s off duty cycle 561nm yellow laser.	-Reduction of high-frequency power, EEG coastline, and epileptiform events.	-None
Temporal lobe	On-demand optogenetic control of spontaneous seizures in temporal lobe epilepsy ⁵⁴ .	Transgenics: -PV-ChR2 -CAMKII α -NpHR3.0	Mouse	-Kainic acid (chronic)	- dorsal hippocampus -50ms on/ 100ms off -2,000ms on/50ms off	<u>CAMK-HR</u> : -58% seizures stopped within 1s of light delivery. -seizure duration reduced by 70% <u>PV-ChR</u> : -59% seizures stopped within 5s of light delivery. -seizure duration reduced by 43%	-29.6% reduction in behavioral seizures overall

Table 1.3.1. continued

Temporal lobe	Optogenetic delay of status epilepticus onset in an in vivo rodent epilepsy model ²⁵ .	CAMKIIa-NpHR3.0	Rat	-Li-pilocarpine IP injection (acute)	-Hippocampus -Continuous illumination, 1-2min on/1min off	-Both stimulation protocols delayed onset of status by 6 min on average.	-Delayed onset of status by 6 min on average.
	Optogenetic inhibition of chemically induced hypersynchronized bursting in mice ⁵⁶ .	Hsyn-NpHR3.0	Mouse	-Bicuculline Methiodide (BM) infusion by chemical optrode to CA1/CA2 (acute)	-ventro-posterior hippocampus -40s continuous illumination	-reduction of BM induced bursting by 17%.	-N/A (animals under anesthesia)
	Seizure Suppression by High Frequency Optogenetic Stimulation Using In Vitro and In Vivo Animal Models of Epilepsy ²⁶ .	Thy1-ChR2 transgenic	Mouse	-Intracerebral 4-AP (acute)	-Hippocampus -5ms pulses at 20Hz and 50Hz	<u>50Hz stim</u> : -82.4% ipsi, 66.7% contra max suppression. <u>20Hz stim</u> : -80.2% ipsi, 61.2% contra max suppression.	-N/A (animals under anesthesia)
	<i>In vivo</i> evaluation of the dentate gate theory in epilepsy ⁵⁵ .	Transgenics : -GC-NpHR -CAMKIIa-NpHR3.0	Mouse	-Kainic acid (chronic)	-Dorsal hippocampus -473nm: 30s illumination, 50ms on/100ms off -589nm: 30s illumination, 2,000ms on/50ms off	<u>GC-NpHR</u> : -75 ± 7% of seizures stopping within 5 s of light delivery. -66 ± 4% reduction in seizure duration <u>CAMKIIa-NpHR</u> : -72 ± 6% reduction in seizure duration	-N/A (not reported).

Abbreviations: GC: granule cells; NpHR: Halorhodopsin; ChR2: Channelrhodopsin; BM: bicuculline methiodide; Pcp: Purkinje specific; PV: parvalbumin specific; GEPR: genetically epilepsy prone rats; GB: gamma butyrolactone; 4-AP: 4-aminopyridine.

1.4 Current challenges impeding effective translation of optogenetics

As summarized in the previous section, multiple optogenetic approaches have now been utilized to halt or suppress seizure activity in various animal models of epilepsy.

Optogenetics has also been directly utilized as a therapy for treating other diseases such retinopathies, diabetes, pain, Parkinson's⁵⁷, and stroke⁵⁸. This technique has therefore demonstrated great clinical value as a potential therapy for treating various diseases. The challenge now lies in translating these approaches to more clinically-relevant animal models.

However, several technical challenges need to be addressed before optogenetics can be effectively scaled to the brains of larger and more complex animal models. One major challenge is light delivery into the brain. Conventional approaches rely on surgically implanted fiber optics for delivering light into the brain, which are not ideal due to their hardware dependency, associated tissue damage, and limited volume of illumination. This hardware dependency comes from the need of external light sources such as lasers or LEDs to provide the driving light. Although advancements have been made in light delivery technology (e.g. miniaturized LEDs, wireless stimulators, optical commutators, etc.), these devices are still not fully hardware-independent. Another major problem with external light sources is their limited volume of illumination due to light scatter and attenuation as it travels through brain tissue. In fact, most of the light coming out of a fiber optic is completely attenuated within 1 mm from the fiber tip⁵⁹. Although various approaches have been taken to increase light transmittance (e.g. multi-fiber probes, more sensitive/longer wavelength opsins⁶⁰), it is unclear how scalable these will be to the much larger non-human primate or human brain.

Instead of relying on external light sources for driving optogenetic probes, we have explored the option of using biological light sources (i.e. bioluminescence from luciferase enzymes) since they can be genetically encoded, are hardware-independent, and readily scalable to illuminate multiple or large structures in the brain. The next chapter will describe basic concepts and describe methods I have developed for detecting bioluminescence *in vitro* and *in vivo*.

CHAPTER II

BIOLUMINESCENCE: AN ALTERNATIVE LIGHT SOURCE FOR OPTOGENETIC APPLICATIONS

In this chapter, I describe practical methods and principles I have developed for generating and detecting bioluminescence from live cells and animals. We systematically tested various components of our live cell imaging microscope to optimize it for long term bioluminescence imaging. High resolution bioluminescence images from live neurons were obtained with our microscope setup and could be continuously captured for several hours with no signs of phototoxicity. Bioluminescence from the mouse brain was also imaged non-invasively through the intact skull with a conventional luminescence imager. These methods demonstrate how bioluminescence can be routinely detected and measured from live cells and animals in a cost-effective way with common reagents and equipment.

2.1 Introduction

Conventional optical techniques for live cell imaging have generally relied on the use of various fluorescent proteins or synthetic molecules. These imaging techniques require an exogenous light source to excite the fluorescent molecules, where they enter a higher energy state and subsequently emit light of a specific wavelength as they return to their ground state. Fluorescent molecules have proven to be exquisitely versatile reporters for live cell imaging because they span a broad spectrum of colors and can be detected with very high spatial and temporal resolution. Many important neuroscience questions

regarding cellular anatomical structures, neuronal circuitry, molecular interactions, brain dynamics, and brain pathology have been addressed with the use of fluorescent molecules.

In contrast to fluorescence, bioluminescence is light generated from an enzymatic reaction and is routinely demonstrated in nature by various bioluminescent marine species, arthropods, fungi, and bacteria. These organisms generate light via a chemiluminescent reaction, in which a chemical substrate (e.g. luciferin) is oxidized by an enzyme (e.g. luciferase). Bioluminescence is therefore produced without any excitation light source and persists as long as the substrate is present. A variety of bioluminescent proteins spanning a broad spectrum of colors and emission properties have been identified and their genes cloned; the major ones used in neuroscience research are summarized in **Table 2.1**.

Table 2.1: common luciferases used in neuroscience research

	Protein	Species	Emission peak	Mg, ATP?	Substrate	References
Luciferases	FLuc	Firefly	560	Y	D-luciferin	61–71
	VLuc	Cypridina	460	Y	Vargulin luciferin	62
	RLuc	Renilla reniformis	480	N	Coelenterazine	65,72–74
	GLuc	Gaussia princeps	480	N	Coelenterazine	62,75,76
Photoproteins	Aequorin	Aequorea victoria	470	N	Coelenterazine	77–81

Bioluminescence imaging differs from fluorescent readouts in several aspects that, depending on the specific application, can be advantageous or disadvantageous. One major advantage of fluorescent molecules is that they can be far brighter than bioluminescent proteins. One reason is that they can be made brighter by simply increasing the amount of excitation light, whereas bioluminescence intensity is strictly

limited by the number of substrate molecules being catalyzed by the luciferase. Due to the relative dimness of bioluminescent proteins, longer exposure times are generally needed to collect a number of photons comparable to that of a fluorescent molecule. Bioluminescence imaging therefore generally has a limited temporal resolution compared to that of fluorescence imaging⁸².

On the other hand, several unique properties of luciferase reporters also make bioluminescence an attractive imaging modality. First, bioluminescent signals generally have a higher signal-to-noise ratio. This is due to the fact that background luminescence is negligible compared to the signal produced from the luciferase reaction⁸³. Bioluminescent signals can therefore be much more sensitive than fluorescent signals, which generally have to compete with background auto-fluorescence. Second, bioluminescence does not require excitation light, eliminating the risk of photobleaching and phototoxicity that is associated with fluorescence imaging⁸⁴. Bioluminescent signals are therefore well suited for live cell imaging and can be recorded for much longer timescales compared to fluorescent signals without damaging reporter molecules or cells. Lastly, since bioluminescence requires no exogenous excitation light sources, it is a suitable optical readout for imaging light-sensitive cells such as retinal neurons. Luciferase proteins have also undergone significant evolution in their versatility as genetically encoded reporters for neuroscience research. Similar to their fluorescent counterparts, luciferase proteins can also be targeted to specific regions in the cell with the use of trafficking or localization signal sequences to allow for imaging of subcellular structures over time⁷². The concept of fluorescence resonance energy transfer (FRET) has also been translated to bioluminescent proteins to measure molecular interactions. In this instantiation, both the intensity and spectral properties of bioluminescent proteins are altered when they are associated with fluorescent proteins in a process termed bioluminescence resonance energy transfer (BRET)⁸⁵⁻⁸⁷. Luciferase proteins have also been engineered to respond to small molecules such as calcium and ATP⁷², allowing

them to be used for measuring changes in cellular dynamics such as neuronal activity. Protein engineering techniques have also led to the development of brighter and longer wavelength luciferases that are well suited for in vivo imaging⁸⁸⁻⁹².

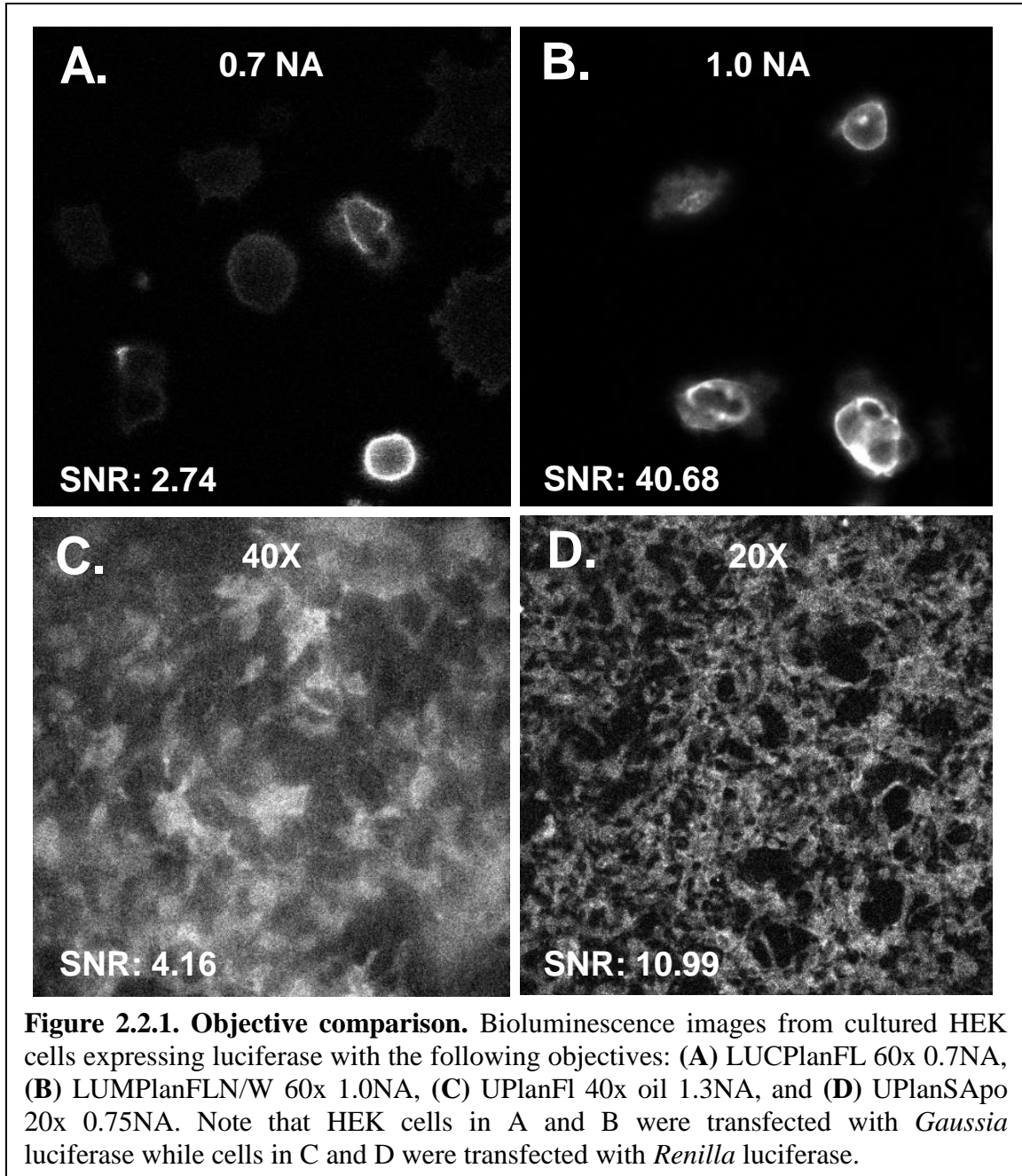
In the rest of the chapter, I discuss advantages and disadvantages of the various methods we have utilized for detection and quantification of bioluminescent signals from live cells and animals.

2.2 Measuring bioluminescence in vitro

2.2.1 Results and discussion

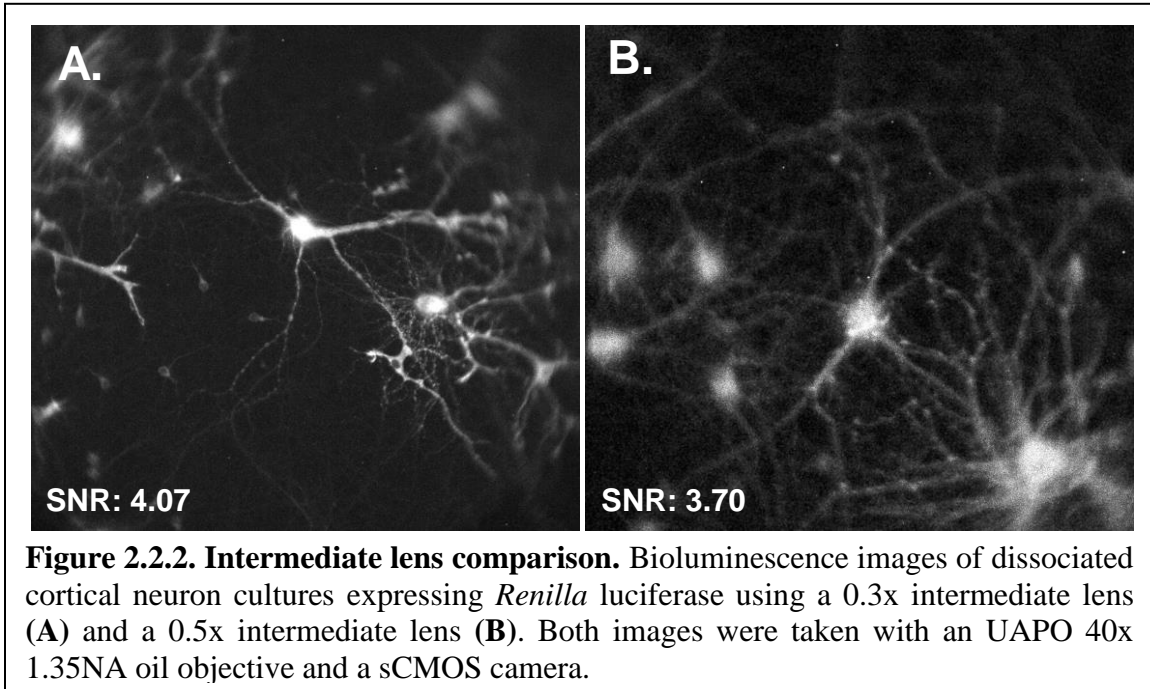
Image brightness is directly related to the light-gathering power of the objective (numerical aperture, NA) and inversely related to the image magnification (M): $\text{brightness} \propto (\text{NA}/M)^2$. We have therefore maximized the image brightness of our samples by optimizing three components of our microscope: the objective, camera, and intermediate optics.

In selecting an appropriate objective lens for bioluminescence imaging, we aimed at finding one with the highest numerical aperture and lowest workable magnification. In comparing various objective lenses, we found that objectives with higher NA produced brighter, higher resolution images (**Figure 2.2.1B vs. 2.2.1A**). Lower magnification objectives were also able to produce higher resolution images (**Figure 2.2.1D vs 2.2.1C**).



We utilized an intermediate demagnifying lens on a camera mount in order to allow more light to be focused onto a smaller area of the camera chip. Each pixel in the illuminated area of the chip therefore receives more light, producing a brighter image. We found that greater demagnification produced brighter images with sufficient spatial resolution to visualize detailed cellular morphology (**Figure 2.2.2A** vs. **2.2.2B**). Note that silhouetting at the periphery of the image may occur with greater demagnification, so the

field of view requirements must be carefully considered.



There are numerous camera options currently available for low-light optical imaging. Charge-coupled device (CCD) cameras are the most popular choice and rely on the photoelectric effect to convert a light signal into an electrical signal. The readout noise of CCD devices was significantly reduced with the advent of electron multiplying charge-coupled devices (EMCCD), making these cameras especially well-suited for low-light imaging applications. Scientific CMOS (sCMOS) devices are a relatively new type of sensor that also offers extremely low readout noise and wide dynamic range, making them a cost-effective alternative for imaging in low-light conditions. We have therefore compared several CCD, EMCCD and sCMOS cameras for bioluminescence imaging (Figure 2.2.3). All of the cameras tested were able to produce bioluminescence images with relatively low background and short exposure times (1-10s). Even though EMCCD cameras generally outperform sCMOS devices at very low light levels, our images were qualitatively similar (most likely due to the fact that RLuc and GLuc are relatively bright luciferases). One should therefore select a camera based on the level of sensitivity

required, as the price difference between EMCCD and sCMOS cameras can be quite significant.

Due to the relatively long exposure times required for bioluminescence imaging, we found that it was important to reduce the amount of ambient light in the room as much as possible to reduce background noise. We routinely turned off or covered light sources (such as an arc lamp for fluorescence observation) near the microscope before bioluminescence imaging. We found that blackout curtains were especially effective at isolating the microscope and camera from any potential light contamination. Cooling the camera to the lowest temperature setting also helped reduce background by limiting dark current noise.

The danger of phototoxicity and photobleaching limits the effectiveness of long-term live-cell imaging with fluorescent molecules. In contrast, we have demonstrated that bioluminescent reporters can be used to image live cells for extended periods of time without any apparent adverse effects. The substrate was supplied by a perfusion system, resulting in a long-lasting bioluminescent signal which could be detected over several hours. We did not observe any apparent adverse effects during this period, making this approach suitable for imaging cellular processes that are directed over long timescales, such as cellular trafficking, synaptogenesis, and migration.

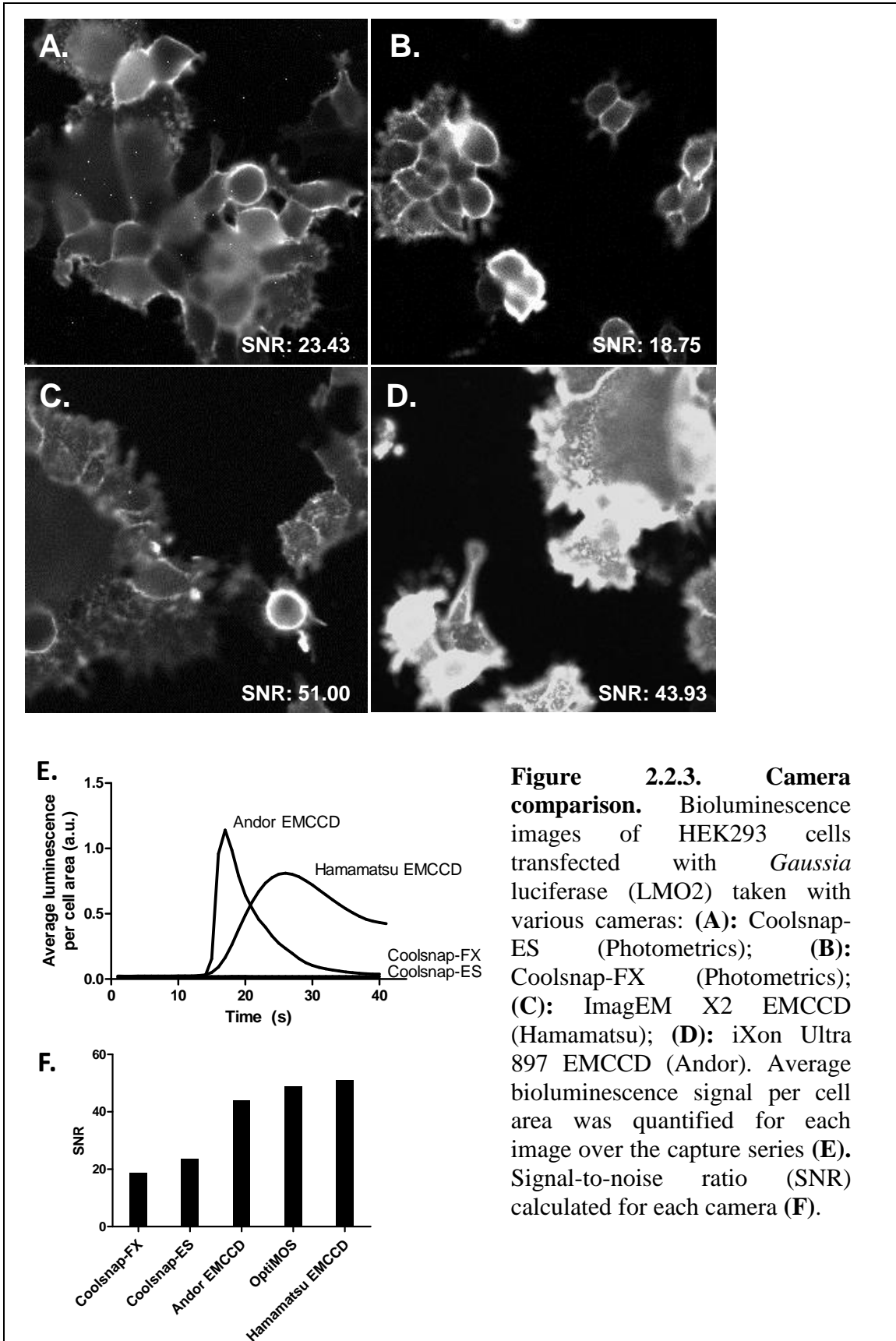


Figure 2.2.3. Camera comparison. Bioluminescence images of HEK293 cells transfected with *Gussia* luciferase (LMO2) taken with various cameras: **(A)**: Coolsnap-ES (Photometrics); **(B)**: Coolsnap-FX (Photometrics); **(C)**: ImagEM X2 EMCCD (Hamamatsu); **(D)**: iXon Ultra 897 EMCCD (Andor). Average bioluminescence signal per cell area was quantified for each image over the capture series **(E)**. Signal-to-noise ratio (SNR) calculated for each camera **(F)**.

2.2.2 Methods

Preparation of coelenterazine substrate

The substrate for Renilla and Gaussia based luciferases, coelenterazine (CTZ), is typically dissolved in nonpolar solvents such as ethanol or methanol. These solvents are not ideal for live cell imaging due to their inherent toxicity. We therefore recommend solubilizing CTZ in aqueous solution with the help of inert chemical agents such as β -cyclodextrin as described by Shimomura et al.⁹³ or by utilizing commercially available solvents. After solubilization, CTZ can be aliquoted and stored at -20°C. It is important to note that CTZ should be protected from light to prevent auto-oxidation.

Cell culture and transfection

HEK293 cells were passaged regularly in Dulbecco's Modified Eagle Medium (DMEM, with 10% FBS, 1% penicillin/streptomycin) and seeded to 90% confluency on glass cover slips the day before transfection. HEK cells were transfected with expression vectors encoding membrane-localized Renilla luciferase⁷³ and membrane-localized Gaussia luciferase protein⁹⁴ using Lipofectamine 2000 (Invitrogen). Transgene expression was confirmed by fluorescence microscopy the following day.

Dissociated cortical neuron cultures were derived from E18 rat embryos. Cortical tissue was digested with 2mg/mL papain and dissociated by mechanical trituration before seeding onto 18 mm diameter German glass coverslips coated with 50 μ g/mL poly-D-lysine (Sigma). Neuronal cultures were grown in serum-free Neurobasal media (w/ 1x B27 supplement, 0.5 mM Glutamine) and media was changed (half-volume) every 3-4 days. Cortical neuron cultures were transduced with viral vectors encoding luciferase 2-3 days after plating.

Live cell bioluminescence imaging

Bioluminescence images were taken on an Olympus inverted fluorescence microscope equipped with a variety of objectives, c-mount adaptors, and cameras:

Objectives	Adaptors	Cameras
PlanApo 60x oil 1.4NA	0.5x	Coolsnap-ES CCD (Photometrics)
UPlanFl 40x oil 1.3NA	0.3x	Coolsnap-FX CCD (Photometrics)
LUMPlanFLN W 60x 1.0NA		ImagEM X2 EMCCD (Hamamatsu)
UPlanSApo 20x 0.75NA		iXon Ultra 897 EMCCD (Andor)
LucPlanFL 60x 0.7NA		QuantEM EMCCD (Photometrics)
		OptiMOS sCMOS (Photometrics)

Cells cultured on glass coverslips were transferred to a perfusion chamber (Warner Instruments) containing phenol-free media at the time of imaging to minimize light absorption and maximize transmission of bioluminescence through the media (this is especially important for upright microscopes). The cells were then checked under fluorescence to confirm transgene expression and determine the right depth of focus for bioluminescence imaging. The microscope was then switched to an empty filter position to collect whole-spectrum bioluminescence.

Images were collected using the open-source Micromanager image acquisition software. Camera settings were standardized and optimized by cooling the chip to the lowest temperature (to minimize dark current) and maximizing the gain. Binning was used only when it was necessary to produce visible images. All of the background light sources in the room (windows, doors, electronics) were covered with blackout material and images were collected at various exposure times (1-40s). Long term bioluminescence images were acquired by using the multi-acquisition feature of Micromanager and a perfusion system to deliver CTZ during the imaging period (up to 3 hours). Image quality was estimated by calculating the signal-to-noise ratio (SNR) of captured images. SNR was calculated by dividing the mean pixel intensity of the bioluminescence

image to the standard deviation of the pixel intensity from a background image (or region with no cells) in ImageJ.

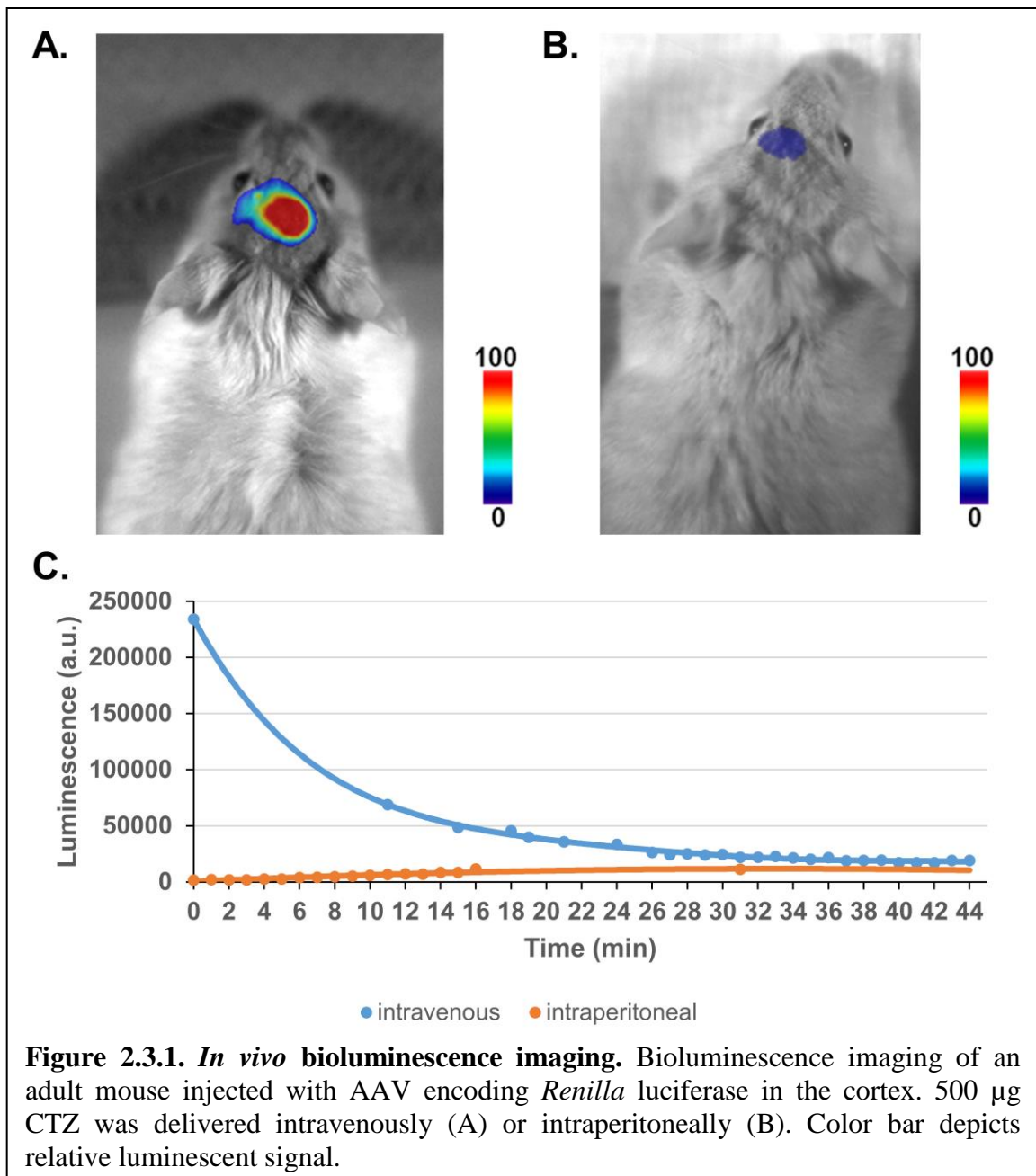
2.3 Measuring bioluminescence in vivo

2.3.1 Results and Discussion

In vivo fluorescence imaging is often compromised by high non-specific background from tissue and cells (auto-fluorescence). In contrast, background bioluminescence from tissues not expressing luciferase is negligible. This property of bioluminescence makes it an ideal signal for imaging whole animals where the number of luciferase-expressing target cells is generally few compared to the surrounding non-expressing tissue. We assessed the usability of Renilla luciferase for in vivo imaging and found that the bioluminescence signal was strong enough to allow detection of signals through the intact skull (**Figure 2.3.1a, b**). Special consideration of the route of substrate administration is needed when selecting a luciferase to use for in vivo bioluminescence imaging. Firefly luciferase (Fluc) has been frequently used for bioluminescence imaging in animals due to the relatively ease of the intraperitoneal route of substrate (D-luciferin) administration. Although we have demonstrated that coelenterazine can also be delivered intraperitoneally, Renilla luciferase is maximally effective when the substrate is administered via intravenous routes (**Figure 2.3.1c**). Since beetle (e.g. Firefly) and marine (Renilla, Gaussia) luciferases utilize different luciferin substrates, it is therefore feasible to multiplex them together due to absence of crosstalk between the two systems.

The low background with bioluminescence makes in vivo bioluminescence imaging particularly sensitive for detecting signals from small areas over extended periods of time. In fact, bioluminescence imaging has been successfully used for

applications from tracking transplanted cells^{95,96} to monitoring cellular processes such as neurodegeneration, inflammation, and neurogenesis⁹⁷. Although *in vivo* bioluminescence signals provide limited spatial information directly, the cell-type specificity of luciferase expression provides indirect spatial information because any detected bioluminescence should ostensibly be coming only from cells expressing luciferase.



2.3.2 Methods

For imaging the mouse brain, an adeno-associated virus (AAV) encoding Renilla luciferase (RLuc) was injected into the cortex of white mice (-1.58 AP, -0.75 ML, -0.8 SI and -1.58 AP, -1.75 ML, -0.5 SI). After 2 weeks, the fur was shaved off the head and the animals were anesthetized with ketamine/xylazine before bioluminescence imaging. 500 µg of CTZ was administered either intraperitoneally or intravenously (via tail vein injection). Bioluminescence images were captured with the animals under anesthesia using a conventional luminescence imager (Fuji LAS-3000). Sequential images of 20s exposure time were captured and the total signal intensity was quantified in ImageJ to achieve a bioluminescence signal time course. Pseudocolor images are displayed showing the relative bioluminescence signal. All procedures were performed in accordance with the US National Institutes of Health guidelines for animal research and were approved by the Institutional Animal Care and Use Committee at Emory University.

2.4 Conclusion

We have demonstrated how bioluminescent proteins can be effectively used as an optical reporter for both *in vitro* and *in vivo* settings. Given the proper detection equipment and scientific question, bioluminescence offers several unique advantages over conventional fluorescence readouts. The major advantage of using bioluminescent signals is that they are detected over little to no background noise, enabling long term imaging applications with no risk of phototoxicity or artifact. With the development of brighter and more responsive luciferase proteins, the use of bioluminescent reporters in neuroscience research will continue to grow more robust and versatile.

CHAPTER III

INHIBITORY LUMINOPSINS

With the ability to generate and characterize bioluminescence from luciferase enzymes (Chapter 2), this chapter will now describe my efforts in coupling these biological light sources to light-sensitive opsins to drive optogenetic inhibition. We have bypassed the challenges of external light delivery by directly coupling a bioluminescent light source (a genetically encoded luciferase) to an inhibitory opsin, which we term an inhibitory luminopsin (iLMO). iLMO was shown to suppress action potential firing and synchronous bursting activity in vitro in response to both external light and luciferase substrate. iLMO was further shown to suppress single-unit firing rate and local field potentials in the hippocampus of anesthetized rats. Finally, expression of iLMO was scaled up to multiple structures in the basal ganglia to modulate rotational behavior of freely moving animals in a hardware-independent fashion. This novel class of optogenetic probes demonstrates how non-invasive inhibition of neural activity can be achieved, which adds to the versatility, scalability, and practicality of optogenetic applications in freely behaving animals.

3.1 Introduction

Optogenetic techniques have revolutionized the field of neuroscience because they have given scientists the ability to selectively activate or inhibit neural activity in the context of exquisitely complex neural circuitry⁹⁸. These techniques rely on the use of light-sensitive ion channels or pumps (opsins), which are expressed in a cell-type specific

manner in the brain and activated by an external light source such as a laser or light-emitting diode (LED).

Although optogenetic techniques generally work well in small rodents, several technical challenges with light delivery into the brain still need to be addressed before these techniques can be routinely used in freely behaving animals or translated into larger and more complex animal models. The most common solution for delivering light into the brain is via a surgically implanted optical fiber coupled to an external light source. Not only do these chronically implanted optical fibers pose risk for infection and tissue damage, but they also raise practical impediments (e.g. limited range of movement or need for extra hardware such as optical commutators) for conducting experiments with freely moving animals. Transmission of external light through the brain is also extremely inefficient due to light scatter and tissue absorption^{99,100}. In fact, most of the light emitted from an implanted fiber optic is completely attenuated within 1 mm of the fiber tip¹⁰¹. Optogenetic applications in other tissues (e.g. heart¹⁰² and peripheral nerves¹⁰³) share similar challenges with light delivery, where light scatter and attenuation can also be a significant problem¹⁰⁴. While progress has been made towards developing optogenetic tools that require less light (i.e. more sensitive and red-shifted opsins^{60,105,106}), the scalability of this approach to larger non-human primates or human patients is still unclear.

We have bypassed the challenges of external light delivery by directly coupling bioluminescent proteins to conventional light-sensitive opsins. Specifically, we have utilized luciferase enzymes (which emit bioluminescence in the presence of a chemical substrate, luciferin) as an alternative light source for activating light-sensitive opsins. Since luciferase enzymes can be genetically encoded and expressed together with opsins in a cell-type specific manner, these bioluminescent light sources obviate any need for chronic implants or external hardware for delivery of light into the brain. A genetically encoded light source also offers much versatility in illuminating large, multiple, or

complex structures in the brain due to the ability to scale up expression in a cell-type dependent manner.

Building upon the previously demonstrated feasibility of coupling bioluminescent proteins to excitatory channelrhodopsins in a single fusion protein termed a luminopsin (LMO)⁹⁴, we describe here a new class of inhibitory luminopsins (iLMOs) consisting of Renilla luciferase (Rluc) and Natronomonas halorhodopsin (NpHR) and demonstrate their ability to silence neural activity in vitro and in vivo in response to both external light and chemical substrate. This new class of optogenetic probes not only allows for optogenetic inhibition without external hardware, but also permits multi-modal (i.e. optical and chemical) methods of neuromodulation that can result in varying temporal effects.

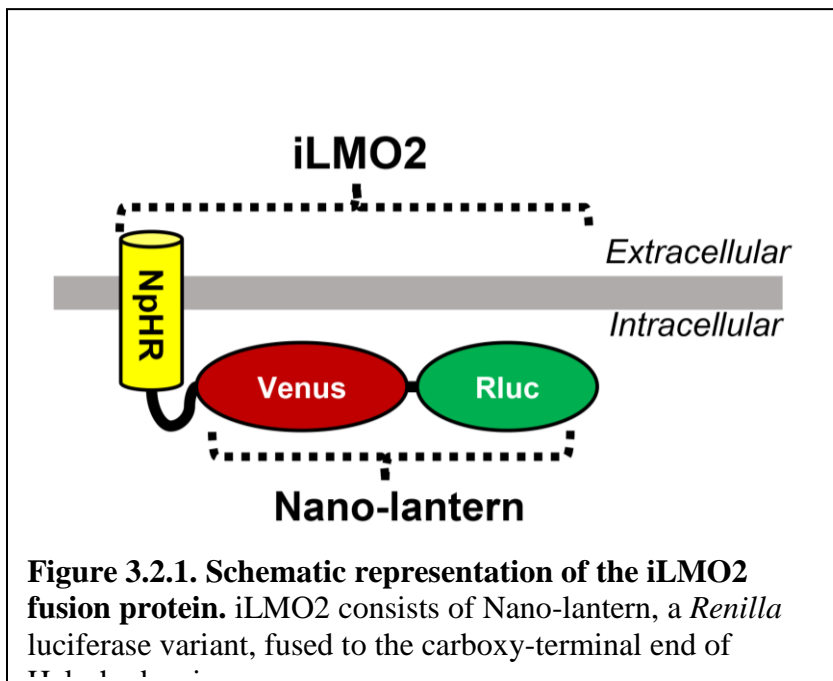
Here we demonstrate how the versatility of conventional light-sensitive opsins can be increased when they are converted into luminopsins, enabling a readily scalable and non-invasive means of neuromodulation that may have unique advantages over other chemical-genetic approaches.

3.2 Design and construction of iLMOs

3.2.1 Results

In search of a luciferase most suitable for activating NpHR, we characterized bioluminescence from several luciferase proteins that have compatible emission spectra with NpHR: a red-shifted Renilla luciferase (TagRFP-RLuc¹⁰⁷), a brighter Renilla luciferase variant (Nano-lantern⁷²), and firefly luciferase (FLuc¹⁰⁸). HEK293 cells were transiently transfected with these luciferases and were characterized in a plate reader by measuring bioluminescence intensity and emission spectrum. The emission spectra for all the luciferases peaked at ~525-nm, with TagRFP-RLuc and Nano-lantern having a wider emission spectrum compared to Fluc (**Figure 3.3.1a**) due to bioluminescence resonance

energy transfer (BRET)^{109,110}. Although the red-shifted emission spectrum of TagRFP-RLuc appeared to be more preferable for activating NpHR, total luminescence from RLuc appeared to be more preferable for activating NpHR, total luminescence from TagRFP-RLuc was significantly lower than that from Nano-lantern by a factor of 12.3 ($p < 0.001$ by one-way ANOVA with Bonferroni posthoc test; $n = 3$ for each group) (Figure 3.2). Fluc did not appear to be a suitable luciferase because it is ATP dependent (which could potentially influence neural activity directly¹¹¹) and its bioluminescence intensity was lower than the RLuc variants by several orders of magnitude. We therefore decided to couple TagRFP-RLuc and Nano-lantern to NpHR by cloning each luciferase to the 3' end of NpHR to create two fusion proteins, which we term iLMO1 and iLMO2 (Figure 3.2.1), respectively. Endoplasmic reticulum export sequences described by Gradinaru et al.²⁴ were also included at the 3' end of the fusion protein to improve membrane trafficking. Here we present the results for iLMO2 since it proved to be more robust. The results for iLMO1 are presented in Appendix A.



3.2.2 Methods

Plasmid construction. All constructs were initially cloned into the pCDNA3 backbone (Invitrogen) for ease of comparison. The luciferase constructs (TagRFP-Rluc8.6⁸⁵ was a gift from Dr. Sanjiv Gambhir; Firefly luciferase¹⁰⁸ was a gift from Dr. Phil Sharp, Addgene plasmid #11510; Nano-lantern⁷² was a gift from Dr. Takeharu Nagai, Addgene plasmid # 51970) were all PCR amplified and cloned into the pCDNA3 vector for direct comparison of expression and bioluminescence. The NpHR coding sequence was PCR amplified from the pAAV-eNpHR3.0-EYFP plasmid (gift from Dr. Karl Deisseroth) and inserted into the pCDNA3 vector. The EYFP coding sequence was digested out of this plasmid using EcoRI/NotI restriction sites to leave a backbone containing NpHR. iLMO1 was created by PCR amplifying out the TagRFP-Rluc8.6 cassette and inserting it in-frame downstream of NpHR. iLMO2 was created in a similar fashion, where the Nano-lantern cassette was PCR amplified (Forward primer: 5' ATCGGAATTCGTGAGCAAGGGCGA, Reverse primer: 5' ATCGCTCGAGTTACACCTCGTTCTCGTAGCAGAACTGCTCGTTCTTCAGCAC) and cloned downstream of the NpHR coding sequence. Both constructs also included an ER-export sequence¹¹² at the 3' end of the fusion protein. The iLMO1 and iLMO2 cassettes were subsequently cloned into the FUGW lentiviral backbone and the pAAV backbone for production of 2nd generation lentivirus and AAV2/9, respectively.

3.3 Characterization of iLMOs in HEK293 cells

3.3.1 Results

We first examined the bioluminescence from iLMO2 and compared it to that of Nano-lantern in transfected HEK293 cells to see whether the creation of the fusion protein had altered the functionality of the luciferase. Both the bioluminescence intensity and emission spectrum of iLMO2 were not significantly different from that of Nano-lantern

alone (**Figure 3.3.1a, b**), which suggests that the functionality of the luciferase moiety is preserved in the fusion protein.

Next, we evaluated the functionality of the NpHR moiety in iLMO2. Judging from the localization of the fluorescence tag, HEK293 cells transfected with iLMO2 efficiently expressed the fusion protein in the cell membrane (**Figure 3.3.1c**). Whole-cell patch clamp recordings revealed that iLMO2-expressing HEK293 cells produced hyperpolarizing outward currents in response to green lamp illumination (Figure 1e), which was not significantly different in peak amplitude from cells expressing NpHR alone or from cells co-expressing NpHR and Nano-lantern separately ($p > 0.05$; one-way ANOVA with Bonferroni posthoc test; $n = 5$ for all groups). These results therefore indicated that NpHR functionality was not significantly affected by fusion or co-expression with Nano-lantern.

We next tested the capability of luciferase-driven activation of NpHR in iLMO2-expressing HEK293 cells. CTZ application in cells expressing iLMO2 generated outward currents that were significantly greater than the negligible CTZ-induced current in cells expressing NpHR alone ($p < 0.05$; one-way ANOVA with Bonferroni posthoc test; $n = 5$ for all groups), indicating a specific effect of CTZ on cells expressing iLMO2 and bioluminescence-mediated photocurrent (**Figure 3.3.1d**). Interestingly, the response of iLMO2-expressing cells to CTZ was not significantly different from cells co-expressing Nano-lantern and NpHR separately, which suggests that bioluminescence from Nano-lantern can activate NpHR whether or not they are physically coupled together.

To assess the efficiency of bioluminescence-driven activation of NpHR, the coupling efficiency (peak CTZ-induced photocurrent divided by peak lamp-induced photocurrent) was calculated. The mean coupling efficiency was higher when Nano-lantern and NpHR were expressed together as the iLMO2 fusion protein compared to when they were co-expressed separately (**Figure 3.3.1e**), but this difference was not statistically significant ($p > 0.05$; one-tailed Student's t-test, $n = 5$ for each group).

These results demonstrate that Renilla luciferase can activate NpHR when they are either co-expressed or coupled together as a single fusion protein. Although co-expression of opsin and luciferase has been shown to be technically feasible by us and others¹¹³, the single fusion protein approach provided more robust responses and practical means of gene delivery.

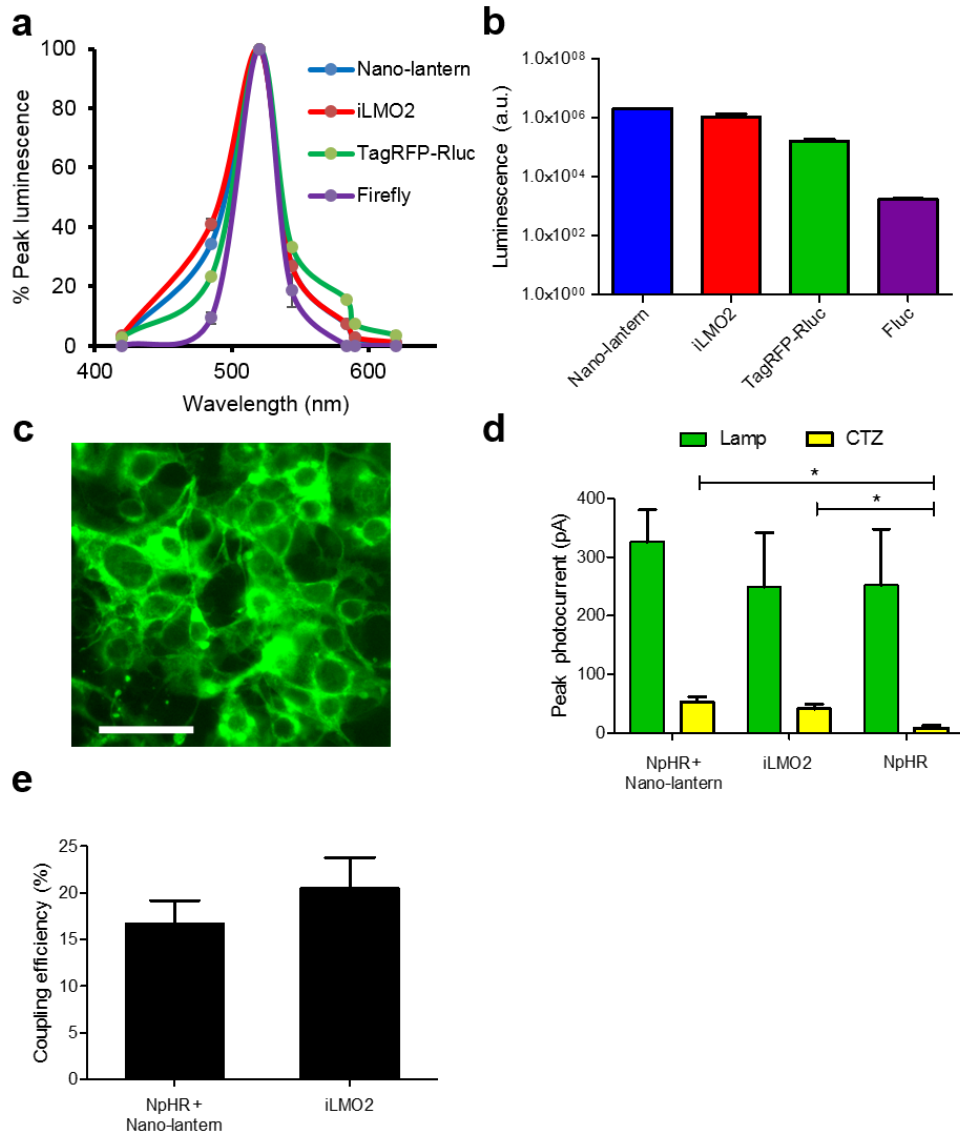


Figure 3.3.1. Characterization of iLMO2 in HEK293 cells demonstrates potential of both direct light and luciferase-driven activation of NpHR. (a) Emission spectra and (b) Total luminescence measured from transfected HEK293 cells expressing various luciferases (Nano-lantern, TagRFP-Rluc, Firefly) and iLMO2. (c) Fluorescence image showing membrane-localized expression of iLMO2 in transfected HEK293 cells. Scale bar: 50 μm (d) Average peak photocurrent responses to green lamp illumination and CTZ measured from HEK293 cells transfected with NpHR and Nano-lantern separately (NpHR + Nano-lantern), iLMO2 fusion protein, and NpHR alone (n = 5 for each group). Mean responses to CTZ are significantly different (*p < 0.05) but light responses were not significantly different (p > 0.05) by one-way ANOVA with Bonferroni posthoc test. (e) Coupling efficiency (peak photocurrent from CTZ divided by peak photocurrent from lamp) of transfected HEK293 cells expressing NpHR and Nano-lantern separately (NpHR + Nano-lantern) (n = 5), and iLMO2 fusion protein (n = 5). Error bars indicate standard error of the mean.

3.3.2 Methods

Coelenterazine preparation. Coelenterazine-h was purchased from Promega and was solubilized in 20 mM β -cyclodextrin (Sigma) in PBS as described by Dr. Osamu Shimomura⁹³. Frozen stock aliquots were kept at -20°C and protected from light. For rotational experiments, CTZ was purchased from Nanolight and solubilized in their proprietary Inject-a-lume solvent immediately before use.

Cell culture and transfection. HEK293 cells were grown in Dulbecco's Modified Eagle Medium (DMEM) containing 10% fetal bovine serum (FBS) and 100U/mL Penicillin/Streptomycin at 37°C with 5% CO₂, and were regularly passaged with 0.25% Trypsin/EDTA every 3-4 days. HEK293 cells were transfected with plasmids using Lipofectamine 2000 (Invitrogen) following manufacturer recommended protocols. Cortical neuron cultures were derived from E18 rat embryos. Cortical tissue was digested with Papain (2 mg/mL) and mechanically dissociated by trituration with a fire-polished glass pipette. Dissociated cortical neuron cultures were seeded on poly-D-lysine coated 18 mm glass coverslips (NeuVibro) and were grown in Neurobasal media containing 1% FBS and 1X Glutamax (Invitrogen). The media was fully changed the day following plating with Neurobasal media containing B27 supplement and 1X Glutamax. Neuronal cultures were typically transduced with viral vectors 1 day in vitro at a multiplicity of infection (MOI) greater than 10 to ensure near 100% transduction efficiency. Half-volume media changes were subsequently given every 3-4 days.

Plate reader assay. For direct comparison of bioluminescence intensity, HEK293 cells seeded at the same density were transfected with 200 ng of luciferase construct (all in the pCDNA backbone) in triplicate wells of a 96-well white luminescence plate (Costar).

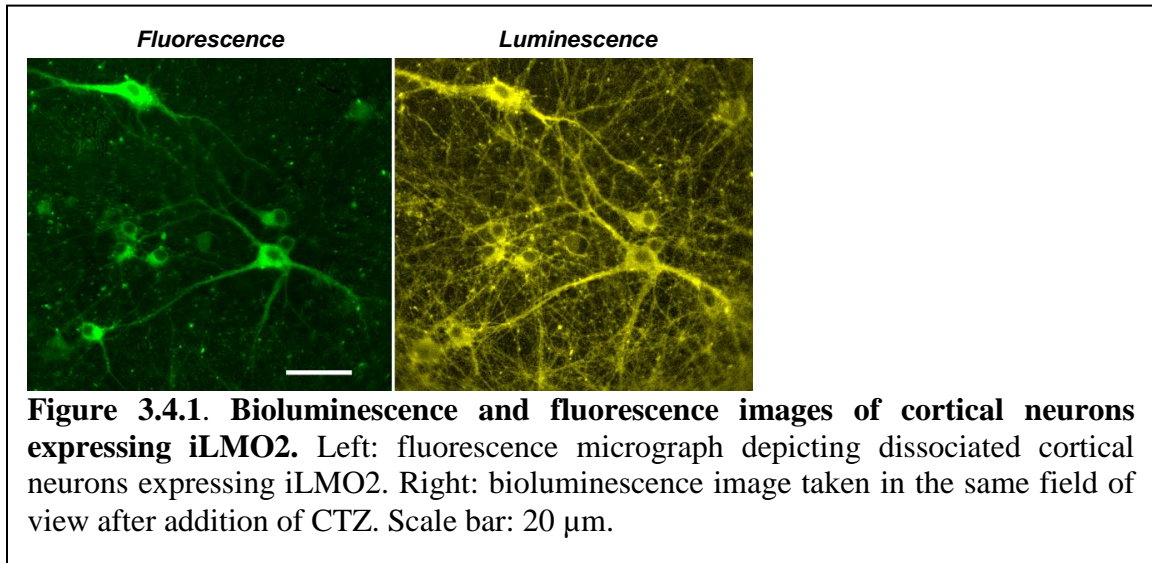
Total luminescence was detected with a commercial plate reader (BMG Labtech) after adding CTZ or D-luciferin (Sigma) to each well (final concentration of 20 μ M). The same gain and integration times were used for measuring all wells. For estimation of emission spectra, luminescence was similarly measured with the use of a filter wheel equipped with 420-nm, 485 nm, 520-nm, 544-nm, 584-nm, 590-nm, and 620-nm bandpass filters.

3.4 Characterization of iLMO2 in cortical neurons

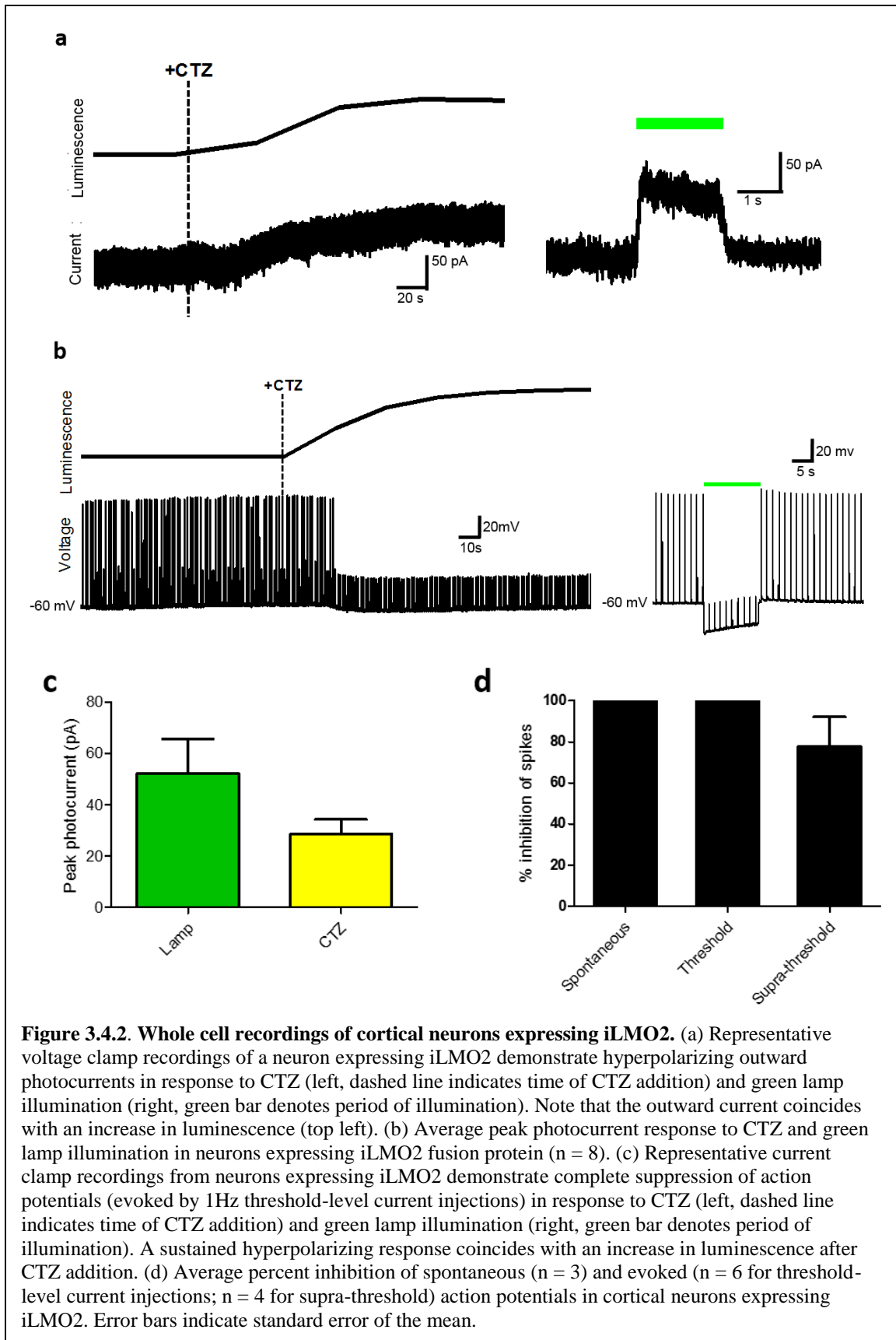
3.4.1 Results

To express iLMO2 in neurons, the iLMO2 cassette was cloned into a lentiviral vector and used to transduce dissociated cortical neurons *in vitro*. Fluorescence micrographs showed strong membrane-localized expression of iLMO2 (**Figure 3.4.1, left**) with no obvious morphological signs of toxicity. After addition of CTZ, robust bioluminescence signal was detected and could be imaged with resolution comparable to that of fluorescence imaging (**Figure 3.4.1, right**). Whole-cell patch clamp recordings showed that neurons expressing iLMO2 generated hyperpolarizing outward currents in response to both direct lamp illumination and CTZ application (**Figure 3.4.2a**). Although direct light illumination was able to generate larger photocurrents than CTZ application, the difference was not statistically significant ($p > 0.05$; two-tailed paired Student's t-test, $n = 8$ for each group). The time course of the CTZ-induced photocurrents corresponded to the bioluminescence signal that was simultaneously detected from the same cells, which suggests that the outward currents seen after CTZ application were due to the activity of luciferase. These effects were not directly caused by CTZ itself because negligible photocurrent responses were seen when CTZ was added to non-transduced cells. The coupling efficiency of iLMO2 in cortical neurons was $72.6 \pm 14.4\%$ (mean \pm

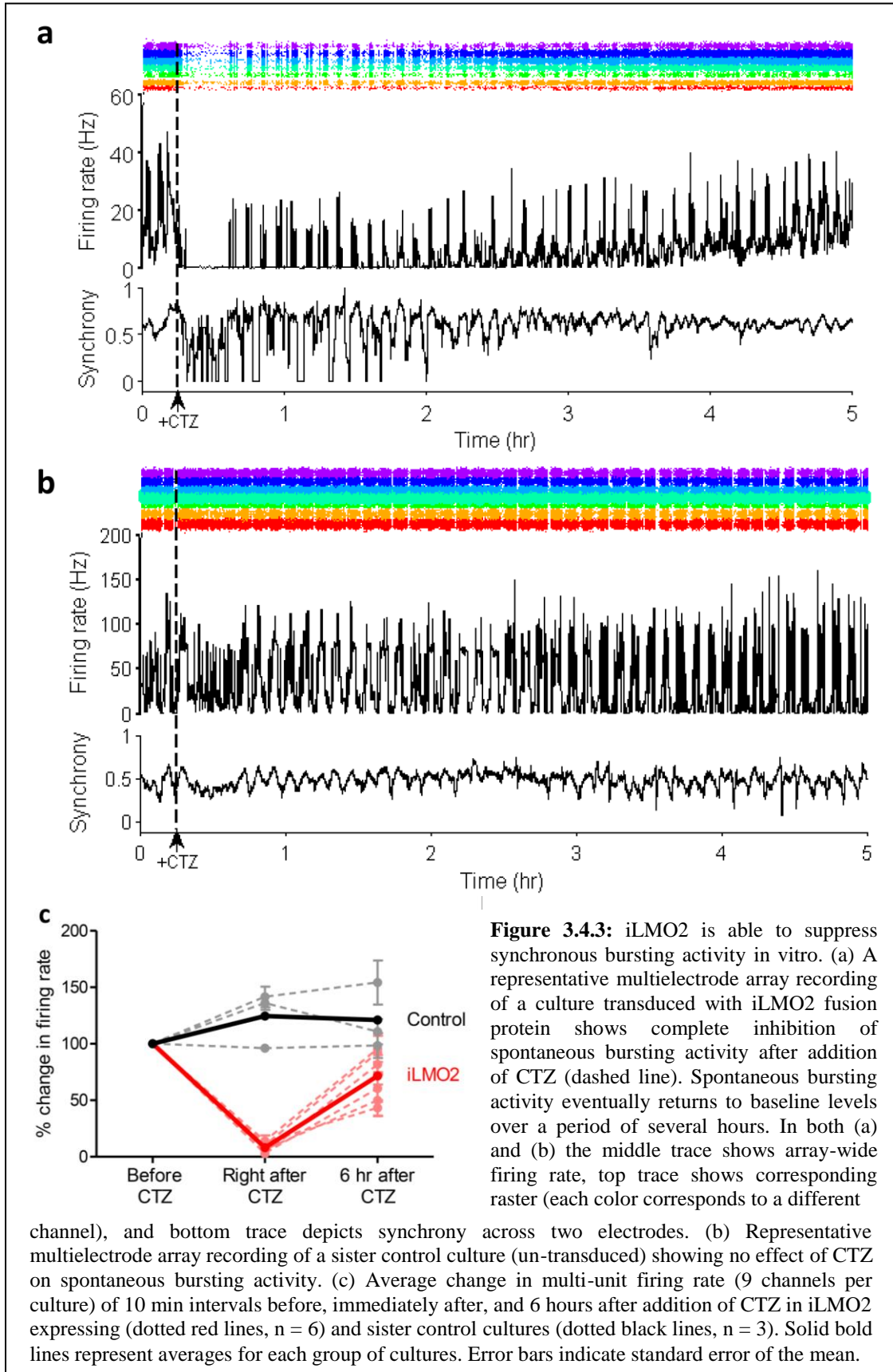
SEM; $n = 8$), which was significantly higher than that found in HEK cells ($p < 0.05$; one-tailed Student's t -test; $n = 5$).



Next, iLMO2 was tested in the context of suppressing both spontaneous and evoked action potentials in dissociated cortical neuron cultures. Similar to direct lamp illumination (**Figure 3.4.2b, right**), CTZ application was able to completely inhibit action potentials evoked by threshold-level (rheobase levels where action potentials are evoked ~50% of the time) current injections given at 1 Hz (**Figure 3.4.2b, left**). In addition, iLMO2 was able to completely suppress spontaneous action potential firing after CTZ application (**Figure 3.4.2d**). In contrast, action potentials evoked by supra-threshold (action potentials evoked 100% of the time) current injections were only partially suppressed by CTZ (**Figure 3.4.2d**), which was most likely due to the inability of iLMO2 to overcome the relatively larger inward current injections. These experiments corroborate our previous findings in HEK293 cells and demonstrate that iLMO2 can inhibit neuronal firing in single cells in response to both external light and luciferase substrate.



To test the ability of iLMO2 to silence neuronal activity of a population of neurons, we cultured cortical neurons on multielectrode arrays (MEAs) and transduced them with iLMO2 lentivirus. When cortical neurons are cultured on MEAs at high density, they spontaneously exhibit synchronous burst-firing activity across the culture^{114,115}. Addition of CTZ inhibited burst-firing activity in a period of minutes, resulting in near-zero total firing rate across all the electrodes in the array (**Figure 3.4.3a**). This effect persisted for up to 20 minutes before bursts returned and total firing rate gradually recovered back to baseline levels. Recovery back to baseline required several hours, which is consistent with the amount of time these cultures take to recover from transient suppression of bursting activity¹¹⁶. The synchrony (a measure of concurrent spike times across electrodes) of cultures expressing iLMO2 also transiently decreased during periods of suppressed burst-firing, confirming that CTZ was suppressing synchronous bursting activity. These changes induced by CTZ were not seen in sister control cultures that were not transduced with iLMO2 lentivirus (**Figure 3.4.3b**), indicating that CTZ was specifically acting through iLMO2. On average, multiunit activity in each electrode of the array slightly increased in control cultures after addition of CTZ (**Figure 3.4.3c**, black trace), whereas cultures expressing iLMO2 showed an unequivocal marked reduction in multiunit activity in each electrode of the array after addition of CTZ (**Figure 3.4.3c**, red trace). These results all suggest that iLMO2 is able to suppress synchronous bursting activity across the entire neural network.



3.4.2 Methods

Viral vector production. iLMO2 lentivirus driven by the ubiquitin promoter (lenti Ub-iLMO2) was made in-house based on methods described by Dr. Trono Didier¹¹⁷. In brief, 293FT cells were grown in multiple 10 cm cell culture dishes to 90% confluency on the day of transfection. Each dish was then transfected with 7.5 μ g Δ 8.9 packaging vector, 3 μ g VSVG envelope vector, and 10 μ g of the iLMO2 transfer vector by calcium phosphate precipitation. Transfection efficiency was confirmed the following day by fluorescence microscopy and lentivirus was subsequently harvested for 2 days following transfection. The harvested lentivirus was purified through a 0.45 μ M PES filter and concentrated by ultracentrifugation to an approximate titer of 10⁸ infectious particles/mL. AAV2/9 CAMKII α -iLMO2 was produced by the Emory viral vector core at a titer of 10¹² viral genomes/mL.

Intracellular recordings. Intracellular recordings were taken from 12 day old dissociated cortical neurons cultured on glass coverslips. The glass coverslips were transferred to an 18 mm low profile recording chamber (Warner Instruments) and perfused using a Quick Exchange platform (Warner Instruments) with external solution containing 135 mM NaCl, 5mM KCl, 1 mM MgCl₂, 2 mM CaCl₂*2H₂O, 10 mM HEPES, 10 mM Glucose. Whole cell patch clamp recordings were obtained with glass pulled recording pipettes with 5-10 m Ω resistance containing internal solution consisting of 120 mM potassium gluconate, 2 mM MgCl₂, 1 mM CaCl₂*2H₂O, 10 mM EGTA, 10 mM HEPES, 2 mM ATP. Recordings were sampled at 10 kHz with an EPC-9 amplifier (HEKA) and Patchmaster software for online analysis and later exported to Matlab for offline analysis. Membrane potential was clamped to -60 mV for voltage clamp recordings while current was clamped at 0 \pm 20 pA for current clamp recordings in order to maintain a resting membrane potential of -60 mV. Action potentials were evoked by either giving threshold-

level (rheobase levels evoking spikes ~50% of the time) or supra-threshold level (spikes evoked 100% of the time) current injections. Bioluminescence imaging was concurrently taken throughout the whole cell recordings with a 1.35 NA oil immersion objective, 0.35x demagnifying lens, and a scientific CMOS camera (QImaging). CTZ was bath applied through a 4 channel micro-manifold (AutoMate Scientific) to reach a final concentration of 40 μM in the recording chamber. Cells were illuminated through the objective with green light (532-554 nm TRITC filter cube at 35 mW/mm²) using an electronic shutter. Percent inhibition of spikes were calculated as the peak reduction of firing rate across the recordings taken in 10 s bins.

In vitro multielectrode recordings. High density cortical neuron cultures grown on multielectrode arrays were prepared and recorded using the same equipment and methods described by Hales et al ¹¹⁸. Briefly, approximately 50,000 dissociated cortical neurons were seeded in each well of a 6-well multielectrode array (Multichannel Systems). Each well contained 9 recording electrodes, in which multiunit activity was detected and acquired by a custom-built NeuroRighter data acquisition system¹¹⁹. The cultures were covered with a Teflon lid to prevent evaporation and kept in a humidified incubator set at 35°C and 5% CO₂. The cultures were infected 1 day in vitro with Ub-iLMO2 lentivirus at >10 MOI to ensure near 100% transduction efficiency, and the media was subsequently changed (half-volume) every 3-4 days with Neurobasal media containing 2% FBS. Approximately 2 weeks later, the MEA was connected to a pre-amplifier located inside an incubator kept at 65% humidity, 35°C, and 5% CO₂. Spiking activity in the cultures was confirmed and the MEA was allowed to equilibrate in the incubator overnight. On the day of the experiment, 5 μl of CTZ was added to the media of each culture to reach a final concentration of 12 μM . Recordings were taken up to 6 hours after addition of CTZ and analyzed offline using custom Matlab scripts. Synchrony was calculated using custom Matlab scripts developed by Quiroga et al¹²⁰. Percent change in firing rate was

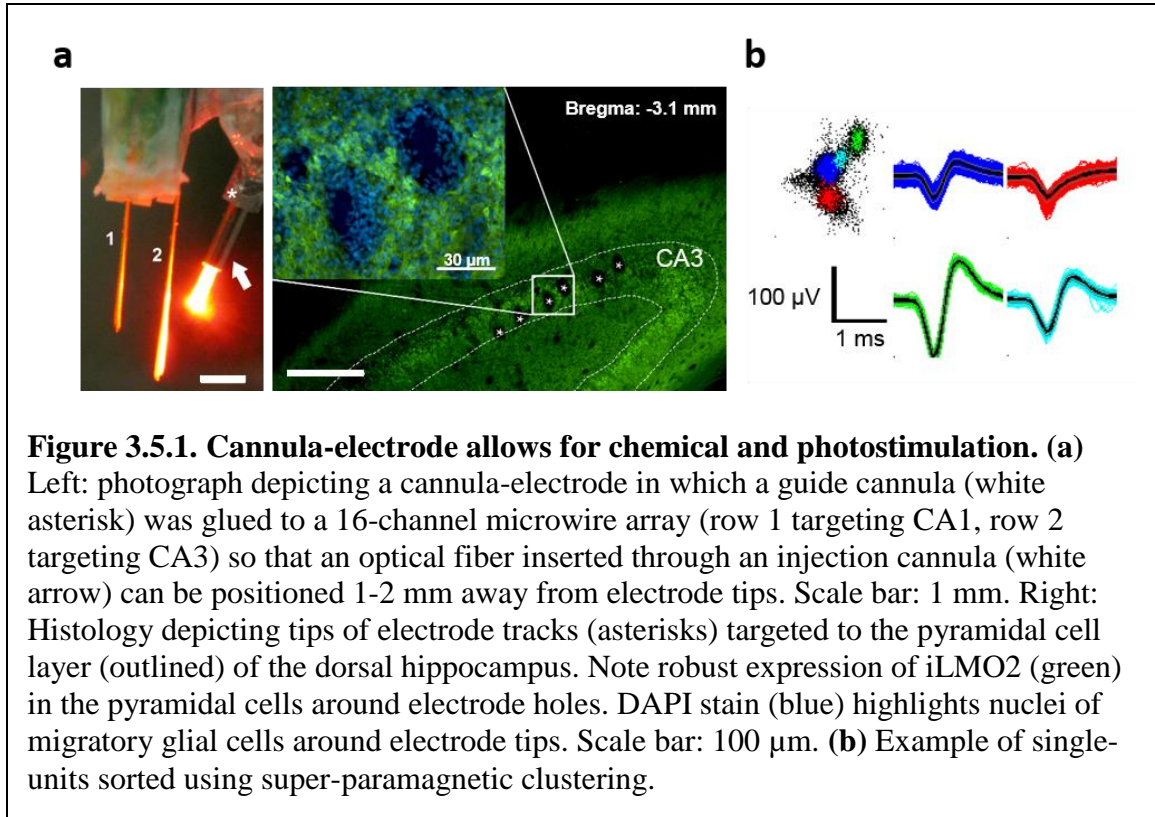
calculated by averaging the firing rate of each electrode in the culture across a 10 min window immediately after and 6 hours after the addition of CTZ.

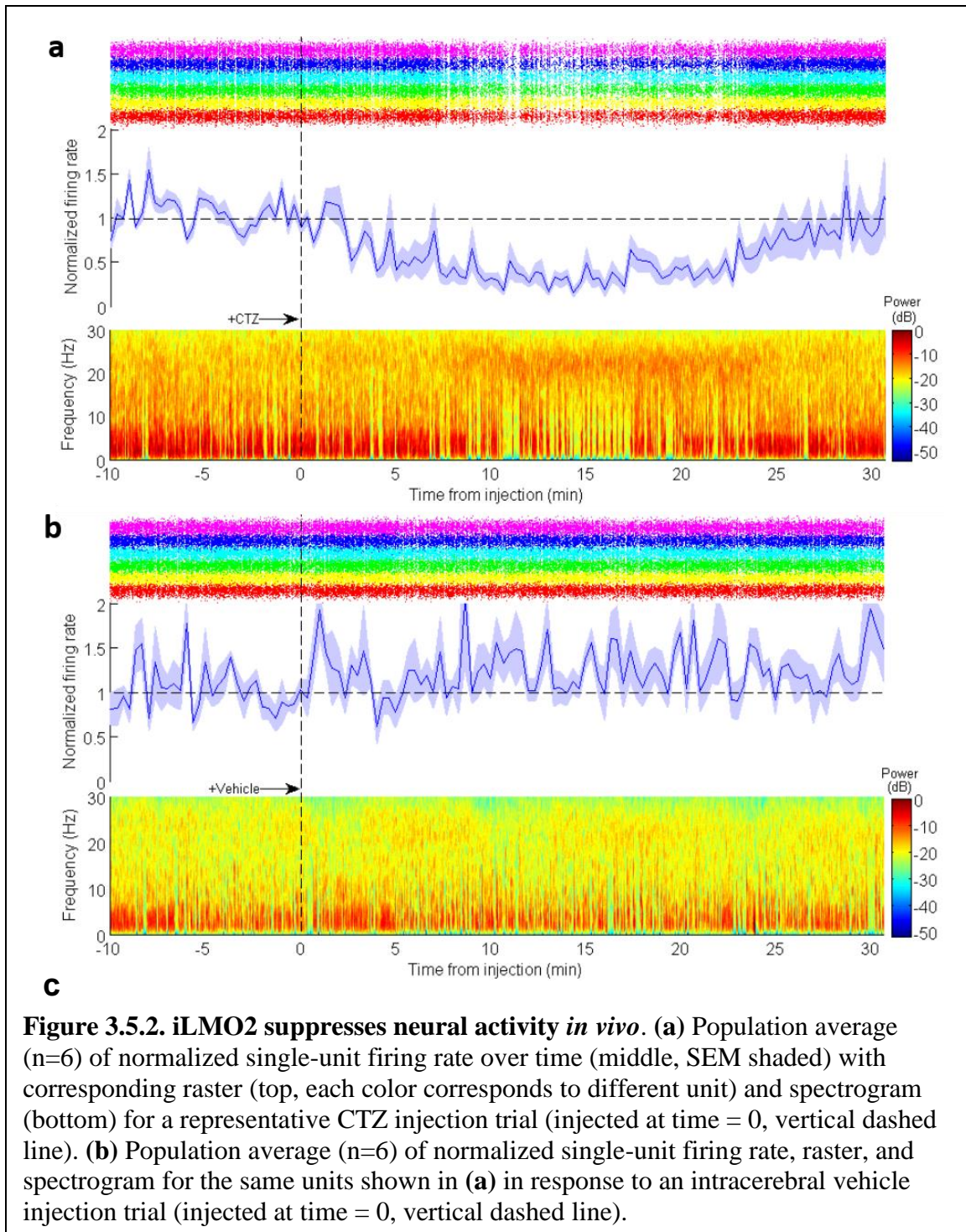
3.5 Characterization of iLMO2 in vivo

3.5.1 Results

Next, we examined the ability of iLMO2 to suppress neural activity in anesthetized and awake rats. The iLMO2 cassette was cloned into an adeno-associated viral (AAV) vector under the control of the CaMKII α promoter, and the virus was stereotaxically injected into the dorsal hippocampus of rats to selectively target expression of iLMO2 to pyramidal cells of CA3 and CA1 (**Figure 3.5.1a, right**). A cannula-electrode consisting of a 16-channel microwire array and a guide cannula (**Figure 3.5.1a, left**) was fabricated and subsequently implanted in the same area, where each row of the array targeted a different pyramidal cell layer of CA3 and CA1. The cannula-electrode was then chronically implanted, which allowed for easy insertion of an injection cannula or optical fiber for intracerebral injections and optical stimulation, respectively, to the same area in each animal over multiple trials under anesthesia. Before each injection trial, single-units whose firing rate was significantly reduced by conventional photostimulation (525-nm or 620-nm LED) were first identified for subsequent single-unit analysis. The optical fiber was then replaced with an injection cannula that contained either 2 μ l of CTZ or vehicle. When CTZ was injected intracerebrally over 5 minutes, single-unit firing rate (of those units that responded previously to photostimulation) decreased and reached peak inhibition about 15 minutes after injection (**Figure 3.5.2a, top and middle**). The firing rate subsequently returned back towards baseline levels over the next 15 minutes. In addition to reducing single-unit firing rate, CTZ also reduced the low frequency power (1 – 10 Hz) in the local field potential of the same electrodes (**Figure 3.5.2a, bottom**), indicating that the dominant theta rhythms in the hippocampus¹²¹ were suppressed. In

contrast, when vehicle was injected in the same animal as a control, an increase in single-unit firing rate and no change in the local field potential were observed (**Figure 3.5.2b**). These trials of intracerebral CTZ and vehicle injection were repeated daily with an alternating order over a period of 5-7 days. The average peak response to CTZ (**Figure 3.5.3a, red trace**) was comparable to conventional photostimulation by LEDs: single-unit firing rate was reduced on average by $52.1 \pm 5.4\%$, $37.5 \pm 6.9\%$, and $45.0 \pm 4.6\%$ (mean \pm SEM; n = 24 units each) by 620-nm light, 525-nm light, and CTZ, respectively. On average, vehicle injections increased single-unit firing rate by $44.6 \pm 9.6\%$ (mean \pm SEM; n = 24 units; **Figure 3.5.3a, blue trace**). Across all animals tested, the average peak inhibition of single-unit activity was $60.3 \pm 11.56\%$ by intracerebral CTZ injection, $58.9 \pm 4.18\%$ by 620-nm light, and $40.2 \pm 2.7\%$ by 525-nm green light (mean \pm SEM, n = 3 animals; **Figure 3.5.3b**). These effects were replicated in the awake behaving animal (**Figure 3.5.4a**). CTZ was thus able to suppress neural activity on both a cellular and network level in vivo and its efficacy was comparable to conventional photostimulation through a fiber optic.





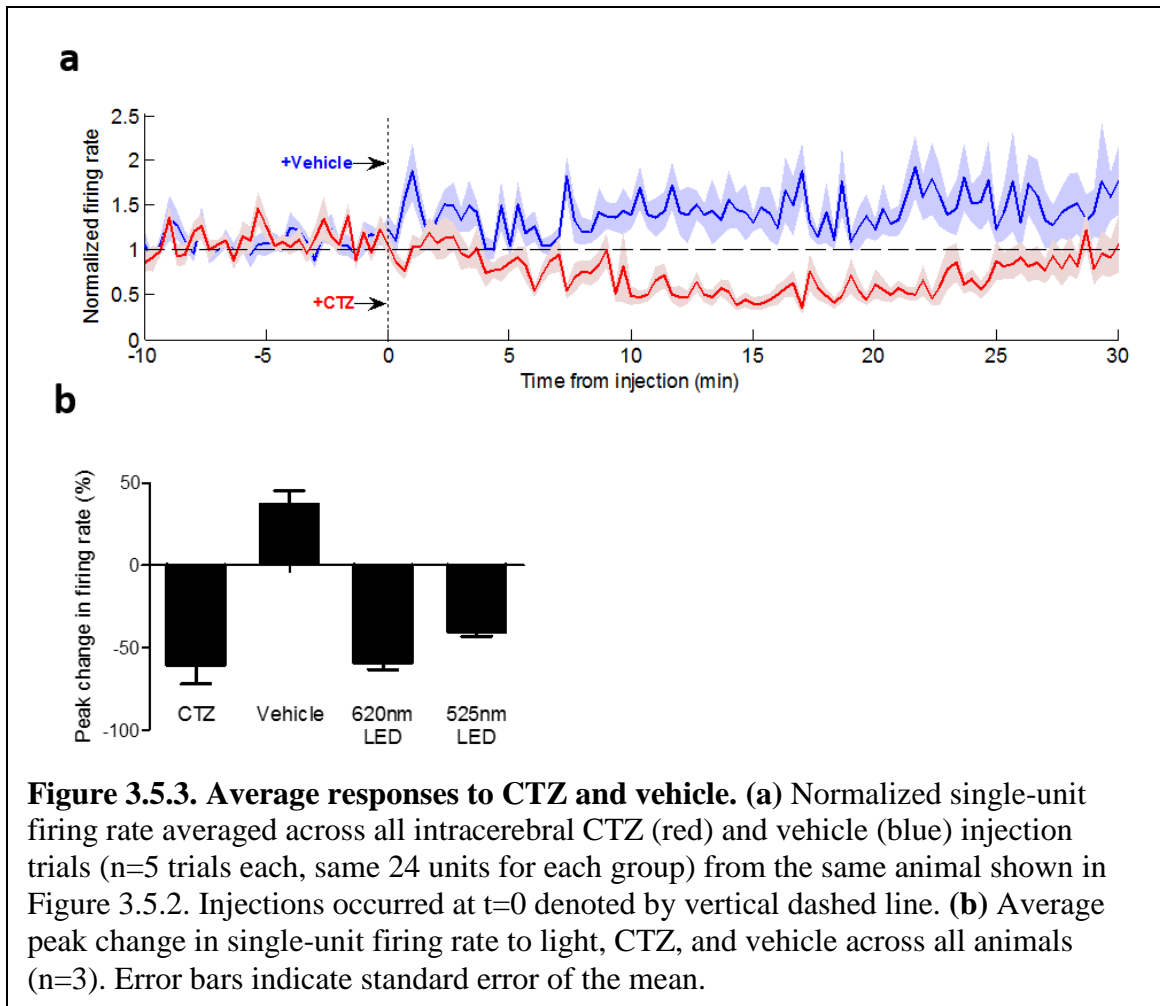
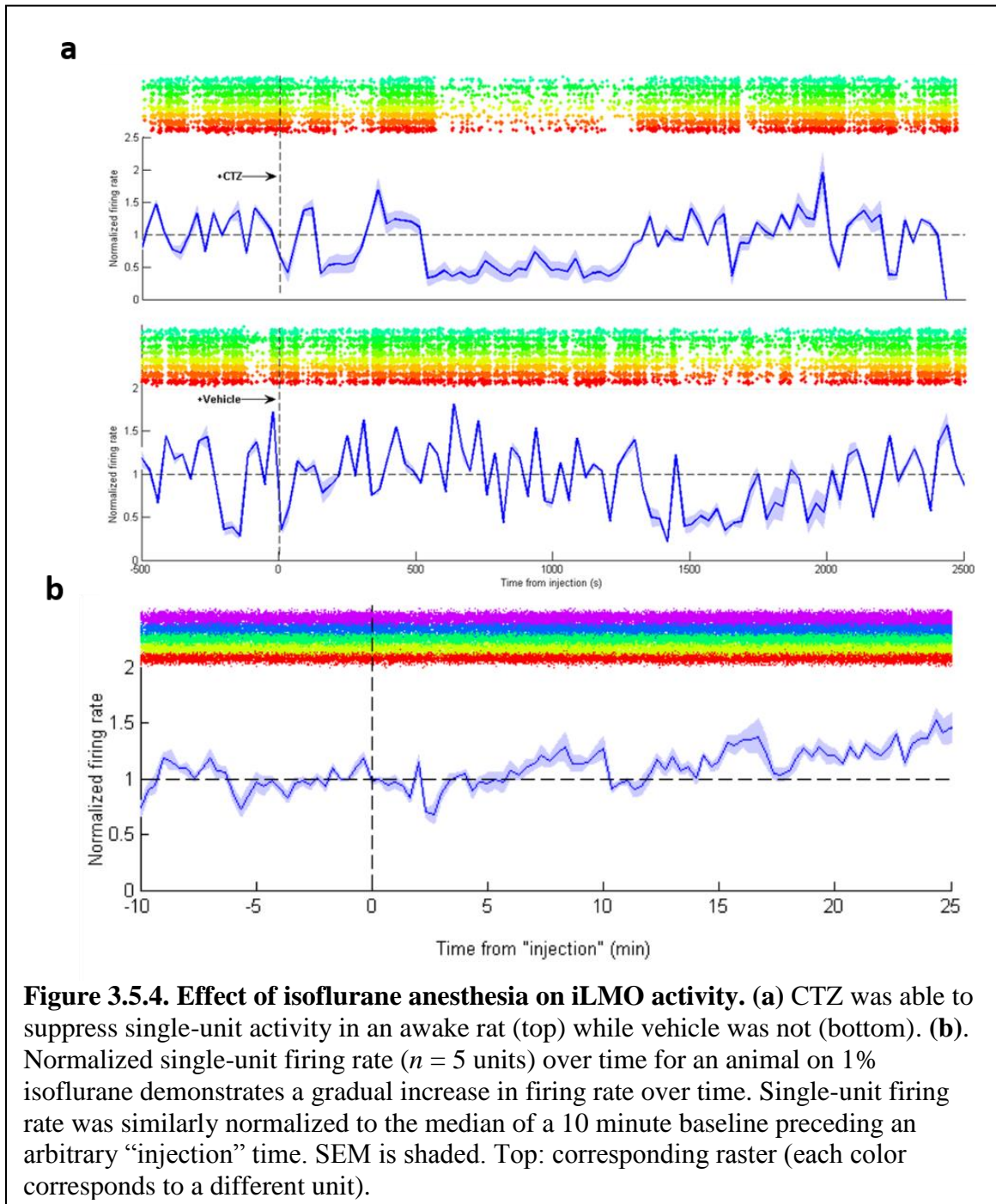


Figure 3.5.3. Average responses to CTZ and vehicle. (a) Normalized single-unit firing rate averaged across all intracerebral CTZ (red) and vehicle (blue) injection trials (n=5 trials each, same 24 units for each group) from the same animal shown in Figure 3.5.2. Injections occurred at t=0 denoted by vertical dashed line. (b) Average peak change in single-unit firing rate to light, CTZ, and vehicle across all animals (n=3). Error bars indicate standard error of the mean.



3.5.2 Methods

Animal experiments. All animals were purchased from Charles River Laboratories and were housed in the Emory animal vivarium with a 12hr light/ 12hr dark cycle. All

procedures were conducted in accordance to approved guidelines from the Emory University Institute for Animal Care and Use Committee.

Stereotaxic viral injections. For animals implanted with a cannula-electrode, two month old male Sprague-Dawley animals (200-250 g) were anesthetized with 1.5-4% inhaled isoflurane and a craniectomy was made 3.3 mm posterior and 3.2 mm lateral to bregma. 1.8 μ l of AAV2/9-CAMKII α -iLMO2 was stereotaxically injected at a depth of 3.1 mm ventral to pia targeting the dorsal hippocampus. Virus was injected through a glass-pulled pipette using a Nanoject injector (Drummond Scientific) at a rate of 275 nl/min. After viral injection was completed, the scalp was stapled closed and animals were allowed to recover for up to two weeks.

In vivo electrophysiology. Animals were implanted with a cannula-electrode two weeks after the viral injection. We have found that two weeks is sufficient for expression of optogenetic vectors delivered by AAV. A guide cannula (Plastics One) was glued to a 16-channel microwire array (Tucker Davis Technologies) so that a 0.39 NA, 200 μ m core diameter bare fiber optic (Thorlabs) inside an injection cannula could be inserted into the guide cannula and positioned 1-2 mm away from the electrode tips. Four skull screws and one cerebellar reference screw were implanted into each animal. A craniotomy was then made over the dorsal hippocampus (array angled 50° from midline and centered 3.5 mm posterior and 2.9 mm lateral to bregma) and the cannula-electrode was manually driven into the brain while continuously recording to ensure ideal placement of electrodes. The correct stop depth was determined by identifying responsive single-units after repeated optical stimulation (10s continuous pulses) with green (625-nm, 2.8 mW from fiber tip) and orange (520-nm, 1.3 mW from fiber tip) light from externally coupled LEDs (Plexon). Electrophysiologic recordings were sampled at 25 kHz using our custom built NeuroRighter data acquisition system¹²². Local field potentials were bandpass filtered (1-

500 Hz) from the raw signal and analyzed offline using custom Matlab scripts and the Chronux toolbox¹²³. Single-units were detected from the bandpass filtered (500-5 kHz) signal and sorted offline using superparamagnetic clustering (Wave Clus) scripts developed by Quiroga et al¹²⁴. The entire cannula-electrode was then sealed in place with dental acrylic (Lang Dental), the optical fiber was retracted from the guide cannula and replaced with a dummy cannula, and the animal was allowed to recover several days before further experimentation.

Intracerebral injections. After the animals recovered from surgery, their electrophysiological responses to light, CTZ, or vehicle were investigated. The chronically implanted cannula-electrode allowed for multiple trials to be conducted for each animal, where each trial consisted of an intracerebral injection of CTZ and vehicle (in alternating order) on one particular day. The animals were first lightly anesthetized by 0.5-1.5% inhaled isoflurane. Responsive units were then identified by optically stimulating through the guide cannula with an optical fiber coupled to a 625-nm orange and 520-nm green LED as described above. Only responsive units were used for subsequent single-unit analysis. The optical fiber was then removed from the guide cannula and replaced with an injection cannula connected to a Hamilton syringe containing either 2 μ l of CTZ (600 μ M) or vehicle (20 mM β -cyclodextrin in PBS). A baseline recording of at least 10 minutes was recorded before CTZ or vehicle was injected (over a period of ~5 minutes) into the brain parenchyma. After injection was completed, the animal was recorded under constant levels of anesthesia for up to 1 hr. Single-unit activity was normalized to the median firing rate 10 minutes before injection. Percent inhibition of spikes to CTZ was calculated by averaging the percent reduction in firing rate \pm 1 min from the point of maximum inhibition. Percent inhibition of spikes to vehicle injection was calculated in the same fashion using the same time interval used in the analogous CTZ calculation.

Histology. After all experiments were completed, animals were sacrificed by intraperitoneal injection of Euthasol (Virbac). Animals were then transcardially perfused with 4% paraformaldehyde (PF). The heads of animals implanted with the cannula-electrodes were decapitated and kept in PF at 4°C overnight to allow for visualization of the electrode tracks. Otherwise, the brains were dissected out and allowed to fix in PF for 1 hr. After fixation, the brains were cryoprotected in 30% sucrose before sectioning on the microtome. 50 µM thickness sections were collected and mounted onto glass slides for imaging on an upright fluorescence microscope using NIS-elements acquisition software (Nikon).

3.6 Application of iLMO2 in behaving animals

3.6.1 Results

Lastly, we tested the ability of iLMO2 to modulate motor behavior in awake behaving rats. Unlike conventional optogenetic stimulation, luminopsins do not require external light delivery and can instead be activated by systemic CTZ administration, facilitating long-term studies of freely behaving animals in a non-invasive manner. Unilateral lesions of the globus pallidus in rats have been demonstrated to produce a consistent and predictable increase in ipsilateral rotation after administration of stimulants such as amphetamine or apomorphine¹²⁵. We therefore sought to mimic these motor effects with optogenetic inhibition of the globus pallidus with iLMO2. AAV encoding iLMO2 was unilaterally injected into the globus pallidus of rats, and two weeks later they underwent multiple amphetamine-induced rotation tests. For each test, a baseline recording of at least 10 minutes was first obtained before the animal was intravenously injected with either CTZ or vehicle through a jugular vein catheter. CTZ injections resulted in a significant increase in mean net ipsilateral rotations above the baseline (**Figure 3.6.1, red**

trace). The effect of CTZ persisted for more than 1 hour before rotational preference returned back to baseline. When vehicle was injected in the same animal, such an effect was not observed (**Figure 3.6.1, black trace**). To confirm the activation of iLMO2 upon CTZ administration, in vivo bioluminescence imaging was conducted in these animals after conclusion of the rotation experiments. After intravenous injection of CTZ, a robust bioluminescence signal was detected through a craniotomy above the virus injection site (**Figure 3.6.2a**), confirming that CTZ was crossing the blood-brain-barrier and reaching cells expressing iLMO2. These results also demonstrate a convenient means to functionally detect and confirm expression of iLMOs in deep structures of the brain. To estimate the extent of activation of iLMO2 in the brain, acute coronal brain slices were prepared and imaged after bath application of CTZ. Bioluminescence was detected throughout the basal ganglia circuitry (**Figure 3.6.2b**), suggesting widespread activation of iLMO2. Post mortem histology confirmed that expression of iLMO2 was found throughout the cell bodies and projections of the globus pallidus and striatum (**Figure 3.6.3**). These results demonstrate iLMO2's ability to manipulate multiple circuits underlying complex behavior in freely moving animals in a non-invasive manner.

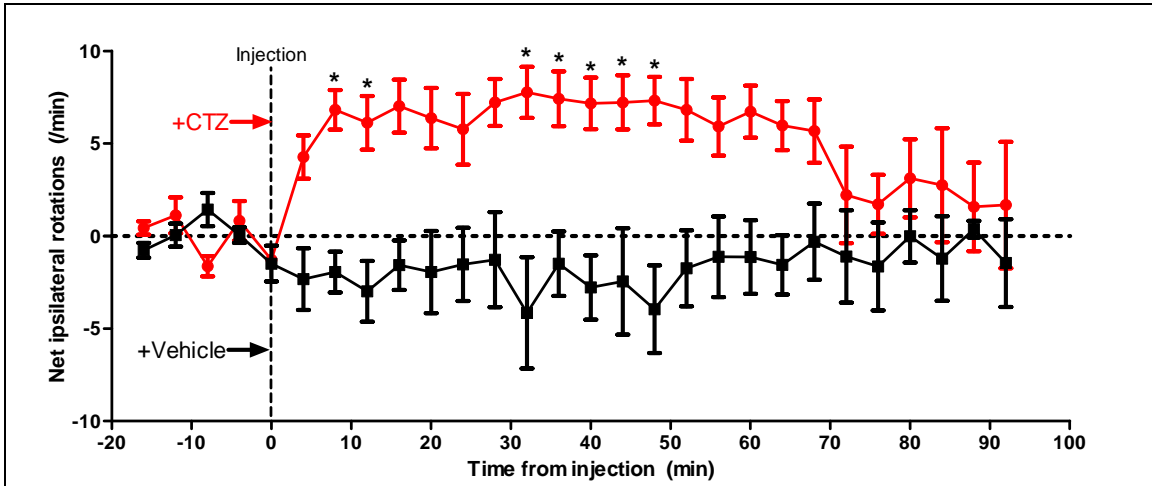


Figure 3.6.1. Rotation testing. Intravenous administration of CTZ was able to significantly increase net ipsilateral rotations over mean baseline rate in rats unilaterally expressing iLMO2 in the striatum and globus pallidus. CTZ or vehicle was injected through a jugular venous catheter at t = 0 (dashed line). The response to CTZ was significantly different than vehicle by two-way ANOVA with Bonferroni posthoc test (*p < 0.05; n = 5 trials for CTZ, n = 6 trials for vehicle across 3 animals).

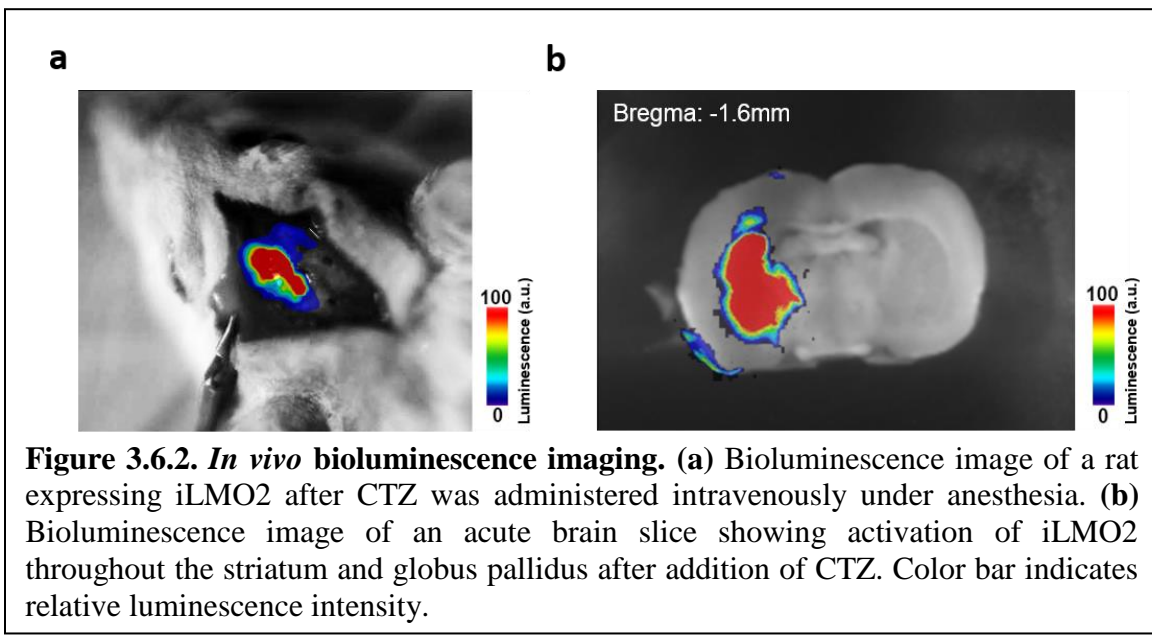
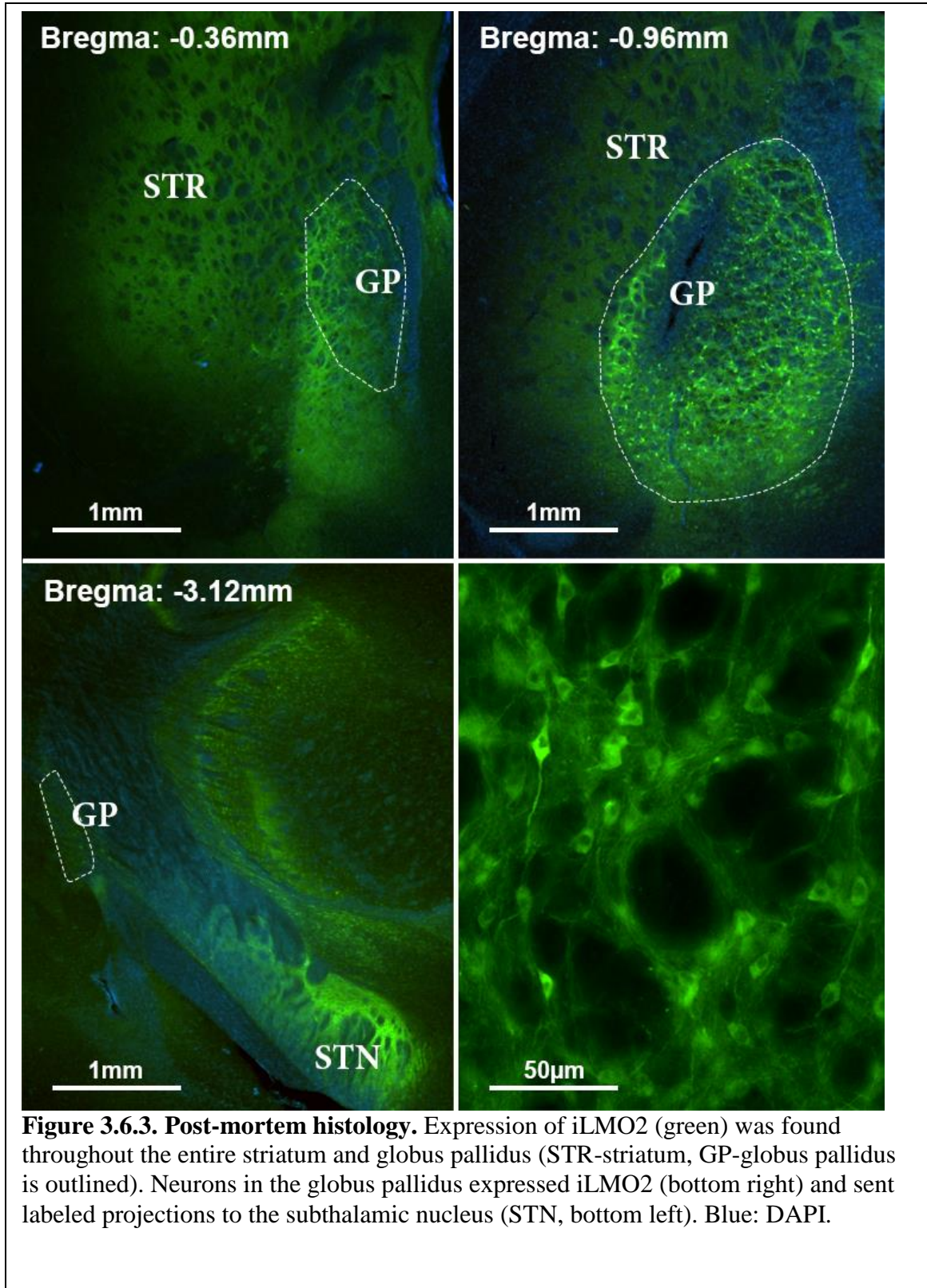


Figure 3.6.2. In vivo bioluminescence imaging. (a) Bioluminescence image of a rat expressing iLMO2 after CTZ was administered intravenously under anesthesia. (b) Bioluminescence image of an acute brain slice showing activation of iLMO2 throughout the striatum and globus pallidus after addition of CTZ. Color bar indicates relative luminescence intensity.



3.6.2 Methods

Stereotaxic virus injections: Same as described above in section 3.5. For animals used in behavioral rotation tests, iLMO2 was unilaterally expressed in the striatum and globus pallidus of rats by two stereotaxic injections (-0.4 mm AP, \pm 3.5 mm ML, -5.0 mm SI; +1.0 mm AP, \pm 2.8 mm ML, -5.2 mm SI) of AAV2/9-CAMKII α -iLMO2 as described above.

Rotation tests. One week after virus injection, animals were implanted with a jugular venous catheter to allow for convenient intravenous injections of CTZ or vehicle during rotational testing. Therefore, each animal could undergo multiple trials of both CTZ and vehicle injections. At the start of each trial day (beginning in the mornings between 10-12pm), animals were given amphetamine (2.5 mg/kg) by intraperitoneal injection and placed into a cylindrical chamber where an automated rotation counter (Columbus Instruments) was used to quantify both partial and full rotations. When the animals reached a steady baseline, they were injected with either 250 μ l of CTZ (1 mg) or vehicle through a syringe connected to the catheter by polyethylene tubing. The number of total rotations per two minute intervals was then recorded for up to 1.5 hours following injection.

In vivo bioluminescence imaging. Bioluminescence imaging was conducted after the conclusion of the amphetamine-induced rotation tests. A craniotomy was first performed over the injection sites to allow for direct visualization of the intact brain and overlaying dura. The animals were then deeply anesthetized with 100 mg/kg Ketamine/Xylazine and injected with 0.5 mg of CTZ through the jugular catheter. Bioluminescence images were taken using 10 - 20s exposure times in a Fuji LAS-3000 dark box equipped with a cooled CCD camera. The animal was subsequently sacrificed after the imaging session by Euthasol injection and acute brain slices were collected and imaged in a similar fashion

(after bath application of CTZ to reach final concentration of 30 μ M) using 1-2 s exposure times.

Histology. Same as described above in section 3.5.

3.7 Discussion

We report here a novel optogenetic probe that is capable of suppressing neural activity in response to both external light and chemical substrate. In contrast to previously described excitatory luminopsins that were shown to modulate neuronal excitability *in vitro*⁹⁴, we have demonstrated robust inhibition of action potential firing in various scenarios *in vitro* and *in vivo*. First, we rationally designed inhibitory luminopsins by characterizing the bioluminescence emission properties of various luciferase proteins and selecting the most suitable ones to couple with an inhibitory opsin, NpHR. We then demonstrated that bioluminescence from the Renilla luciferase variant, Nano-lantern, could be used to activate NpHR when both are coupled together as the iLMO2 fusion protein or co-expressed in the same cell (Figure 1). Although co-expression of opsin and luciferase uniquely allows for the possibility of transcellular optogenetic modulation if different cells are targeted, we pursued the single fusion protein approach due to its more effective transgene delivery and greater coupling efficiency. iLMO2 was then utilized to suppress single-cell action potentials and synchronous bursting activity *in vitro* (Figures 2 and 3). These effects were translated *in vivo*, where bimodal activation of iLMO2 was able to suppress single-unit firing rate and local field potential in the hippocampus of anesthetized rats (Figure 4). Finally, iLMO2 was used for hardware-independent optogenetic inhibition of the basal ganglia, where its effects increased ipsilateral rotations for more than an hour in awake behaving rats (Figure 5).

We have bypassed the challenges of delivering external light into the brain by making the opsin-expressing cells their own light source with the use of bioluminescent

proteins. The major advantage of utilizing luminopsins is that both the light source and opsin are genetically encoded and expressed as one molecule, which allows for modulating neural activity without the need for invasive hardware, as well as the ability to selectively target expression in a readily scalable manner. We demonstrated these advantages by modulating behavior in freely moving rats without the need for any chronically implanted devices or external light sources. Our results demonstrate that large structures in the brain can be targeted with luminopsins, which can be advantageous when multiple brain regions or diffuse circuits need to be manipulated. Indeed, expression of iLMO2 was found in both cell bodies and projections of the striatum and globus pallidus in animals used for the rotation tests, which suggests that inhibition of the direct pathway (striatal-nigral) and disinhibition of the indirect pathway (striato-pallido-subthalamic-nigral) acted synergistically to modulate rotational behavior. Expression of iLMO2 was estimated to span a total volume greater than 20 mm³ in the brains of these animals, which is far greater than the predicted volume of light illumination achieved with a single optical fiber (the predicted spherical volume illuminated with at least 3.5 mW/mm², an intensity shown to reliably activate eNphR3.0¹²⁶, is 1.15 mm³ using a 630-nm, 20 mW output, 200 μm core diameter, 0.39 NA fiber¹²⁷).

Although we were able to influence a large volume of tissue in the brain by delivering iLMO2 with a non-specific viral vector, one could also spatially restrict the expression of luminopsin to genetically defined cell populations with the use of cell-specific promoters or transgenic animals. In addition, luciferase-derived bioluminescence can also be spatially localized within the cell with the use of various targeting motifs¹²⁸, which could potentially be useful for limiting optogenetic manipulation to subcellular components or preventing off-target activation of surrounding opsin-expressing cells. A genetically encoded luminopsin can therefore achieve high spatial resolution when expression is carefully controlled for (e.g. with cell-specific promoters, localization motifs, or precise virus injections). Utilization of a genetically encoded light source can

also yield distinct advantages over external light sources particularly when targeting complex structures (e.g. cerebellum) that are problematic for efficient light transmission¹⁰⁴ since the light source is directly coupled to the opsin.

iLMO2 was able to generate enough hyperpolarizing photocurrent to completely suppress neural activity *in vitro*, but was only able to suppress single-unit firing rate by 60.3% on average *in vivo*. Our data suggests that this degree of inhibition is underestimated because single-unit firing rates actually increased after vehicle was injected. This increase in firing rate was likely not directly due to the injection itself; rather, baseline activity gradually increased from exposure to isoflurane anesthesia. Indeed, recordings from animals on low levels of isoflurane (0.5-1.5%) showed a gradual increase in hippocampal activity over time (Supplementary Figure 2), which agrees with previous findings demonstrating the excitatory effects of low dose isoflurane on hippocampal activity^{129,130}. Despite this excitatory effect of isoflurane, CTZ was still able to suppress single-unit activity just as well as 620-nm light delivered by optical fiber. The challenges of delivering external light into the brain were markedly illustrated by the fact that luciferase-derived light actually outperformed external light of the same peak wavelength (525-nm) given from the same location in the brain. The utilization of brighter and more red-shifted luciferases may help improve the performance of iLMO2 further, since better spectral overlap with NpHR and greater tissue penetration with longer wavelength light could improve both the coupling efficiency and volume of activation, respectively.

Luminopsin activity is contingent on the presence of either externally delivered light or luciferase substrate. Luminopsins therefore have a wide dynamic range of temporal control due to two modes of activation: temporally precise activation (on the order of milliseconds) with external light to more gradual and longer lasting activation (on the order of minutes) with luciferase substrate. Luminopsin activity triggered by either of these modes can also be temporally tuned based on the amount of light or

substrate administered. The mode of activation can therefore be selected at the discretion of the user, where one mode can have substantial advantages or disadvantages over the other depending on the experimental context. For example, the gradual off-kinetics of the chemically activated approach can be leveraged to avoid the risk of rebound excitation that is exhibited by NpHR with conventional photostimulation¹³¹. Combining both modes of activation can create even more intricate duty cycles where external light can potentially add spatially and temporally precise periods of optogenetic manipulation over a network state primed by luciferase substrate. Since the modes of luminopsin activation can be both wide-acting and spatially precise, they could be appropriately utilized together for determining the influence of network activity (altered by luciferase substrate) on the activity of a particular subpopulation of neurons (altered by external light). These types of experiments would be more readily realized *in vivo* compared to other approaches utilizing multiple fibers or different combination of molecules¹³² since only one single molecule is needed.

The chemical genetic approach to light production by luminopsins is reminiscent of DREADD (Designer Receptors Exclusively Activated by Designer Drugs) technology^{133,134}, where a physiologic actuator (G protein in the case of DREADDs, opsin in the case of luminopsins) is specifically activated by an otherwise biologically inert molecule (CNO for DREADDs, CTZ for luminopsins). Although DREADDs have been shown to inhibit neural activity *in vitro* and *in vivo*, they face several unique challenges that are not necessarily shared with the luminopsin approach. First, DREADDs rely on secondary endogenous signaling proteins (e.g. G proteins), which are not necessarily present or active in every target population of neurons. In contrast, everything required to manipulate neural activity is encoded in a single molecule for the luminopsin approach. Second, these signaling proteins are involved in a variety of endogenous cell signaling pathways. The downstream effects of DREADD activation can therefore have very diverse, unintended effects other than altering membrane

conductance compared to opsins. Third, only a single DREADD ligand (CNO) currently exists, which prevents the use of different DREADDs for both excitation and inhibition in the same experimental paradigm. In contrast, a vast number of luciferases (each with their own spectral properties and substrate specificity) currently exist that can be coupled to compatible opsins. For example, CTZ-h specifically generates bioluminescence with Renilla luciferase but not Gaussia luciferase (which can only catalyze native CTZ¹³⁵). Thus, iLMO2 can be potentially employed together with a Gaussia luciferase-based excitatory luminopsin (i.e. LMO1 and LMO2⁹⁴) without the risk of crosstalk. Fourth, CNO undergoes back-metabolism to clozapine in humans which has multiple targets and effects in the brain, which makes it prohibitive for clinical translation¹³⁶. Although CTZ has been widely used for in vivo imaging studies in rodents, no adverse effects of CTZ or its metabolite have been reported. Lastly, luminopsins may not necessarily suffer the same degree of limited temporal control seen with other chemical genetic approaches. With the advent of activity-dependent luciferases (e.g. calcium dependent photoproteins like Aequorin¹³⁷), luminopsin activity may be made responsive to neural activity in a closed-loop fashion and thus be activated only when it is needed. The luminopsin approach is thus unique in the fact that it combines the advantages of optogenetics (i.e. versatile and robust modulation of neural activity) with those of the DREADD approach (i.e. non-invasive chemical activation) into one single molecule capable of enabling responsive control of neural activity.

The luminopsin approach can be readily applied to existing and new optogenetic probes as they are continually developed. With the advent and discovery of new luciferases and opsins (each with their own different kinetics and spectral properties), much freedom and versatility exists in expansion of the luminopsin toolbox.

CHAPTER IV

APPLICATION OF INHIBITORY LUMINOPSINS TO EPILEPSY

The previous chapters have described my efforts in developing and validating inhibitory luminopsins in various *in vitro* and *in vivo* models. The ability of iLMO2 to suppress epileptiform activity *in vitro* (section 3.4) as well as inhibit neural activity in limbic structures that are highly implicated in seizures (i.e. hippocampus, section 3.5) provides a just rationale to test its ability to modulate seizure activity in animal models of epilepsy. Although our laboratory has experience with a spontaneous seizure model in rats (via hippocampal tetanus toxin injection¹³⁸), I have elected to test iLMO2 with acute seizure models to facilitate the ease of substrate administration with the timing of seizures. I have chosen to develop two different epilepsy models: an acute focal seizure model (via intracerebral bicuculline injection) to investigate the ability of iLMO2 for suppressing epileptiform discharges and an acute generalized seizure model (via systemic pentylenetetrazol) to demonstrate the scalability of the luminopsin approach.

4.1 Introduction

Epilepsy is a disorder characterized by seizures that arise spontaneously from excessive synchronous discharges of neurons in the brain. Choosing an appropriate seizure model is a constant struggle for anyone in the field, given that each model has its own advantages and disadvantages¹³⁹. These epilepsy models can be broadly classified into acute (seizures that are triggered) or chronic (seizures that arise spontaneously) epilepsy models. Although chronic models of epilepsy generally have better face validity due to the fact that seizures arise spontaneously in patients with epilepsy, acute seizure models

can provide a convenient platform for testing and screening new anti-epileptic therapies. I have taken the approach of utilizing multiple acute epilepsy models as a means for testing the efficacy of optogenetic inhibition of seizure activity with inhibitory luminopsins.

Acute focal blockade of inhibitory transmission has frequently been used to induce epileptiform discharges in animals. Bicuculline is a specific GABA_A antagonist that has been shown to generate discharges akin to inter-ictal spikes seen in human patients with epilepsy. Because the mechanism of action for seizure generation is well known (i.e. impaired network inhibition), bicuculline has been a useful model for testing various anti-epileptic drugs that aim to increase inhibitory drive¹⁴⁰⁻¹⁴². Optogenetic inhibition with halorhodopsin has also been utilized to attenuate seizure activity generated from focal injection of bicuculline *in vivo*²¹, which provides a good rationale for testing the ability of inhibitory luminopsin (which is also halorhodopsin based) to suppress seizure activity in this same context.

Pentylenetetrazol (PTZ) is another GABAergic transmission blocker that has been utilized for generating generalized seizures. It has been particularly useful for screening anti-convulsant compounds because it has been shown to be sensitive to molecules with varied mechanisms of action¹⁴³. Although systemic administration of PTZ affects multiple regions in the brain, its excitatory effects are especially strong in the structures found in the limbic system (e.g. hippocampus, anterior thalamus). Indeed, electrical stimulation of certain thalamic nuclei (anterior nucleus, thalamic reticular nucleus) has been shown to be effective for suppressing PTZ-induced seizures^{144,145}. The luminopsin approach to optogenetic inhibition is also particularly well-suited for intervening with PTZ-induced seizures given the fact that multiple brain structures are involved in an acute setting. Trying to target multiple structures with conventional optical or electrical means would not only be technically difficult, but also impractical for clinical translation.

I have chosen to target the granule cells of the dentate gyrus and the anterior nucleus of the thalamus with iLMO2 for testing its effectiveness in suppressing PTZ-

induced seizures. The granule cells of the dentate gyrus appear to be a suitable target for optogenetic intervention because this area is highly active during PTZ-induced seizures as determined by c-fos immunohistochemistry¹⁴⁶ and fMRI¹⁴⁷. Furthermore, optogenetic inhibition of the dentate granule cells has been shown to prevent propagation of seizure activity throughout the hippocampus (i.e. the ‘dentate gate’ hypothesis of epilepsy)⁵⁵. The anterior nucleus of the thalamus was targeted because it is the first structure activated after administration of PTZ¹⁴⁷ and has also been shown to increase seizure threshold with high frequency electrical stimulation¹⁴⁵.

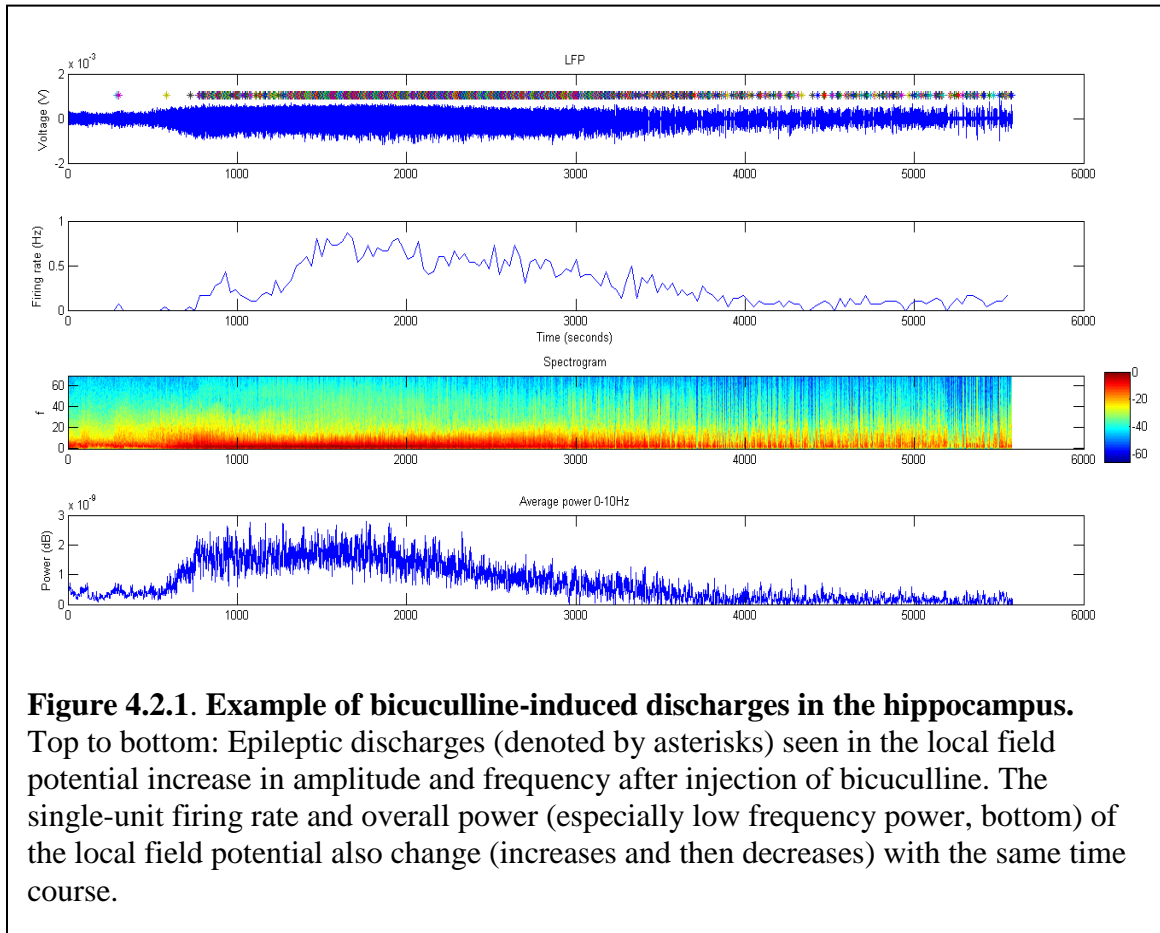
4.2 Optogenetic inhibition of acute focal epileptic discharges with iLMO2

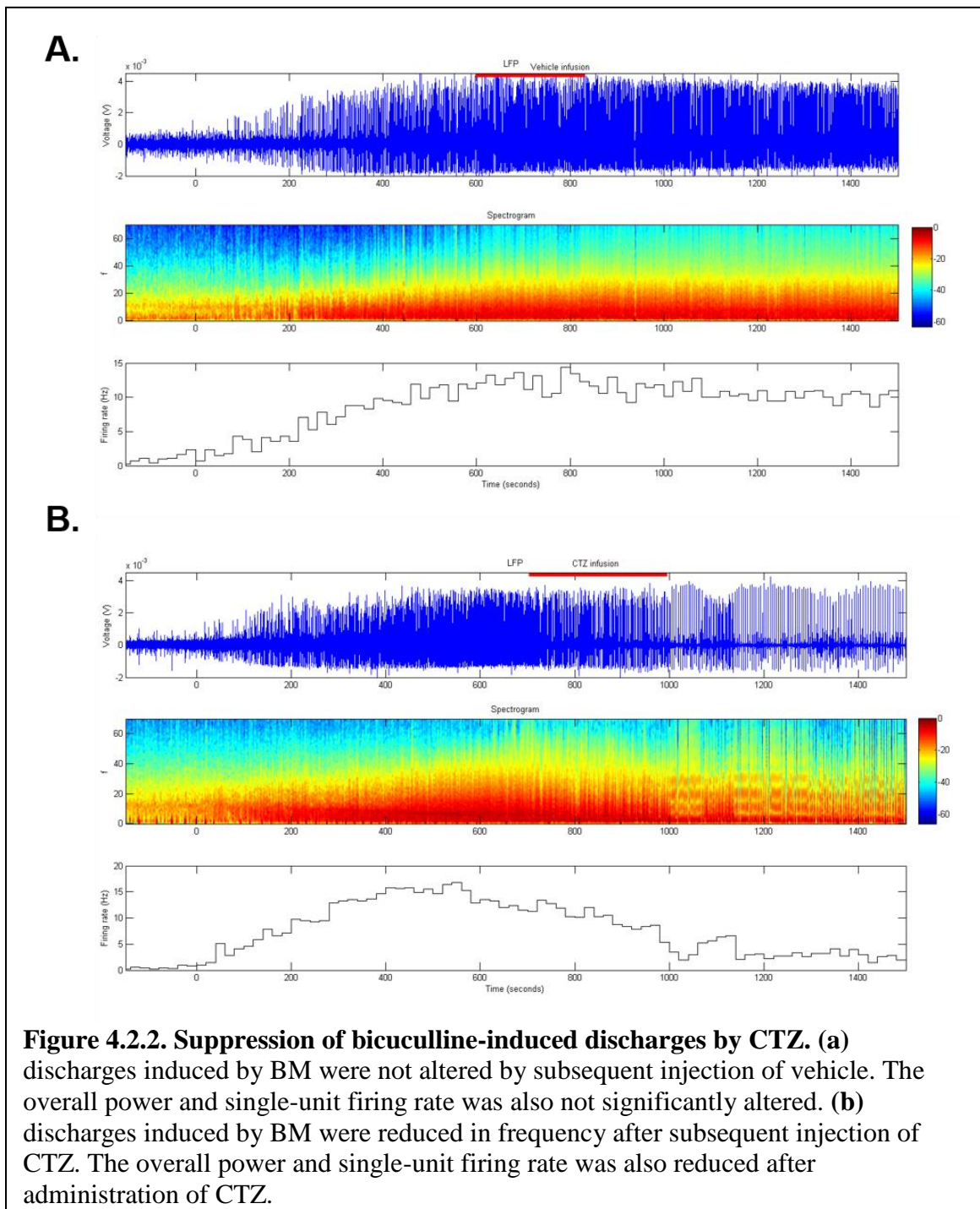
4.2.1 Results

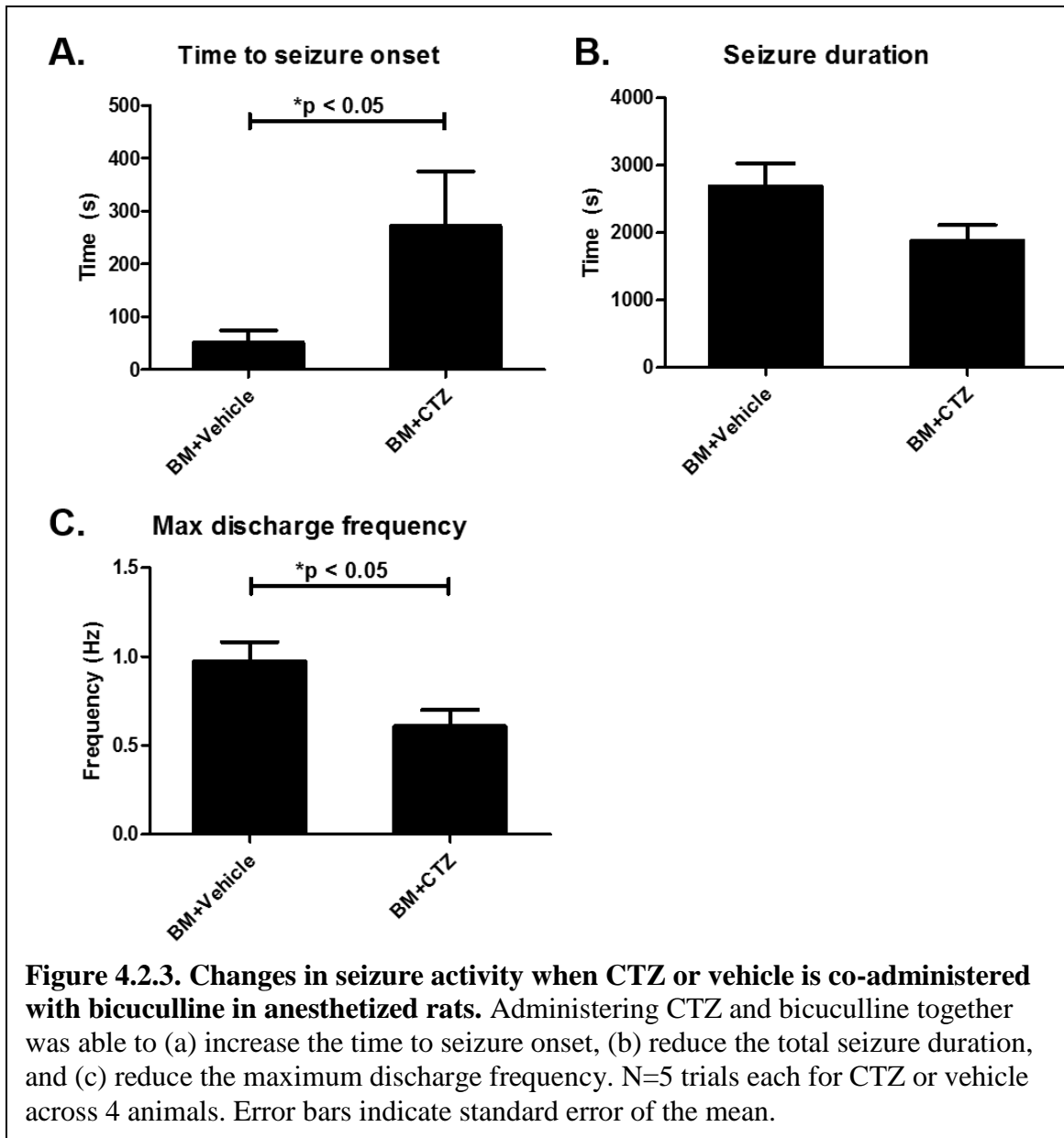
To investigate the ability of iLMO2 to modulate seizure activity, focal epileptic discharges were induced in the hippocampus with intracerebral injections of bicuculline methiodide (BM) in anesthetized rats expressing iLMO2 in the dorsal hippocampus. iLMO2 was first expressed in the dorsal hippocampus by stereotaxic injection of AAV and then chronically implanted with a cannula-electrode as described previously⁷³. The chronically implanted cannula-electrode allowed for multiple injection trials to be conducted in the same animal. 1 µl injections of 20 mM BM typically induced discharges within 5 minutes that increased in amplitude and frequency until plateauing around 15 minutes and returning back to baseline after about 45 minutes (**Figure 4.2.1**).

To investigate the ability of iLMO2 in preventing BM-induced discharges, CTZ was administered together with bicuculline. CTZ was able to suppress the BM-induced discharges when it was acutely administered during the development of the discharges (**Figure 4.2.2**). Compared to vehicle, CTZ was able to significantly increase the time to seizure onset, decrease the seizure duration, and significantly ($p < 0.05$; two-tailed

student's t-test; $n = 5$ trials each) reduce the maximum discharge frequency (**Figure 4.2.3**).







4.2.2 Methods

Stereotaxic viral injections. Two month old male Sprague-Dawley animals (200-250 g) were anesthetized with 1.5-4% inhaled isoflurane and a craniectomy was made 3.3 mm posterior and 3.2 mm lateral to bregma. 1.8 μ l of AAV2/9-CAMKII α -iLMO2 was stereotaxically injected at a depth of 3.1 mm ventral to pia targeting the dorsal hippocampus. Virus was injected through a glass-pulled pipette using a Nanoject injector

(Drummond Scientific) at a rate of 275 nl/min. After viral injection was completed, the scalp was stapled closed and animals were allowed to recover for up to two weeks.

In vivo electrophysiology. Animals were implanted with a cannula-electrode two weeks after the viral injection. We have found that two weeks is sufficient for expression of optogenetic vectors delivered by AAV. A guide cannula (Plastics One) was glued to a 16-channel microwire array (Tucker Davis Technologies) so that a 0.39 NA, 200 μm core diameter bare fiber optic (Thorlabs) inside an injection cannula could be inserted into the guide cannula and positioned 1-2 mm away from the electrode tips. Four skull screws and one cerebellar reference screw were implanted into each animal. A craniotomy was then made over the dorsal hippocampus (array angled 50° from midline and centered 3.5 mm posterior and 2.9 mm lateral to bregma) and the cannula-electrode was manually driven into the brain while continuously recording to ensure ideal placement of electrodes. The correct stop depth was determined by identifying responsive single-units after repeated optical stimulation (10s continuous pulses) with green (625-nm, 2.8 mW from fiber tip) and orange (520-nm, 1.3 mW from fiber tip) light from externally coupled LEDs (Plexon). Electrophysiologic recordings were sampled at 25 kHz using our custom built NeuroRighter data acquisition system¹²². Local field potentials were bandpass filtered (1-500 Hz) from the raw signal and analyzed offline using custom Matlab scripts and the Chronux toolbox¹²³. Single-units were detected from the bandpass filtered (500-5 kHz) signal and sorted offline using superparamagnetic clustering (Wave Clus) scripts developed by Quiroga et al¹²⁴. The entire cannula-electrode was then sealed in place with dental acrylic (Lang Dental), the optical fiber was retracted from the guide cannula and replaced with a dummy cannula, and the animal was allowed to recover several days before further experimentation.

Intracerebral injections. After the animals recovered from surgery, their electrophysiological responses to BM with and without CTZ was investigated. The chronically implanted cannula-electrode allowed for multiple trials to be conducted for each animal, where each trial consisted of an intracerebral injection of CTZ and vehicle (in alternating order) on one particular day. The animals were first lightly anesthetized by 0.5-1.5% inhaled isoflurane. An injection cannula connected to a Hamilton syringe containing a 1 μ l mixture of either 60 μ M CTZ and 2 mM BM or 2 mM BM diluted in vehicle (20 mM β -cyclodextrin in PBS). Each animal received either the CTZ or vehicle mixture in a random order. A baseline recording of at least 10 minutes was recorded before CTZ or vehicle was injected (over a period of ~5 minutes) into the brain parenchyma. After injection was completed, the animal was recorded under constant levels of anesthesia for up to 1 hour.

Histology. After all experiments were completed, animals were sacrificed by intraperitoneal injection of Euthazol (Virbac). Animals were then transcardially perfused with 4% paraformaldehyde (PF). The heads of animals implanted with the cannula-electrodes were decapitated and kept in PF at 4°C overnight to allow for visualization of the electrode tracks. Otherwise, the brains were dissected out and allowed to fix in PF for 1 hr. After fixation, the brains were cryoprotected in 30% sucrose before sectioning on the microtome. 50 μ M thickness sections were collected and mounted onto glass slides for imaging on an upright fluorescence microscope using NIS-elements acquisition software (Nikon).

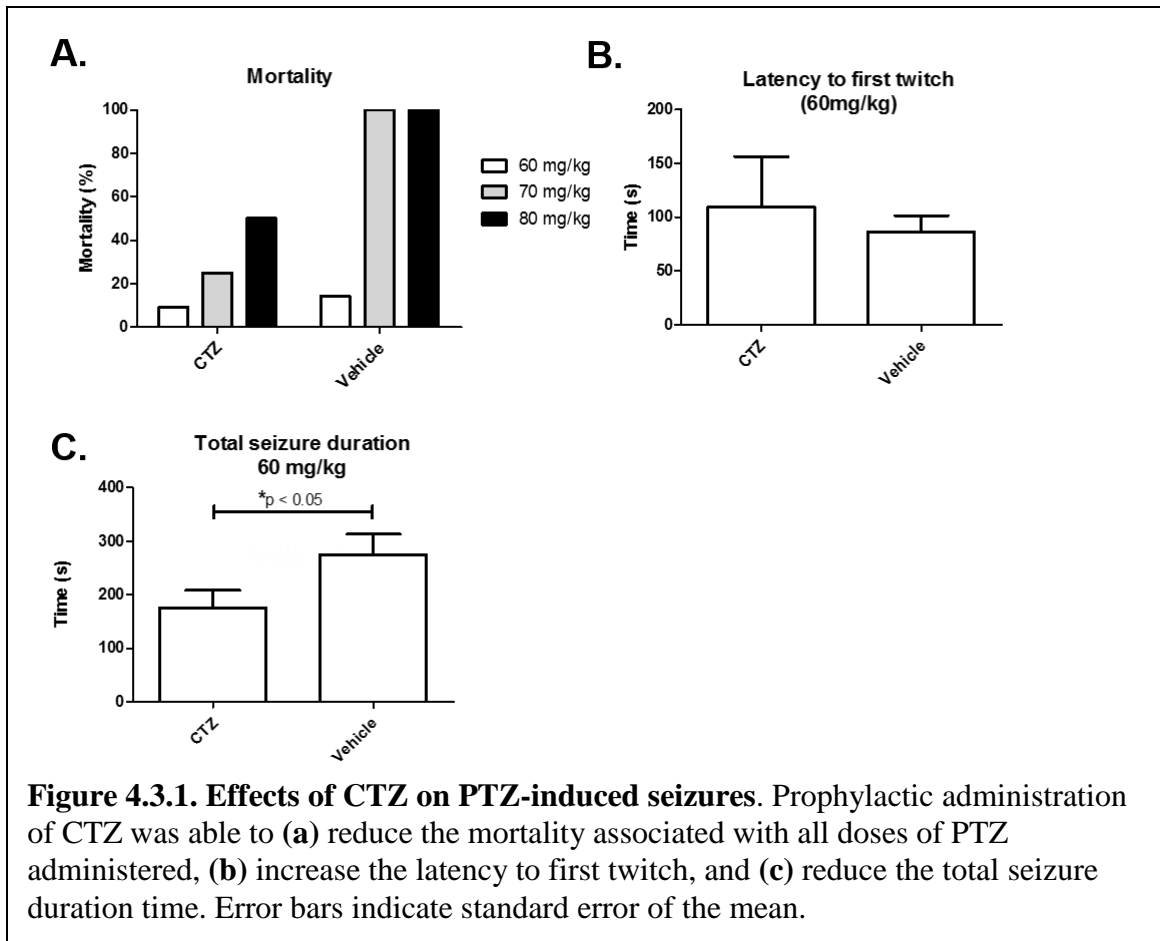
4.3 Optogenetic inhibition of acute generalized seizures with iLMO2

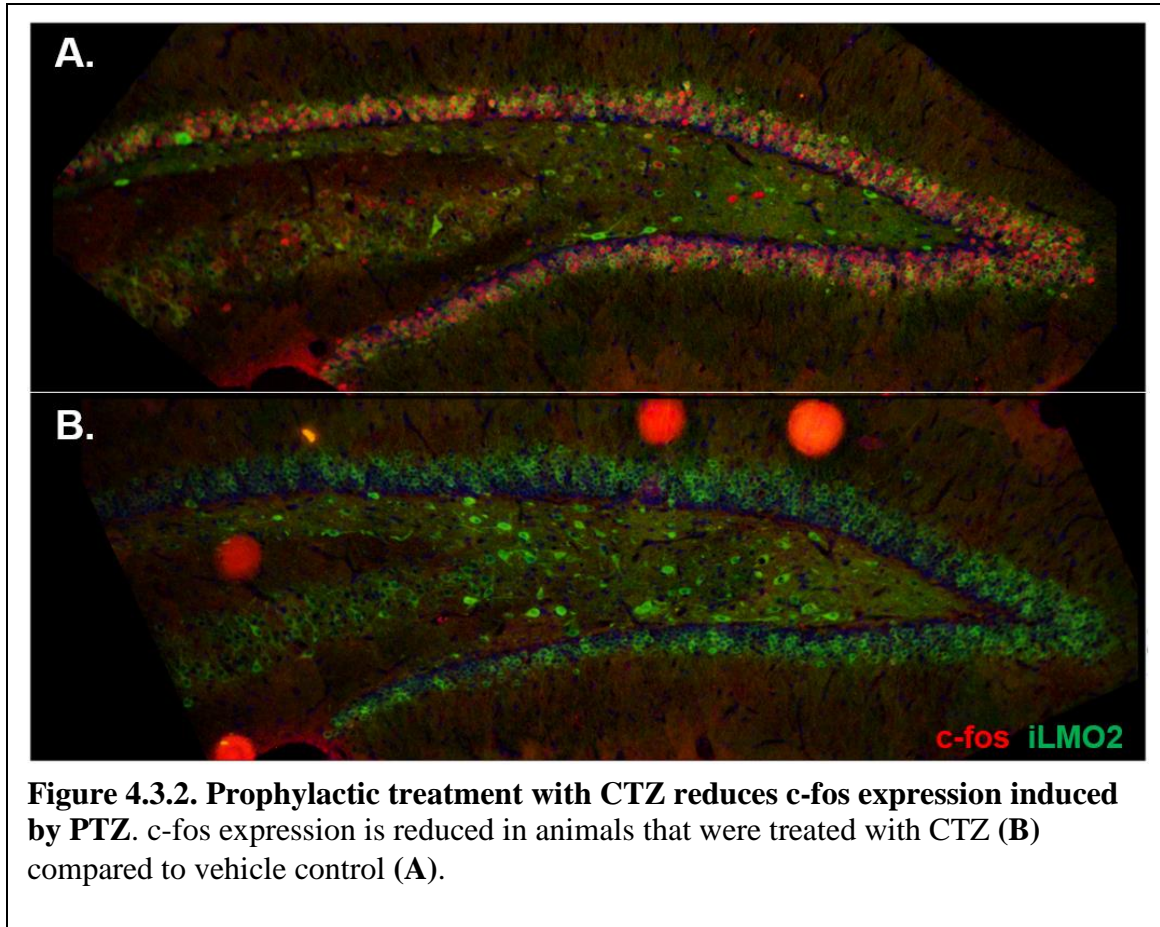
4.3.1 Results

Targeting granule cells of the dentate gyrus

The ability of iLMO2 to attenuate generalized seizures was tested in rats expressing iLMO2 bilaterally in the dentate gyrus of the hippocampus. CTZ was administered via tail vein injection prior to inducing generalized seizures by systemic intraperitoneal injection of pentylenetetrazol (PTZ). At the doses tested, all control animals experienced tonic/clonic seizures (Racine level 5), while some progressed to status epilepticus and died. Prophylactic administration of CTZ was able to reduce the mortality associated with PTZ at all doses given (**Figure 4.3.1a**). At the 60mg/kg dose, CTZ administration was able to increase the latency to seizure onset and significantly ($p < 0.05$, one-way paired t-test; $n = 10$ for each group) reduce the total seizure duration compared to vehicle control (**Figure 4.3.1b, c**).

All animals were sacrificed 40 minutes after the seizure onset for immunohistochemical analysis of c-fos expression. C-fos expression was reduced in animals that received CTZ compared to those who received vehicle (**Figure 4.3.2**).





4.3.2 Methods

Stereotaxic viral injections. Two month old male Sprague-Dawley animals (200-250 g) were anesthetized with 1.5-4% inhaled isoflurane and bilateral craniectomies were made 4.68 mm posterior and 2.9 mm lateral to bregma. 1.8 μ l of AAV2/9-CAMKII α -iLMO2 was stereotaxically injected at a depth of 3.2 mm ventral to pia targeting the dentate gyrus. Virus was injected through a glass-pulled pipette using a Nanoject injector (Drummond Scientific) at a rate of 275 nl/min. After viral injection was completed, the scalp was stapled closed and animals were allowed to recover for up to two weeks.

Seizure induction. After animals had recovered from the viral injection surgery, they were habituated in a tail vein restrainer (Braintree LLC) and handled every day until the day of injection. On the day of injection, the lateral tail vein was visualized by soaking the tail in warm water. Cage-matched litter mates were randomly selected to either receive 200 µl of CTZ-e (1 mg total) or 200 µl of vehicle (Inject-a-lume solvent, Prolume) by tail vein injection. Animals were immediately returned to their home cage after injection, where they subsequently received an intraperitoneal injection of PTZ (60, 70, or 80 mg/kg). Animals were then video recorded for up to 40 minutes, where they were immediately sacrificed and perfused for immunohistochemical analysis.

Histology. Animals were sacrificed by intraperitoneal injection of Euthazol (Virbac) following induction by Isoflurane. Animals were then transcardially perfused with 4% paraformaldehyde (PF). The brains were dissected out and allowed to fix in PF for 1 hr. After fixation, the brains were cryoprotected in 30% sucrose before sectioning on the microtome. 10 µM thickness sections were collected onto gelatin coated glass slides for immunohistochemistry. Sections were stained with primary c-fos antibody (Santa Cruz, 1:100 dilution) and fluorescent secondary antibody (Alexa 594, 1:1000) before imaging on an upright fluorescence microscope using NIS-elements acquisition software (Nikon).

Behavior analysis. Video recordings of animals were viewed by 2 blinded viewers where annotations about all changes in behavior were made using a modified Racine scale.

4.4 Discussion

iLMO2 was previously shown to inhibit neural activity in the hippocampus and in multiple structures of the basal ganglia⁷³. In this study, we aimed to see whether this inhibitory effect could be translated to pathological states of seizure activity. Focal administration of bicuculline was able to induce epileptic discharges in the hippocampus

of rats expressing iLMO2 in the dorsal hippocampus. These discharges could be subsequently suppressed by focal injection of CTZ and also attenuated in their onset and frequency when CTZ was delivered together with bicuculline. Systemic administration of PTZ in animals expressing iLMO2 bilaterally in the granule cells of the dentate gyrus was able to induce generalized seizures that were reduced in severity in animals that received CTZ prophylactically.

These results suggest that iLMO2 can be utilized to focally suppress seizure activity *in vivo*, which agrees with previously published results using optogenetic inhibition to inhibit bicuculline-induced discharges²¹. These combined results therefore signify that optogenetic inhibition of principal cells in the hippocampus can attenuate epileptic activity that is produced from compromised inhibitory drive. PTZ also compromises inhibitory drive through GABA receptor antagonism, and the fact that focal inhibition of granule cells was able to suppress these generalized seizures suggests that optogenetic inhibition with iLMO2 was able to prevent/delay the spread of synchronous activity throughout the limbic structures that are highly involved in this model. Indeed, optogenetic inactivation of the granule cells of the dentate gyrus has been previously shown to prevent the spread of activity throughout the hippocampus and reduce the spontaneous seizure frequency in mice⁵⁵. Prophylactic inhibition of the granule cells was therefore able to raise the threshold for transmitting epileptic activity throughout the hippocampus, providing additional evidence for the dentate gate hypothesis.

There are several unique advantages to the luminopsin approach to suppressing seizure activity compared to conventional photostimulation used in previously published studies. First, optogenetic inhibition was achieved in a hardware-independent fashion via peripheral administration of CTZ. This is of practical and translational importance especially when animals are undergoing tonic/clonic seizures, which can lead to damage or destruction of implantable hardware. Second, optogenetic inhibition could be achieved in a readily scalable manner. Although the expression of iLMO2 in the brain was limited

by focal injections of virus, multiple injections could be utilized to express iLMO2 bilaterally in the targets of interest. This approach could easily be scaled up to include multiple structures (e.g. thalamus) with more injections and other methods to improve viral spread (e.g. convection enhanced delivery, viral vector serotype, virus injection parameters, etc.). Third, this approach did not lead to any rebound bursting that has been reported with conventional approaches of optogenetic inhibition with Halorhodopsin. This is most likely due to the fact that the degree of optogenetic inhibition is slowly tapered off as CTZ substrate was consumed or washed away, allowing time for the cell to return to resting membrane potential and counter any hyperpolarization current.

Although focal injection of bicuculline and systemic administration of PTZ do not necessarily reflect epileptic activity in the human, we have demonstrated that iLMO activity can suppress synchronous discharges in a readily scalable and hardware-independent manner. These results therefore provide motivation to test this approach in other models of epilepsy that may have more construct validity to human temporal lobe epilepsy (e.g. tetanus toxin, kainic acid) and other types of both focal and generalized epilepsy.

CHAPTER V

RESPONSIVE LUMINOPSINS

In the previous two chapters, I have described the development and application of inhibitory luminopsins to epilepsy. Although manual activation of iLMO2 by administration of CTZ substrate was able to suppress and attenuate seizure activity, we aim to make this approach more effective by tying iLMO activation to seizure activity to achieve autonomous closed-loop suppression of seizures. In this chapter, I will describe my efforts in utilizing calcium-dependent luciferases for reporting neural activity and driving optogenetic inhibition. We call these new probes responsive luminopsins (rLMOs) since they are ostensibly activity-dependent.

5.1 Introduction

Neuromodulation that is capable of being delivered in response to a particular signal is a high-level goal that would bring both therapeutic advantages as well as practical advantages in terms of device development. Not only would these ‘closed-loop’ approaches make these devices more efficient in terms of power consumption (a practical consideration given that future implantable devices will require battery packs), but they would also reduce potential side effects by minimizing off-target stimulation. A good example of such a device that has been used for epilepsy treatment is the Responsive Neurostimulation System (RNS[®]) developed by NeuroPace (Mountain View, CA), which is capable of detecting the onset of seizures and automatically delivering therapeutic stimulation to interrupt their progression. Several groups have taken a similar approach to delivering optogenetic stimulation for halting seizure activity^{51,54,55,148}. While it may be possible that closed-loop optogenetic stimulators could eventually be packaged into an

implantable device like the RNS system, optogenetic devices will face unique challenges of miniaturizing light sources and dealing with higher power demands.

Optical reporters of neural activity have undergone significant development over the last decade and have proven useful to visualize activity dynamics within the context of neural circuitry¹⁴⁹. Although genetically encoded calcium indicators (GECIs) have been generally less superior than dyes in terms of sensitivity and signal strength in the past, significant development in recent years has made the GECIs quite comparable, if not better^{150–153}. Moreover, genetically encoded bioluminescent calcium indicators also exist and have been utilized to image neural activity *in vitro*^{78,81,154,155} and *in vivo*¹³⁷. It therefore seems appropriate to utilize these calcium-dependent luciferases to drive optogenetic inhibition in response to neural activity.

5.2 Development and characterization

5.2.1 Results

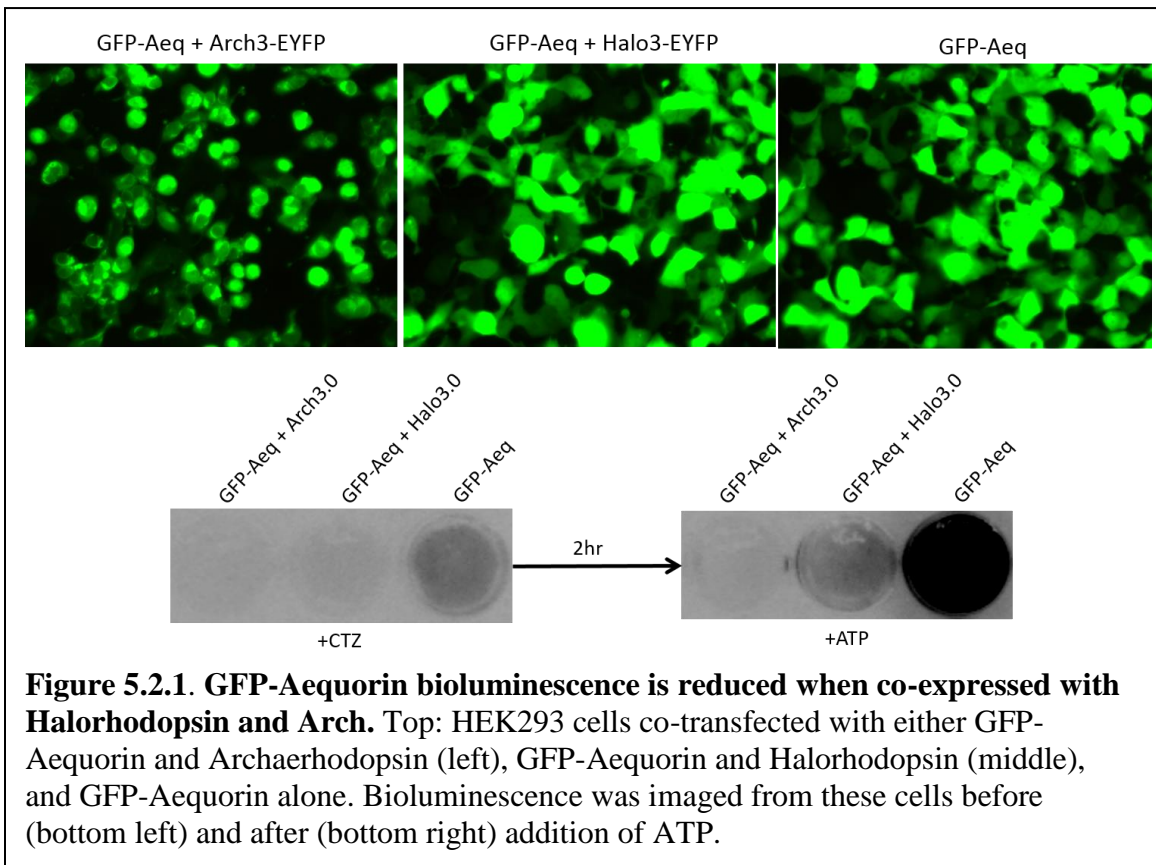
I have cloned several calcium-dependent luciferases to use as potential sensors of neural activity and have tested them with various opsins as summarized in **Table 5.1**. I have measured calcium-dependent bioluminescence by expressing the calcium-dependent luciferases in HEK293 cells by transfection and stimulating them with ATP. Aequorin bioluminescence from transfected HEK293 cells was increased after stimulation with ATP (**Figure 5.2.1**). The bioluminescence intensity was also dependent on the CTZ concentration (**Figure 5.2.2**) and ATP concentration (**Figure 5.2.3**) used to stimulate the cells. However, when Aequorin (either with GFP or Tdt as a fluorescent tag) was co-expressed with opsin (either Halorhodopsin or Arch) bioluminescence was significantly reduced (**Figure 5.2.1** and **Table 5.1**). The presence of aggregates seen by fluorescence microscopy suggests that there is protein misfolding or aggregation occurring when

Aequorin is co-expressed with opsin. I therefore concluded that Aequorin could not be used together with inhibitory opsins for creation of a responsive luminopsin.

Next, I turned to calcium-dependent Nanolanterns as a potential candidate to use with inhibitory opsins. These calcium-dependent Nanolanterns are split *Renilla* luciferases that are linked by M13 and CaM calcium binding motifs. Thus when calcium is present, the split luciferase comes together to become functional and is able to oxidize CTZ to produce bioluminescence. These calcium-dependent Nanolanterns were fused to Halorhodopsin to create several rLMOs with different binding affinities to calcium (rLMO-11, rLMO-300, and rLMO-600 have K_D 's of 11, 300, and 600 nM, respectively). When HEK293 cells expressing these rLMOs were stimulated with ATP, bioluminescence signal increased (**Figure 5.2.4**). These constructs were subsequently packaged into a lentiviral vector and used to transduce dissociated cortical neurons, which increased their bioluminescence by approximately 2-fold after stimulation with 10mM KCl (**Figure 5.2.5**).

Luciferase	Opsin/FP	Luminescence?	Fluorescence
GFP-Aequorin		Yes	Green
GFP-Aequorin	Arch3.0-EYFP	No	Green
GFP-Aequorin	eNphR3.0-EYFP	Maybe (Decreased)	Green
tdTA		Yes	Red
tdTA	eNphR3.0-EYFP	No	Green aggregates + Red
tdTA	EYFP	Yes	Red + Green
eNphR3.0-tdTA		No	Red
tdTA	Arch3.0-EYFP (co-tx or sequential)	No	Green + Red aggregates
Arch3.0-linker-tdTA		No	Red aggregates
Arch3.0-linker2-tdTA		No?	Red

Table 5.1. Summary of results when various calcium-dependent luciferases were co-expressed (either by fusion or co-transfection) with various opsins.



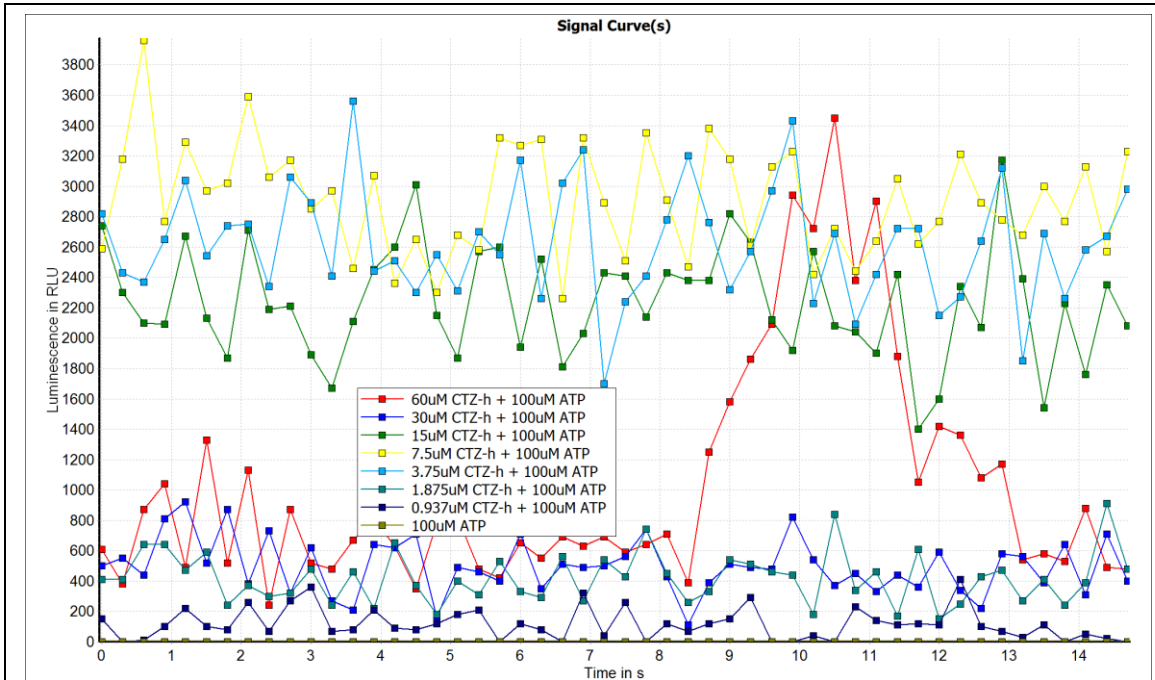


Figure 5.2.2. Dose-dependent bioluminescence over time. Bioluminescence intensity from HEK293 cells expressing Aequorin (tdTA) emit bioluminescence in a dose-dependent fashion. The highest bioluminescence signal was seen at a concentration of 7.5 μ M.

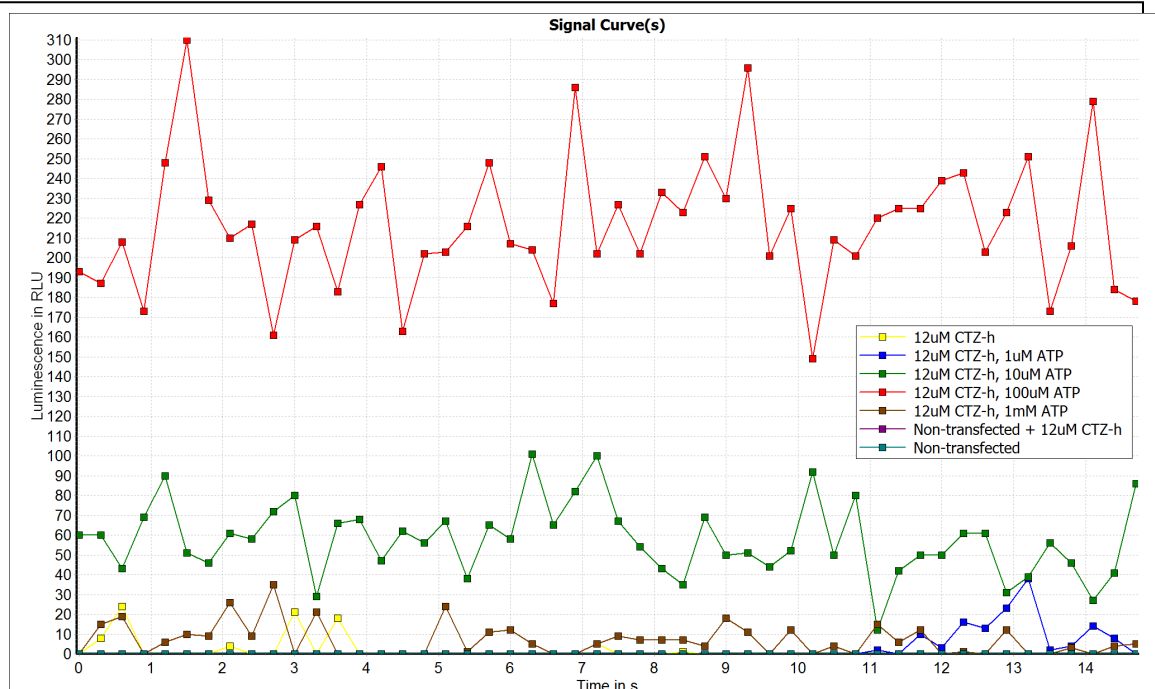
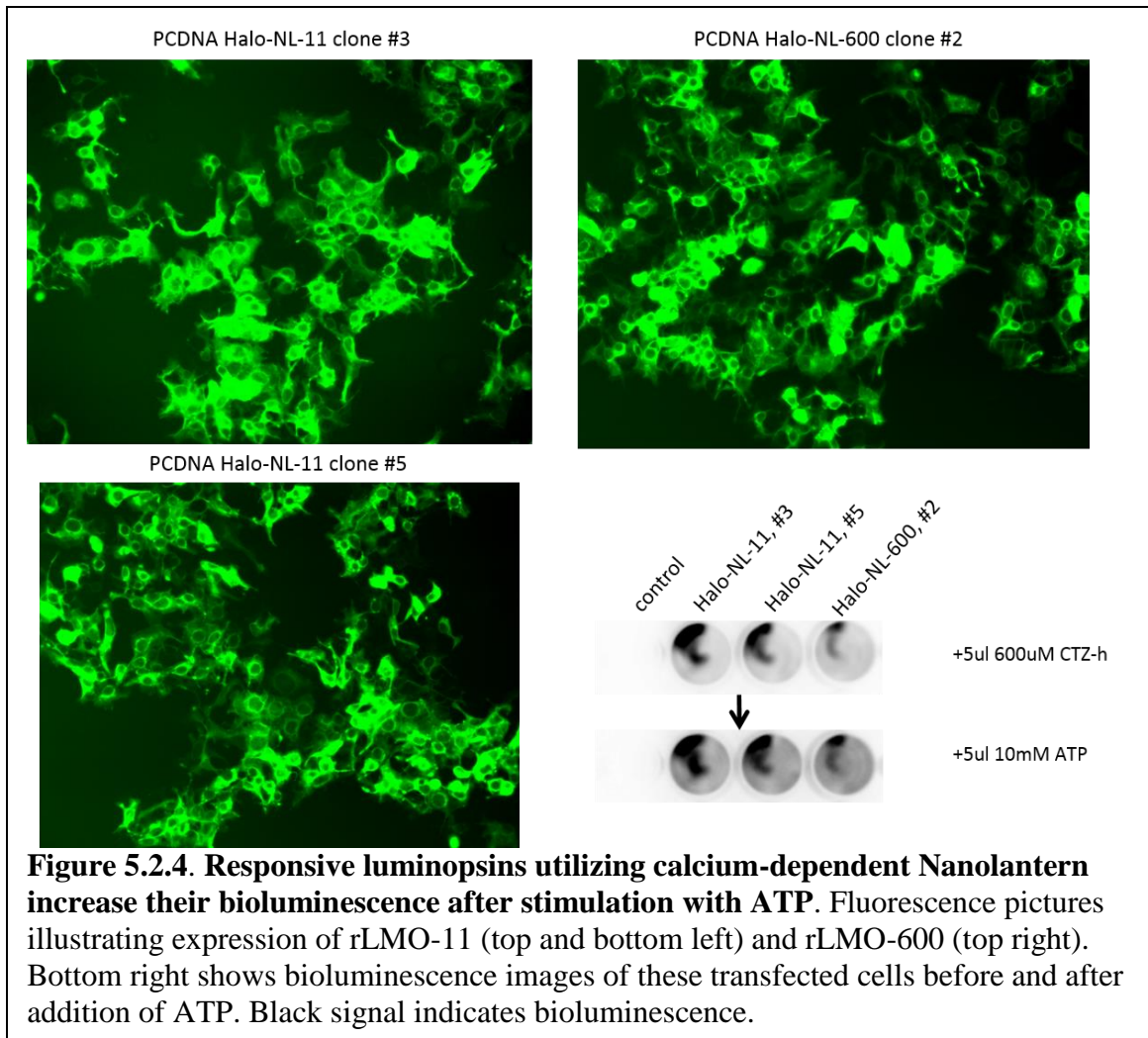
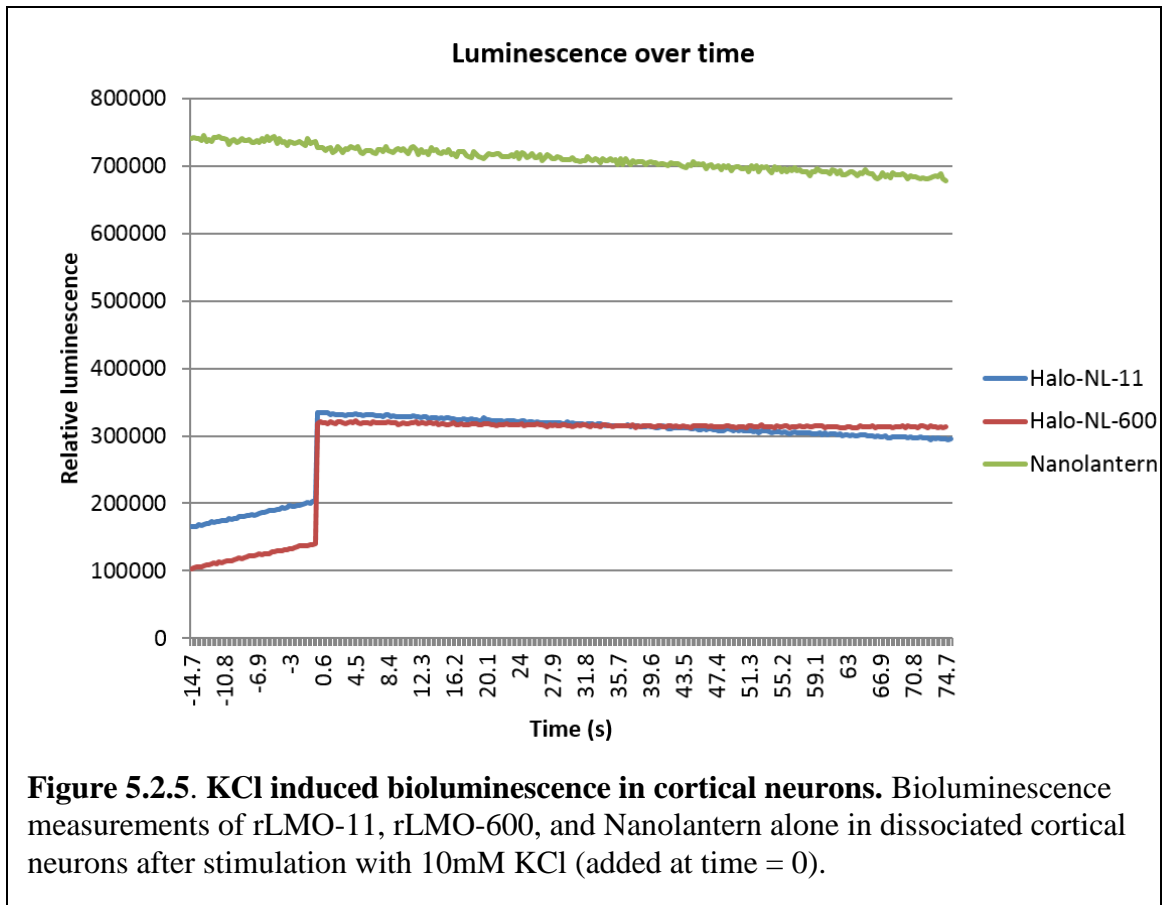


Figure 5.2.3. ATP-dependent bioluminescence over time. Bioluminescence intensity from HEK293 cells expressing Aequorin (tdTA) emit bioluminescence in a dose-dependent fashion. 100 μ M ATP produced the highest bioluminescence intensity.





5.2.2 Methods

Plate imager and reader assays

Luciferase functionality was quickly assessed with a Fuji LAS-3000 gel imager (a light-tight box equipped with a cooled CCD camera). Transfected or transduced cells were placed in the imager and coelenterazine (CTZ-h for Renilla, CTZ-native for Gaussia) was added to each well to reach a final concentration of 12 μ M. Luminescence images (20s exposure times for each image) were then taken and integrated for up to 2 minutes.

Luminescence signals were further quantified in a luminescence plate reader (FLUOstar Optima, BMG Labtech). Cells were seeded and transfected in white 96-well clear-bottom luminescence plates (Corning) and transgene expression was confirmed by fluorescence microscopy the next day. Coelenterazine was then injected into the wells using a

multichannel pipette and the plate was immediately placed into the plate reader for measurement of luminescence. Each sample was measured in triplicates over the specified amount of time.

CHAPTER VI

CONCLUSION AND FUTURE DIRECTIONS

6.1 Conclusion

In this dissertation, I have pursued a simple question that ultimately started this incredible journey: “Can bioluminescence be utilized to drive light-sensitive opsins?” This question was motivated from a purely translational viewpoint, yet required very basic and fundamental science to approach the problem.

To answer this question, I first had to be able to measure bioluminescence. Our laboratory had never worked with luciferase enzymes before, so a lot of effort was spent on getting the right equipment and setup for detecting and imaging bioluminescence *in vitro* and *in vivo* (Chapter 2). The ability to measure bioluminescence was critical for me to be able to quantify and characterize these biological light sources so that I could pair them with the appropriate opsins. Achieving the ability to image bioluminescence from single cells was also critical to be able to concurrently measure bioluminescence along with intracellular recordings; these concurrent measurements allowed me to attribute the electrophysiological changes I was seeing to luciferase activity.

The next step was to develop and characterize the luminopsin constructs. A lot of time was spent cloning these various constructs (summarized in Appendix E), but the biggest challenge was learning the techniques to be able to characterize these constructs (e.g. whole cell patch clamp recording, *in vitro* extracellular recording, *in vivo* recordings). Nevertheless, these constructs were characterized in a step-wise fashion from single-cell recordings to animal behavior (Chapter 3). Although several iterations of luminopsin had to be developed, iLMO2 performed the best and was shown to be able to

suppress neural activity in response to both external light illumination and substrate-induced bioluminescence *in vitro* and *in vivo*.

With a validated tool in hand, the next step was to apply it to animal models of epilepsy. Although our laboratory had an established model of chronic epilepsy (tetanus toxin model), I believed that it was not the best platform for testing the efficacy of inhibitory luminopsins due to the practical challenges of substrate delivery. I therefore developed two acute models of epilepsy using focal injections of bicuculline and systemic administration of PTZ. Although these acute models may not have the same construct validity with human epilepsy, they still allowed me to test the efficacy of iLMOs on affecting seizure activity in a predictable and controllable fashion. It was shown that iLMO2 was able to attenuate seizure activity induced by bicuculline, which demonstrates its potential as a neuromodulatory therapy and corroborates previous studies utilizing conventional optogenetic approaches to halt epileptic discharges in the hippocampus induced by bicuculline. The therapeutic potential of iLMO2 was further supported when it was expressed bilaterally in the granule cells of the dentate gyrus and shown to reduce the seizure burden from acute administration of PTZ. Given that systemic PTZ administration is a model for generalized seizures and affects multiple structures in the brain, this result demonstrated the unique scalability of the luminopsin approach and how it can be applied to multiple areas in the brain.

The overall goal of this project was to not only utilize bioluminescence as an alternative light source for optogenetic applications, but to also tie this bioluminescence to neural activity in an activity-dependent manner. In the beginning of my thesis work, I had focused on the development of inhibitory luminopsins as a proof-of-concept that bioluminescence can indeed be utilized to activate light-sensitive opsins. Chapter 5 described my later efforts in utilizing calcium-dependent luciferases for activity-dependent activation of light-sensitive opsins. I have been able to show that these activity-dependent luminopsins are able to respond to neural activity, but not yet been

able to demonstrate that the resulting activity-dependent bioluminescence is sufficient to drive optogenetic inhibition.

6.2 Future directions

Although iLMO2 has been shown to be effective in suppressing both normal and pathological neural activity, much more can be done to improve the robustness of its effects. For example, the coupling efficiency between the luciferase and opsin can be improved with the use of either brighter luciferases or more sensitive opsins. I have begun preliminary testing with recently described anion channelrhodopsins (e.g. iC1C2¹⁵⁶, SwiChR¹⁵⁶, GtACR1¹⁵⁷), which have unique advantages over halorhodopsin. First, much larger photocurrents can be generated with these channels (on the scale of nano-amps) since they are more efficient at transporting ions across the membrane than pumps. Second, these anion channelrhodopsins offer the possibility of prolonged optogenetic inhibition with step function-like kinetics. Indeed, the Deisseroth lab has taken the same structure-guided approach to decreasing the deactivation kinetics of their light-activated chloride channel to create SwiChR. Utilizing an inhibitory channel with prolonged deactivation kinetics could be potentially useful *in vivo* where the frequency of substrate administration could therefore be minimized.

Much work still needs to be done regarding luciferase substrate delivery *in vivo*. We are currently limited to only acute delivery of substrate either via intravenous injections or intraperitoneal injections. Chronic delivery of substrate could potentially be achieved with implantable osmotic pumps or miniaturized drug delivery devices, but this approach needs to be explored in more detail (especially given the strict storage conditions for CTZ). Furthermore, the solubility of CTZ needs to be improved in order to achieve adequate concentrations *in vivo* without fear of utilizing too much solvent, which can be toxic in high doses. The commercially available solvents we use to solubilize CTZ for *in vivo* use are not ideal because they contain proprietary ingredients that could

potentially confound our results. I have therefore taken the approach of making my own solvent by complexing CTZ with beta-cyclodextrin, but more scalable approaches still need to be developed. With better substrate delivery methods, we could then more readily test inhibitory luminopsins in chronic models of epilepsy.

There is still more work to be done on the activity-dependent luminopsin front. Although progress has been made with calcium-dependent luciferases for reporting neural activity, there are significant challenges that still need to be addressed. First, the brightness of these calcium-dependent luciferases is much lower than the traditional luciferases. This is due to the fact that these probes usually rely on a calcium-dependent ‘gain-of-function’ step in order to produce bioluminescence. For example, the calcium-dependent Nanolantern luciferases are essentially split *Renilla* luciferases that become functional again only when calcium binds. This functionality is never truly the same as the unsplit luciferase since these conformational changes do not occur as cleanly as intended *in situ*. Thus brighter and more responsive probes need to be developed to achieve an adequate dynamic range to report neural activity. Second, the sensitivity of these luciferases to calcium needs to be made more robust. Calcium levels can fluctuate widely in the cell and these sensors therefore need to be appropriately calibrated to detect these changes. Other biological markers of activity-dependence (such as chloride, potassium, transcriptional and translational events, etc.) also need to be explored.

APPENDIX A

ILMO1 DEVELOPMENT AND CHARACTERIZATION

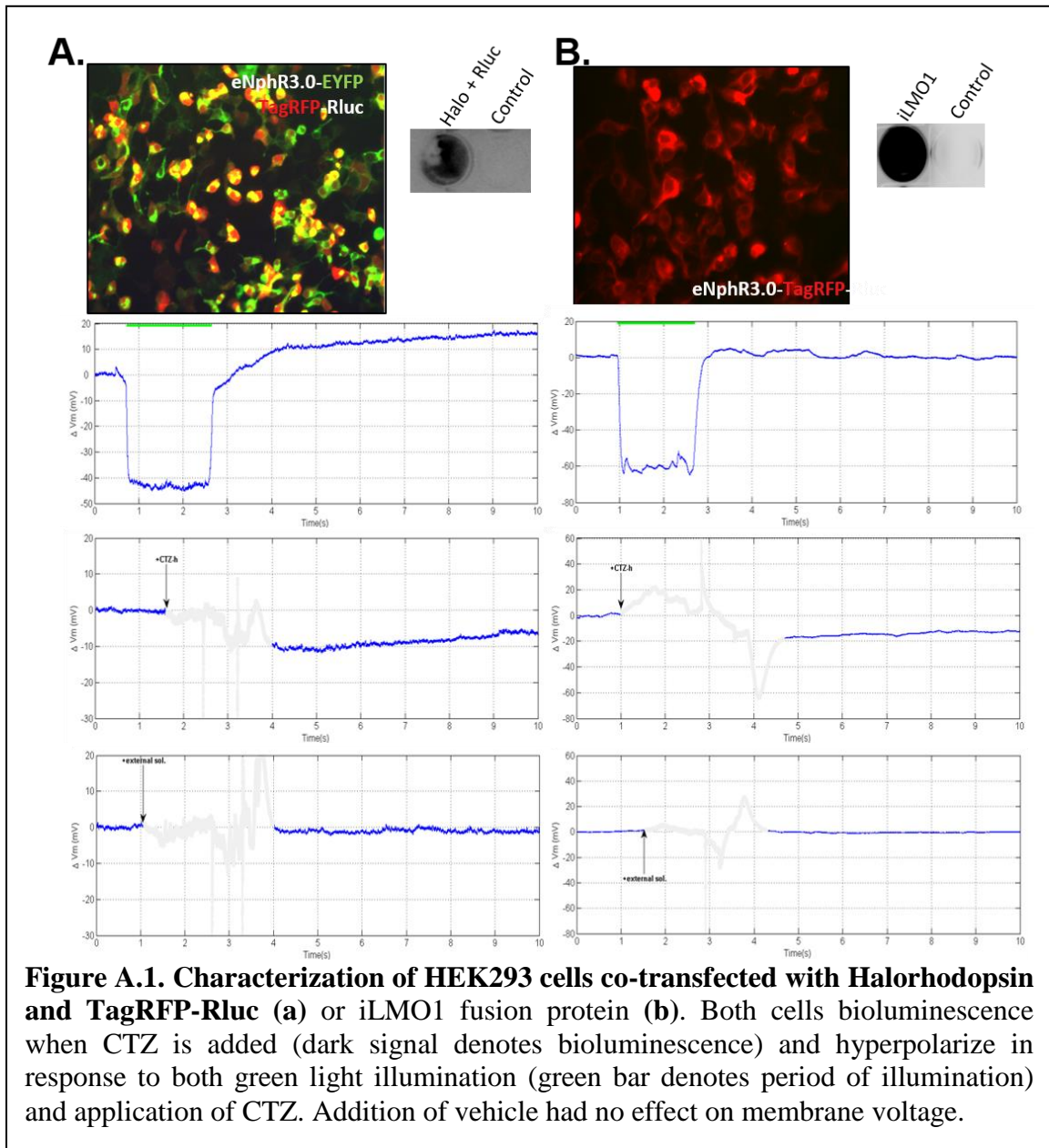
In this appendix, I describe the development and testing of iLMO1, the first attempt at coupling bioluminescent *Renilla* luciferase to Halorhodopsin. These results are described here because the performance of iLMO1 was not as robust as iLMO2. However, this work provided valuable insight into construct and experimental design that was subsequently implemented in the development of iLMO2.

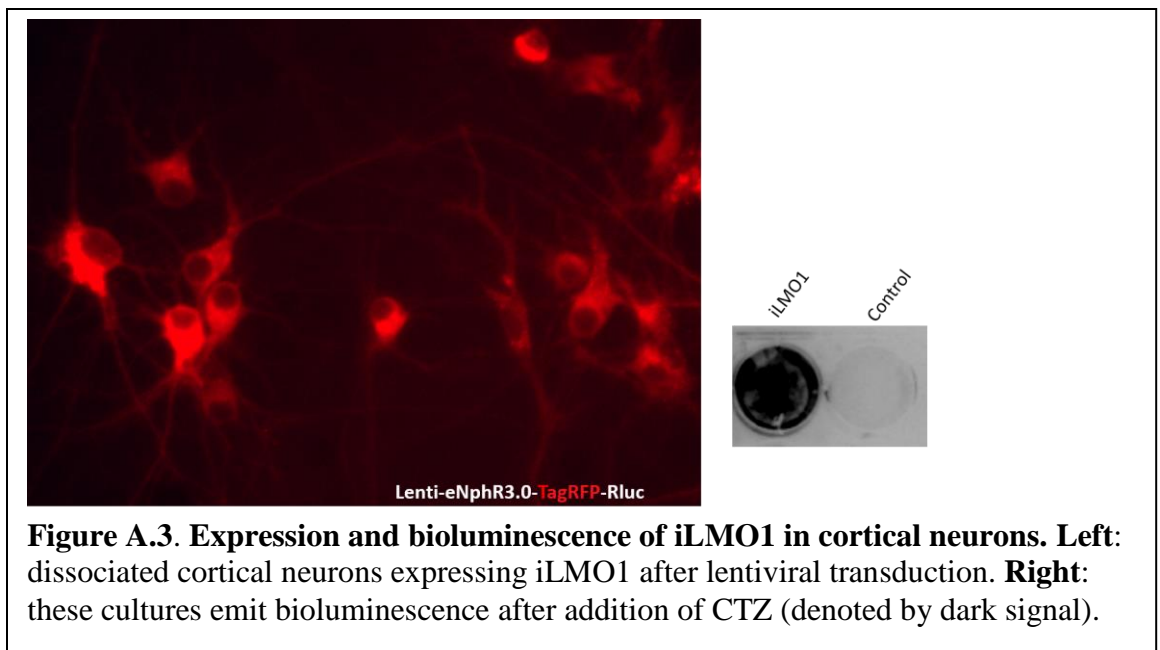
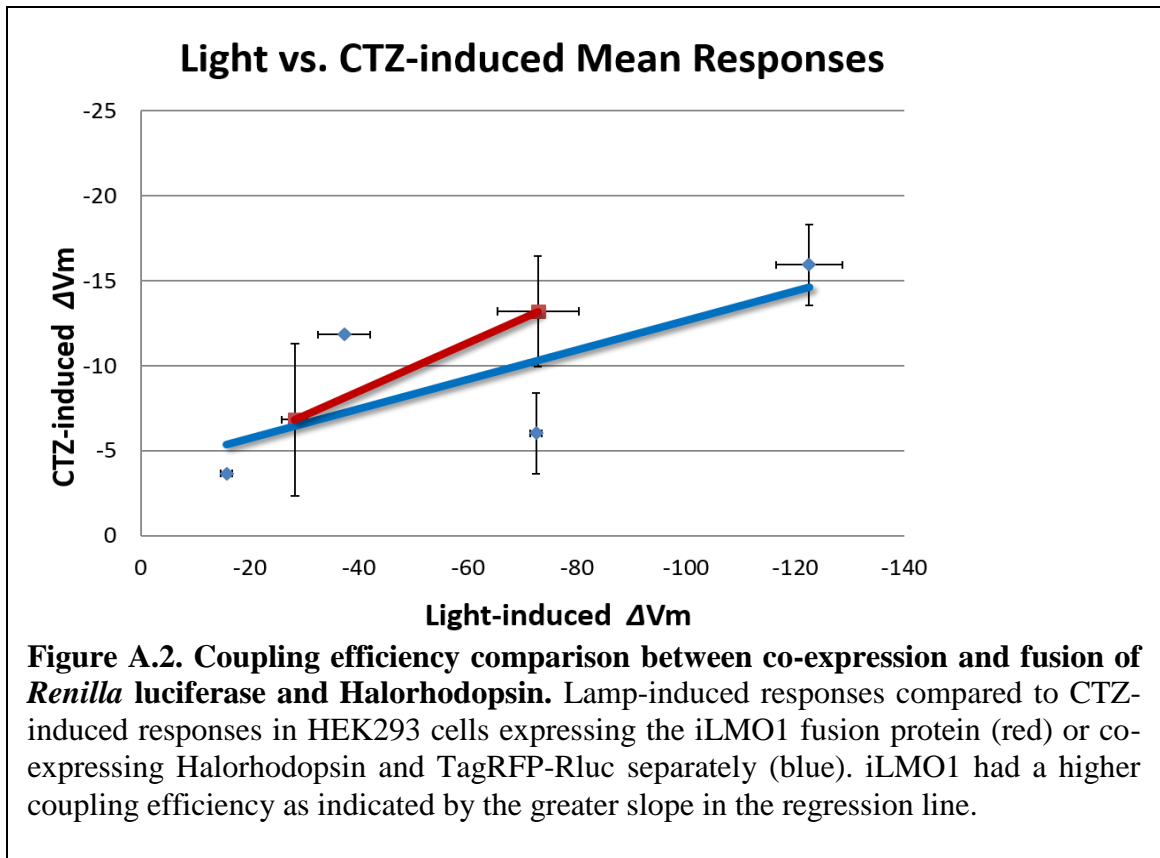
Results

iLMO1 consisted of a single fusion protein between Halorhodopsin and a *Renilla* luciferase BRET (bioluminescence resonance energy transfer) probe, TagRFP-Rluc¹⁰⁷. TagRFP-Rluc was coupled to Halorhodopsin either as a single fusion protein or co-expressed as separate constructs to determine which approach would yield higher bioluminescence-induced inhibition. Both approaches were able to hyperpolarize membrane potential in transfected HEK293 cells (**Figure A.1**). The iLMO1 fusion protein appeared to have a higher coupling efficiency (CTZ-induced response divided by lamp-induced response) compared to cells co-expressing Halorhodopsin and TagRFP-Rluc (**Figure A.2**). It was therefore decided to continue characterizing iLMO1 in dissociated cortical neuron cultures.

The iLMO1 cassette was cloned into a lentiviral vector (FUGW backbone) and lentivirus was produced in house to transduce dissociated cortical neurons (**Figure A.3**). Intracellular recordings demonstrated that addition of CTZ during a 10s current injection could reduce the number of evoked action potentials (**Figure A.4**). On average, CTZ was able to reduce evoked firing rate by 63% (**Figure A.5**). However, this reduction in firing rate is most likely overestimated due to the fact that it does not take into account the

normal decrease in firing rate from desensitization to prolonged current injection. Addition to CTZ to cortical neurons expressing iLMO1 cultured on multielectrode arrays was also able to reduce the array-wide spontaneous firing rate (**Figure A.6**). I have subsequently utilized 1 Hz current injections to evoke activity and a perfusion system to bath apply CTZ (described in methods section 3.4.2) to reduce artifact.





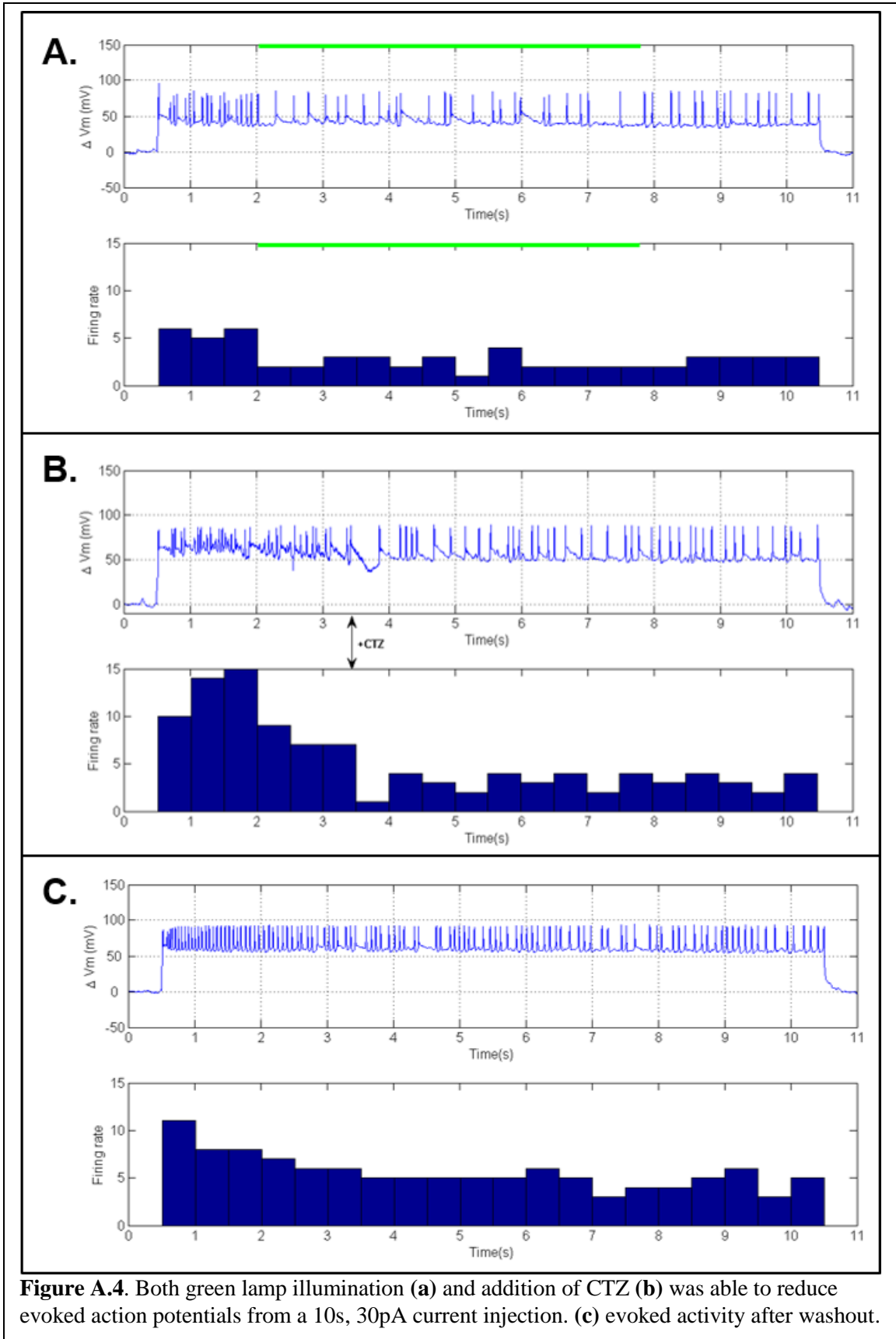
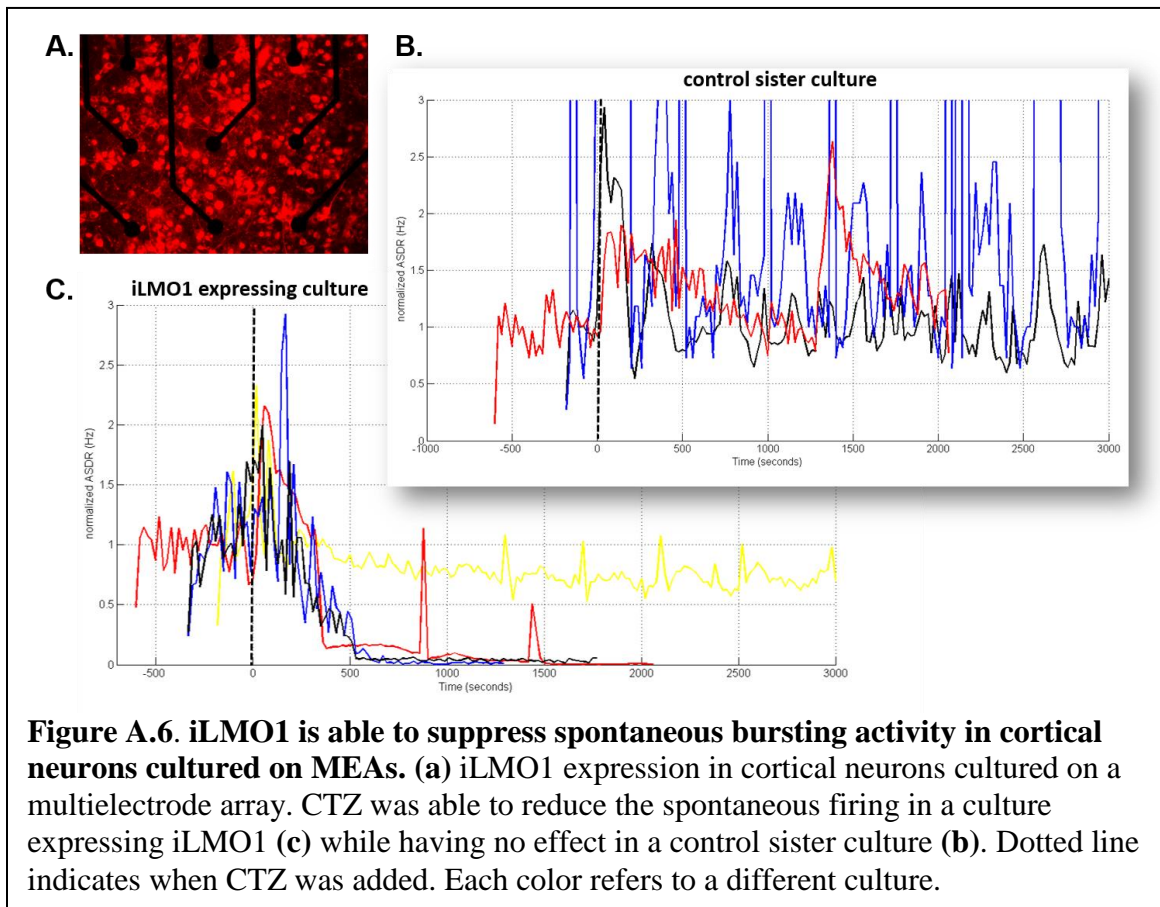
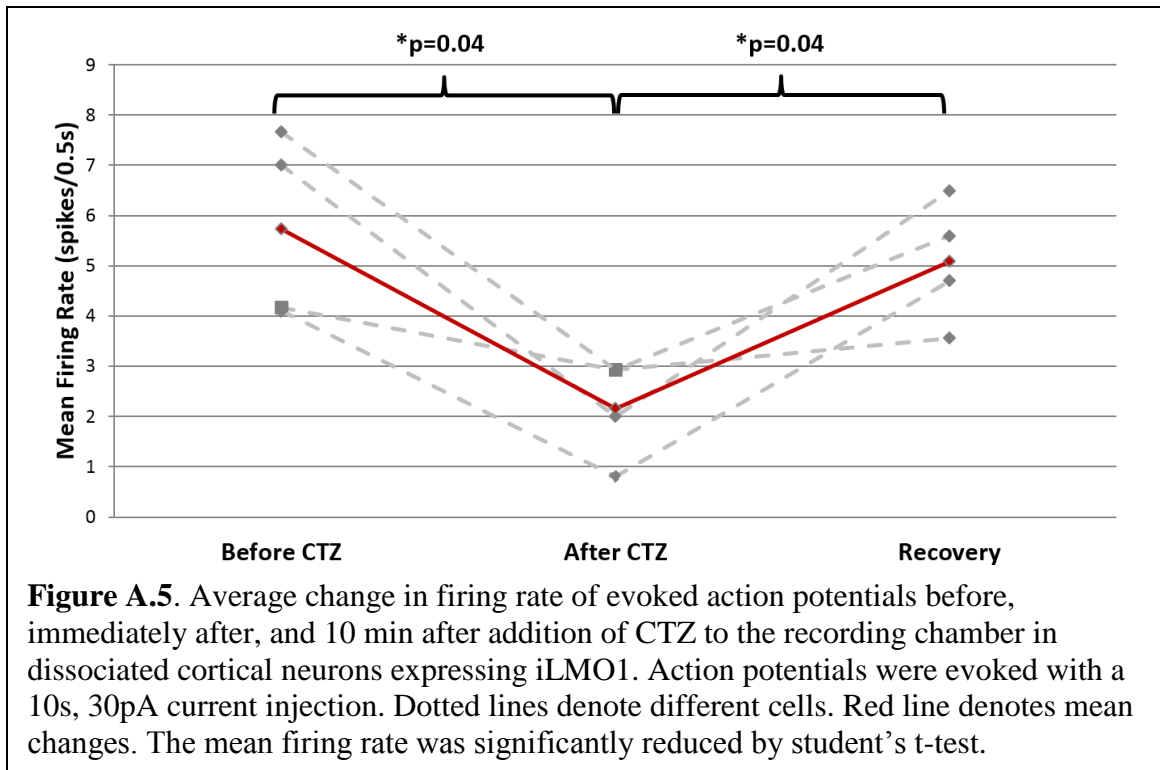


Figure A.4. Both green lamp illumination (a) and addition of CTZ (b) was able to reduce evoked action potentials from a 10s, 30pA current injection. (c) evoked activity after washout.



APPENDIX B

EXCITATORY LUMINOPSINS

In this appendix, I describe my work with channelrhodopin based excitatory luminopsins. This work was done as part of a collaboration between Ute Hochgeschwender at Duke University and Ling Wei and Shan Ping Yu at Emory University using the LMO3 construct (*Gaussia* luciferase and VChR1 fusion protein). In this instantiation, *Gaussia* luciferase emits blue light in the presence of CTZ to activate VChR1, an excitatory channelrhodopsin.

B.1 Intracellular recordings in vitro

To see whether LMO3 could drive excitation in response to CTZ, intracellular recordings were obtained in primary dissociated cortical neuron cultures expressing LMO3. LMO3 was expressed in these cells by transduction with AAV driven by a human synapsin promoter. As a positive control, blue light illumination from an arc lamp was able to evoke action potential firing (**Figure B.1.1**). When CTZ was added to cells expressing LMO3, the rate of spontaneous action potential firing increased (**Figure B.1.2b**). This effect eventually disappeared over time as CTZ washed out and the spontaneous firing rate returned back towards baseline (**Figure B.1.2c**).

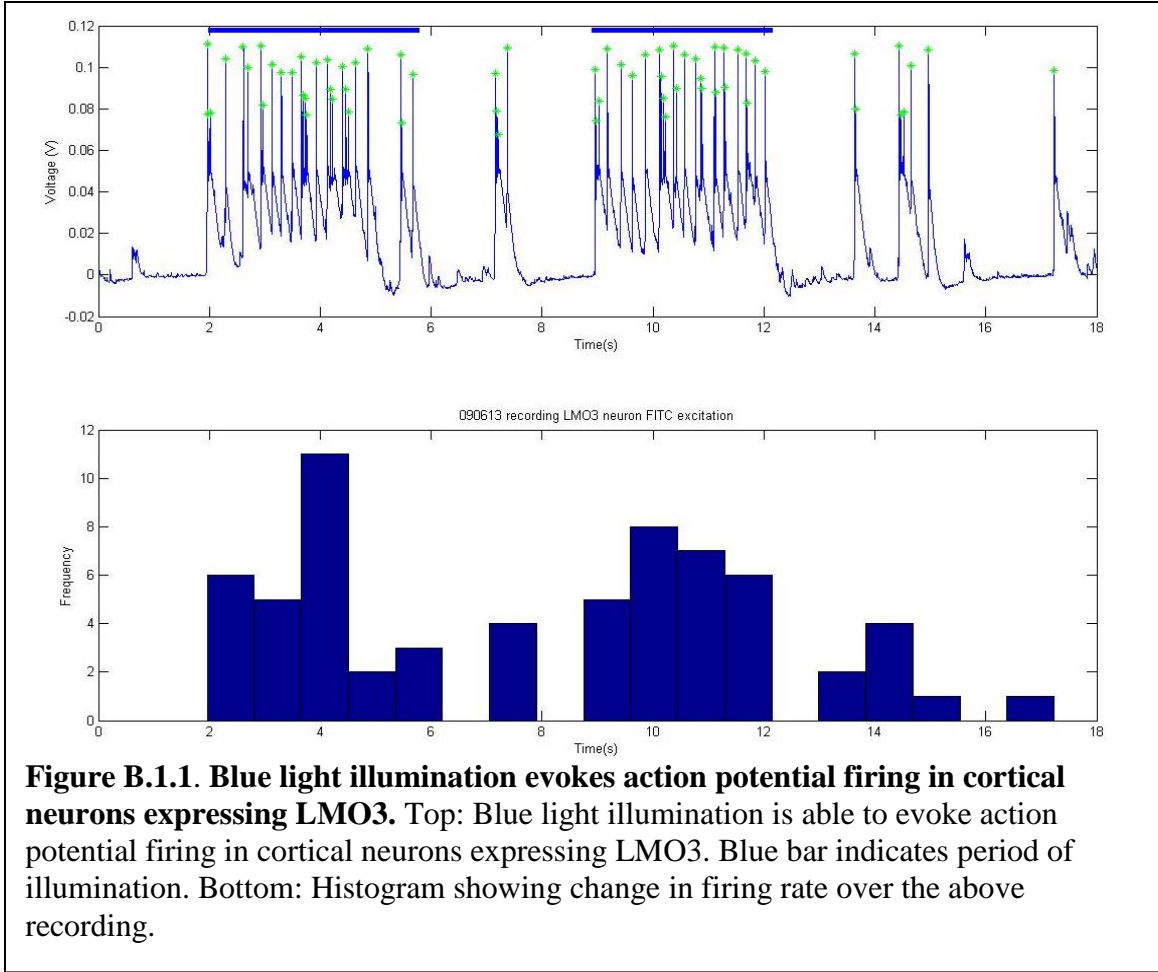
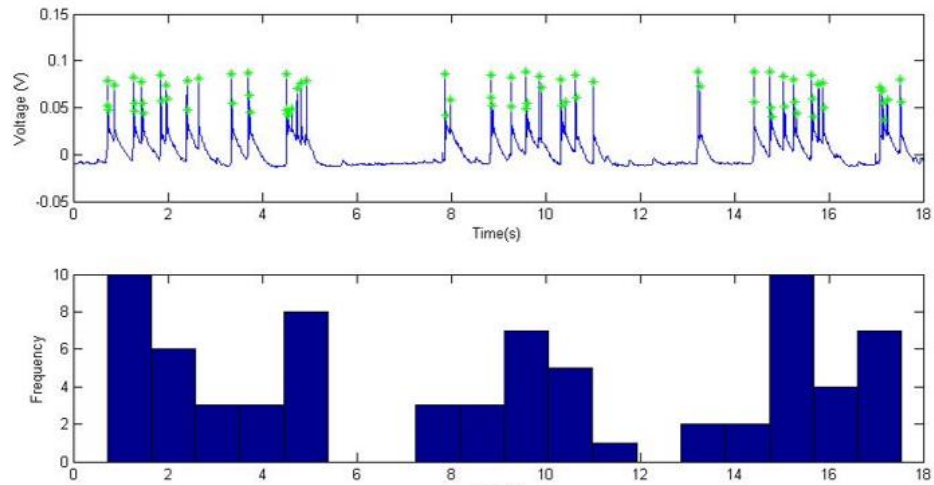
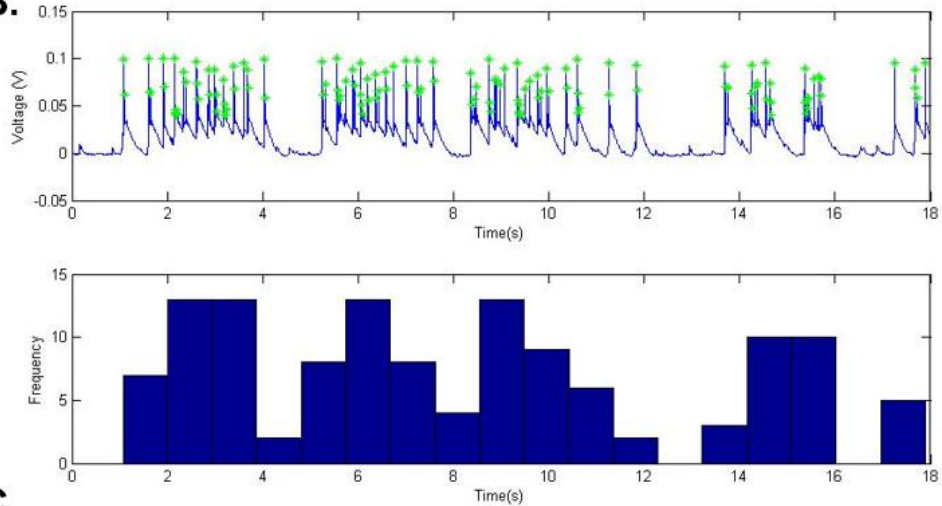


Figure B.1.1. Blue light illumination evokes action potential firing in cortical neurons expressing LMO3. Top: Blue light illumination is able to evoke action potential firing in cortical neurons expressing LMO3. Blue bar indicates period of illumination. Bottom: Histogram showing change in firing rate over the above recording.

A.



B.



C.

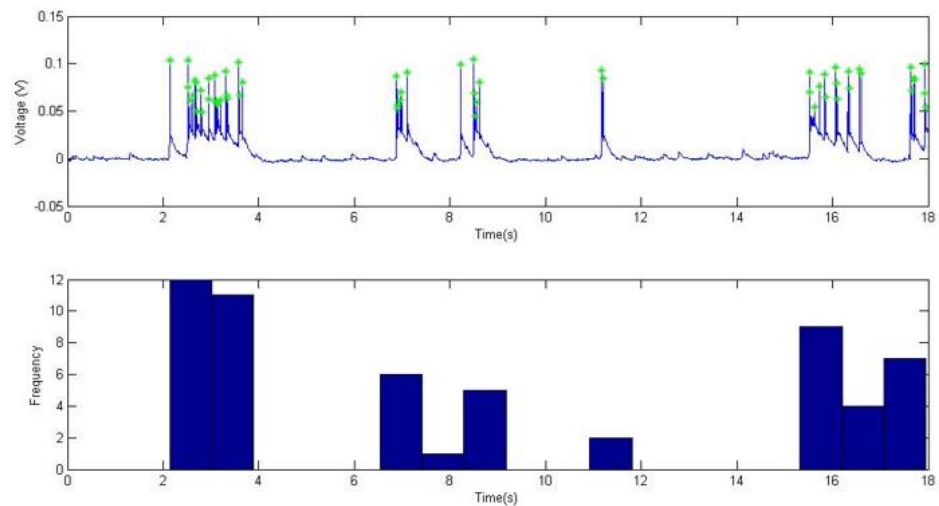
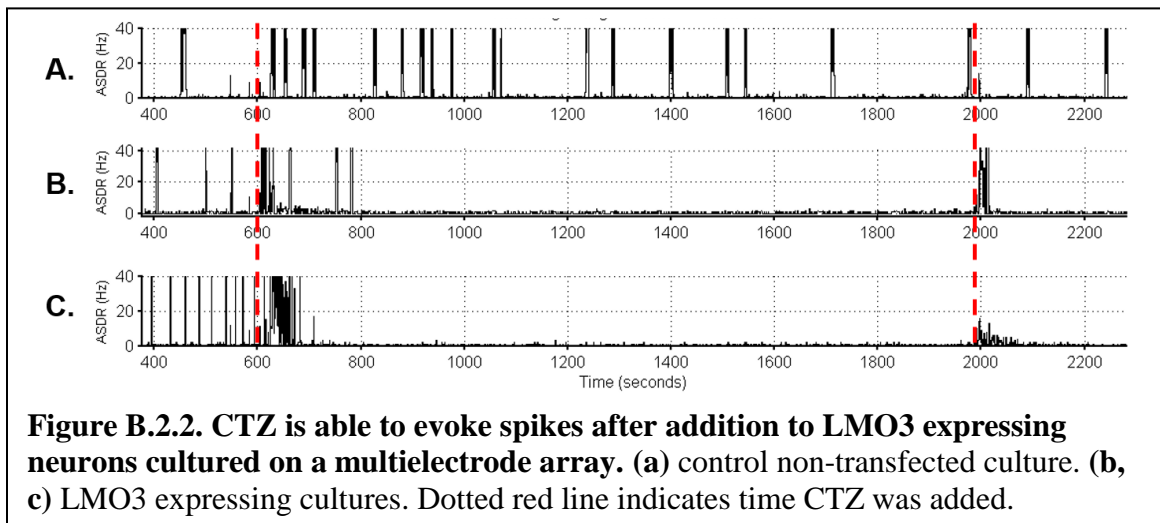
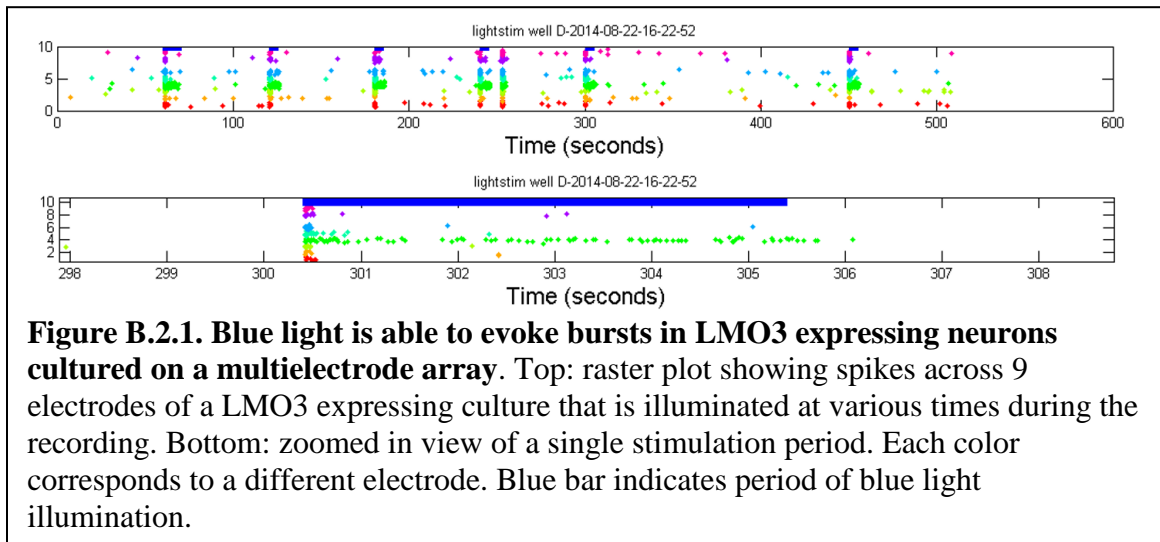


Figure B.1.2. CTZ is able to evoke action potential firing. (a) baseline spontaneous firing. (b) spontaneous firing after addition of CTZ. (c) spontaneous firing 10 min after CTZ was washed out.

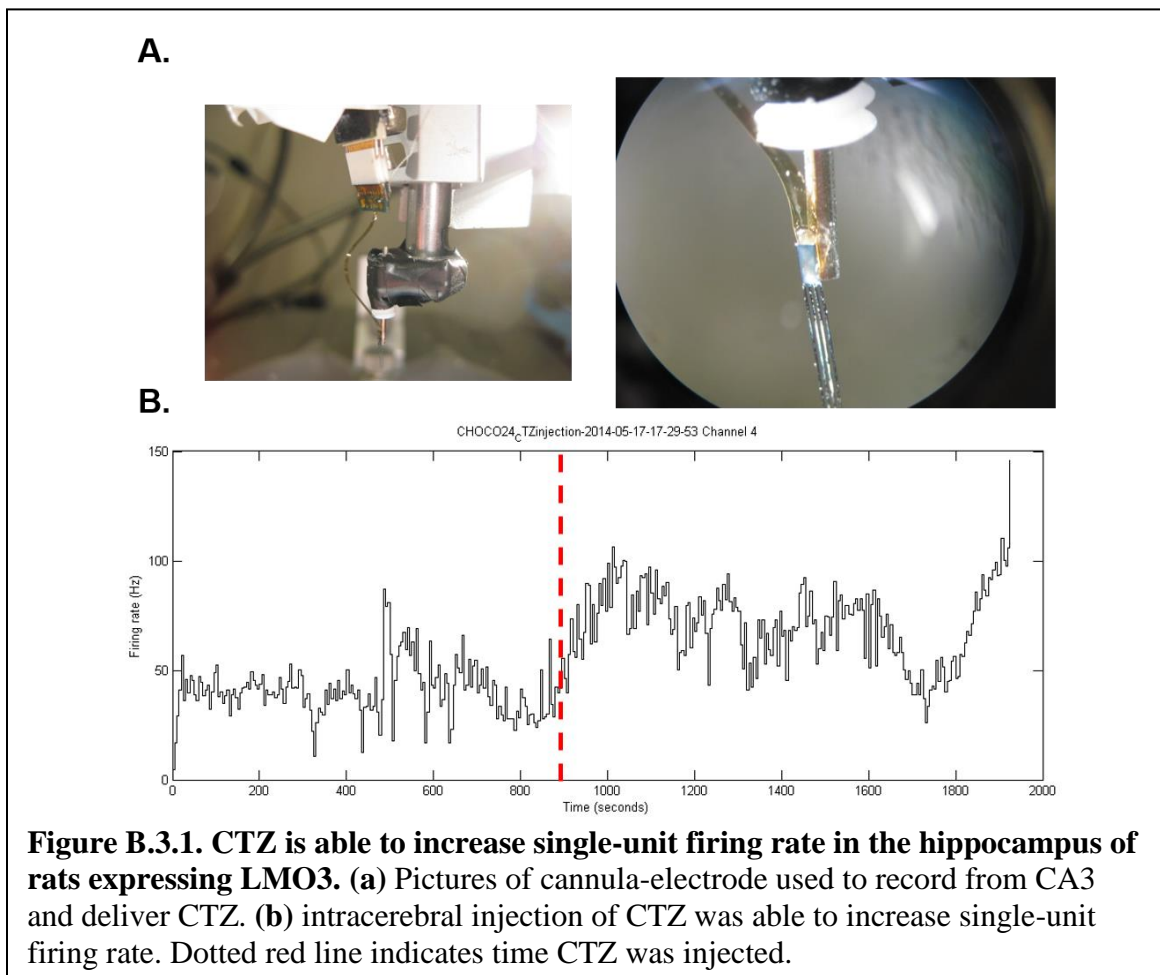
B.2 Extracellular recordings *in vitro*

LMO3 was further tested in the context of *in vitro* multielectrode array recordings using the same methods as those described in section 3.4. Synchronous bursts were able to be evoked when these cultures were illuminated with blue light (**Figure B.2.1**). When CTZ was added, spikes were evoked over an extended period of time lasting several minutes (**Figure B.2.2**)



B.3 In vivo recordings

LMO3 was further tested in vivo, where animals expressing LMO3 were implanted with a cannula-electrode as described in section 3.5. The only difference is that these cannula-electrodes were built from laminar shank-style arrays from NeuroNexus. These cannula-electrodes still allowed recording of local field potential and single-unit activity, albeit with lower fidelity than the microwire arrays. When CTZ was injected through the cannula, single-unit firing rate increased for a period of ~10 minutes (**Figure B.3.1**). Unfortunately the recordings with this cannula-electrode were not stable enough to conduct the appropriate vehicle control, although it was shown that vehicle had no effect in iLMO2 expressing animals in section 3.5.



B.4 In vivo imaging

In vivo bioluminescence imaging was conducted in mice expressing LMO3 as described in section 2.3. When CTZ was delivered intranasally (150 µg in 30 µl, a bioluminescent signal was able to be detected above the injection site (**Figure B.4.1**).



Figure B.4.1. *In vivo* bioluminescence imaging of LMO3 in mice. CTZ delivered intranasally was able to generate bioluminescence above the injection site (somatosensory cortex). Three areas of signal intensity are seen: 1 on the nose, 2 above the injection site.

APPENDIX C

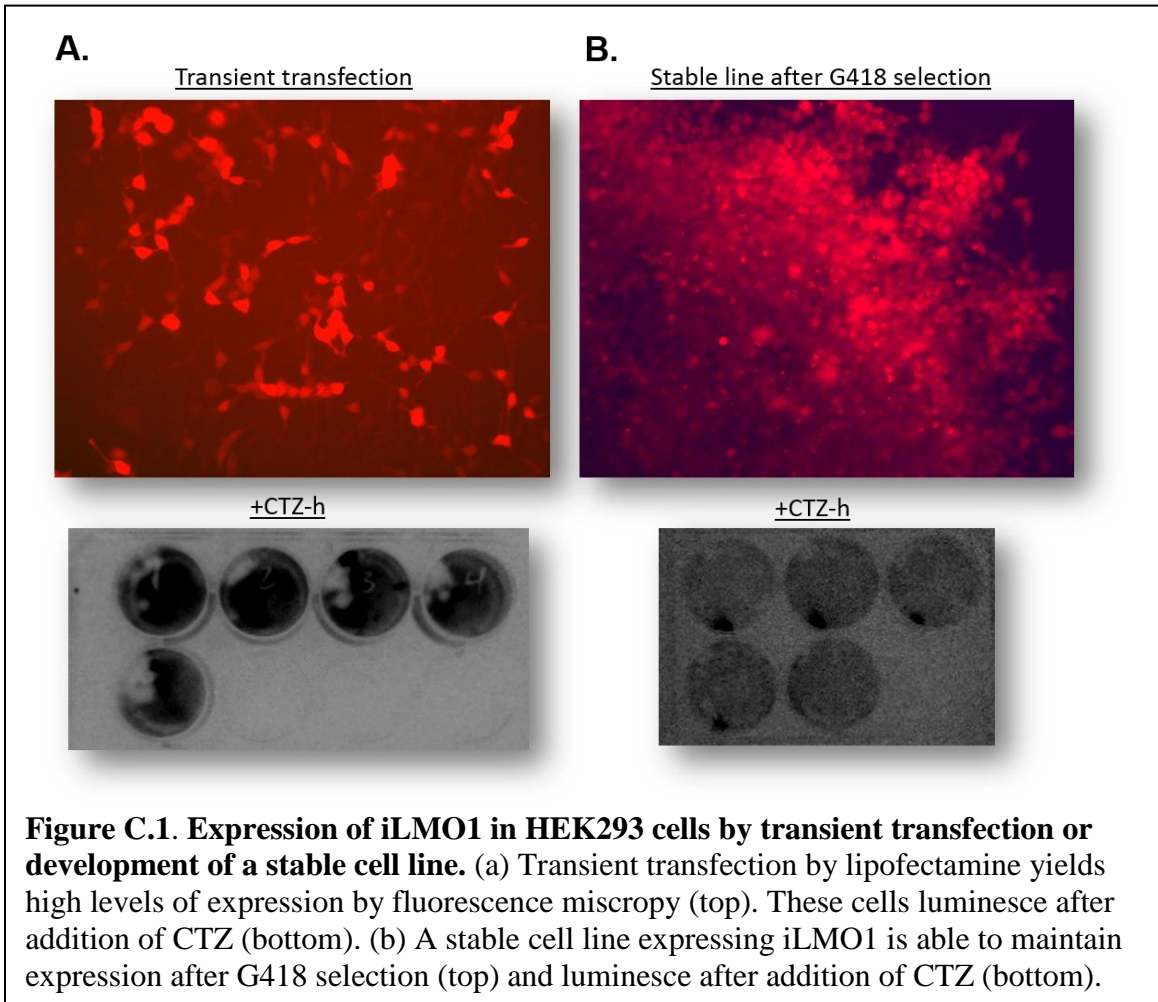
EXPLORING AND OPTIMIZING METHODS OF TRANSGENE EXPRESSION IN VITRO

In this appendix, I describe the methods I have utilized and optimized for expressing constructs in cultured HEK293 cells and primary neuron cultures. For HEK293 cells, I have explored both transient transfection methods and development of stable cell lines. For primary dissociated cortical neuron cultures, there are several methods that are typically used 1.) liposomal delivery, 2.) calcium phosphate precipitation, 3.) electroporation or nucleofection, and 4.) viral vectors. There are advantages and disadvantages to each method¹⁵⁸, but I have explored both liposomal and viral vector delivery methods.

HEK293 cells

HEK293 cells are a convenient cell line for testing expression and functionality of new constructs. They are easy to maintain and easy to transfect. In addition, they can also be patch clamped (albiet a little tricky due to the fact that they are very flat) for intracellular recordings. Transient transfection with lipofectamine 2000 typically yields high levels of expression that is detectable by fluorescence microscopy the next day (**Figure C.1a**). This approach is typically suitable for luminescence assays and intracellular recording the day after transfection. To prevent the need to transfect new cells every time an experiment is planned, I developed a stable cell line expressing iLMO1 (**Figure C.1b**). Although expression in stably expressing cell lines is typically lower than that of transiently transfected cells, these cells were still able to be detected by fluorescence

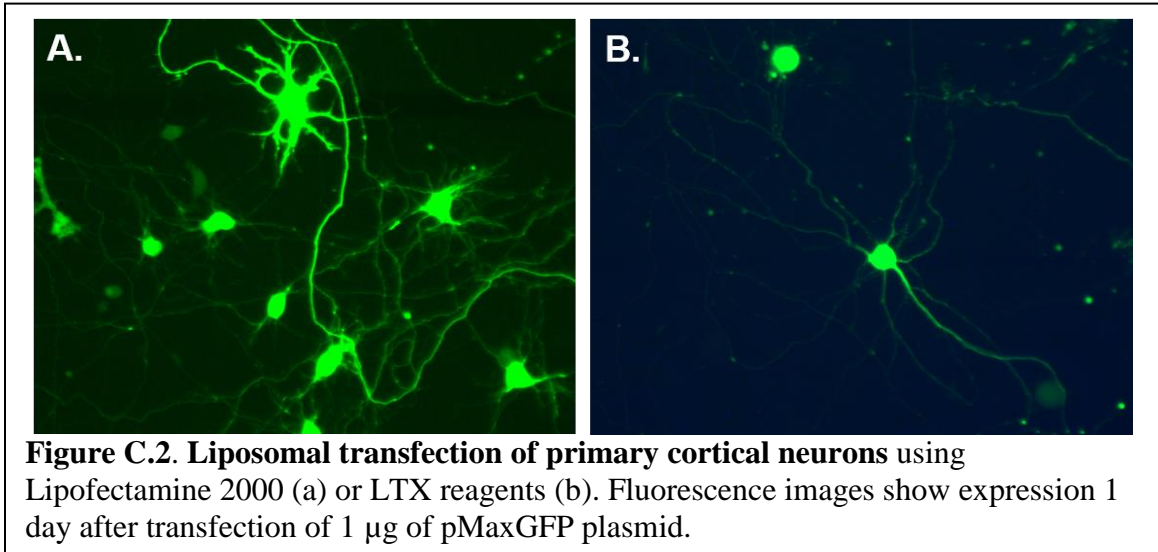
microscopy and bioluminescence imaging. These cells could therefore be utilized whenever they were needed without the need of an additional transfection step.



Primary cortical neurons

Liposomal delivery methods were explored primarily for the reasons of cost-effectiveness and relatively simple procedure. Expression could usually be detected by fluorescence microscopy the day after transfection (**Figure C.2**). Although expression levels were typically very high, there was a high level of toxicity associated with the transfection method as seen by altered cellular morphology and high levels of cell death. The transfection efficiency was also not very high (typically ~10-20%). Since lentiviral vectors allowed me to achieve near 100% transduction efficiency with little or no

associated toxicity, I have primarily utilized this method of transfection for my *in vitro* studies with primary neuronal cultures.



Methods

HEK293 stable cell line development. HEK293 cells were transiently transfected using the same methods described in section 3.3.2. Stable cell lines were obtained in three ways:

- 1.) Re-seeding the transiently transfected cells in media containing 1 mg/mL of G418 Sulfate and continuously passaging at low density in the selection media until the entire population of cells is stably expressing the construct (by visualizing fluorescent tag)
- 2.) A clonal stable cell line can be achieved by re-seeding the transiently transfected cells down to single cell per well (by performing serial dilutions in a 96-well plate) in media containing 1mg/mL G418 Sulfate. Once clonal colonies have developed in each well, they can be continuously expanded to larger dishes.

- 3.) Another alternative for achieving clonal stable cell lines is to manual pick a single cell from the population of transiently transfected cells and expanding it in selection media containing G418 sulfate.

Liposomal transfection of primary neuron cultures. Primary neuron cultures were obtained using the same methods described in section 3.4.2. For lipofection, the manufacturer recommend protocol was utilized except with 1/10th the amount of Lipofectamine 2000 and LTX reagent and 1/4th the amount of DNA for transfection.

APPENDIX D

TARGETED EXPRESSION OF INTERNEURONS

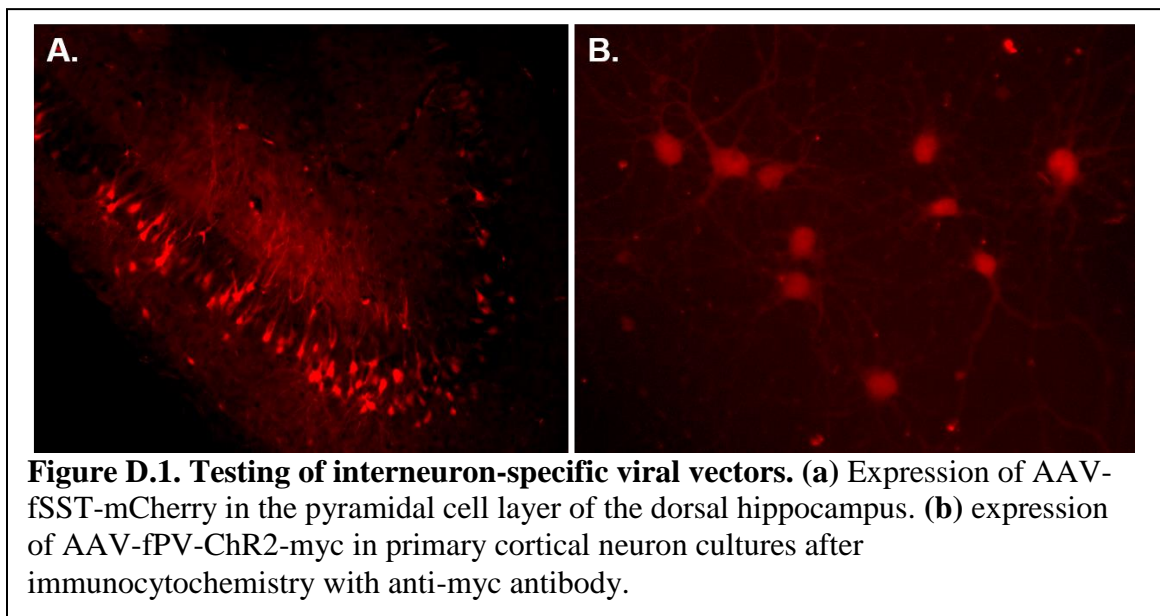
In this appendix, I describe my efforts on developing viral vectors that have selective expression in GABAergic interneuron cell types. The ability to tease apart complex circuitry in the brain in a cell-type specific manner is what has made optogenetics such a powerful technique. Cell-type specific expression of opsins can be achieved in several ways (summarized in section 1.2). The two major approaches include utilizing cell-type specific promoters or the use of CRE-dependent animals.

At the time of this work, there were no CRE-dependent rats that could be utilized to target expression of opsins in GABAergic neurons. Although there were GABAergic specific CRE-driver mouse lines (e.g. PV-CRE, SST-CRE), we did not want to utilize these transgenic animals since our temporal lobe epilepsy model was in rats. We therefore had to turn to promoter-specific expression of opsins. The challenge with this approach is that these cell-type specific promoters are generally quite large (2-3 kb), and are thus difficult to package into a viral vector with limited cargo sizes (i.e. lentiviral constructs typically can only be < 9 kb, while adeno-associated viral vectors can only be < 4.5 kb). Fortunately, Nathanson et. al described the cell-type specificity of various Fugu promoters, which are much smaller in size compared to mammalian promoters, in the mammalian CNS¹⁵⁹. Utilizing these much shorter fugu promoters, I generated two AAV constructs specific to parvalbumin and somatostatin GABAergic interneurons.

Results

I cloned and tested two AAV constructs: 1.) AAV-fSST-mCherry, a somatostatin specific AAV encoding mCherry fluorescent protein and 2.) AAV-fPV-ChR2-myc, a parvalbumin specific AAV encoding Channelrhodopsin. AAV-fSST-mCherry was

injected into the dorsal hippocampus and expression of mCherry could be seen throughout the pyramidal cell layer (**Figure D.1a**). Although these particular cell types were not confirmed by immunohistochemistry, the large morphology and number of cells suggests that they are interneurons. AAV-fPV-ChR2-myc was utilized to infect primary dissociated cortical neurons. A myc tag had to be utilized instead of a fluorescent protein to label channelrhodopsin due to cargo size limitations. Although cell-type specific immunohistochemistry was not performed, expression of ChR2 could be detected in these cells after immunocytochemistry with anti-myc antibody (**Figure D.1b**). More cell-type specific staining needs to be conducted to further validate the specificity of these vectors. However, at the time of this writing there are now transgenic rat CRE-driver lines for both parvalbumin and somatostatin cell types. This is a prime example of why you need to focus on one project at a time.



APPENDIX E

CONSTRUCTS

In this appendix, I list and describe the various constructs I have made over the course of this thesis.

Vector	Promoter	Insert	Description
Opsins			
PCDNA3	CMV	SwiChR2.0-EYFP	Inhibitory step function opsin
PCDNA3	CMV	SwiChR3.0-EYFP	Inhibitory step function opsin
PCDNA3	CMV	NpHR3.0-EYFP	Inhibitory Cl ⁻ pump
PCDNA3	CMV	eArch3.0-EYFP	Inhibitory H ⁺ pump
PCDNA3	CMV	eArch3.0-linker	Inhibitory H ⁺ pump
PCDNA3	CMV	Mac-EGFP	Inhibitory H ⁺ pump
Luciferases			
PCDNA3	CMV	pTurboFP-Rluc	Renilla luciferase
PCDNA3	CMV	pTagRFP-Rluc	Renilla luciferase
PCDNA3	CMV	TagRFP-Rluc	Renilla luciferase
PCDNA3	CMV	Nanolantern	Renilla luciferase
PCDNA3	CMV	Gluc-GFP	Gaussia luciferase
PCDNA3	CMV	Luc-GFP	Firefly luciferase
Luminopsins			
PCDNA3	CMV	NpHR-TagRFP-Rluc	iLMO1
PCDNA3	CMV	NpHR-Nanolantern	iLMO2
PCDNA3	CMV	sbGluc-SwiChR2.0-EYFP	Inhibitory step function luminopsin
PCDNA3	CMV	eArch3.0-TagRFP-Rluc	
Ca-sensitive luciferases			
PCDNA3	CMV	GFP-Aequorin	Ca-dependent luciferase
PCDNA3	CMV	Nanolantern-Ca(11)	Ca-dependent luciferase
PCDNA3	CMV	Nanolantern-Ca(117)	Ca-dependent luciferase
PCDNA3	CMV	Nanolantern-Ca(300)	Ca-dependent luciferase
PCDNA3	CMV	Nanolantern-Ca(600)	Ca-dependent luciferase
rLMOs			
PCDNA3	CMV	NpHR-Nanolantern-Ca(11)	rLMO-11
PCDNA3	CMV	NpHR-Nanolantern-Ca(600)	rLMO-600
PCDNA3	CMV	eArch3.0-linker-tdTA	rLMO
PCDNA3	CMV	NpHR-tdTA	rLMO

Vector	Promoter	Insert	Description
Adeno-associated viral constructs			
pAAV	CAMKII α	NpHR3.0-EYFP	Inhibitory Cl ⁻ pump
pAAV	fPV	hChR2-mCherry	Excitatory cation channel
pAAV	fPV	mCherry	Control vector
pAAV	CAMKII α	Mac-eGFP	Inhibitory H ⁺ pump
pAAV	CAMKII α	NpHR-Nanolantern	iLMO2
pAAV	Ef1 α	DIO-NpHR-Nanolantern	Floxed iLMO2
pAAV	fPV	ChR2-myc	Excitatory cation channel
pAAV	fsST	ChR2-mCherry	Excitatory cation channel
pAAV	fsST	mCherry	Control vector
Lentiviral constructs			
pLenti	Ubiq	NpHR-Nanolantern	iLMO2
pLenti	Ubiq	NpHR-Nanolantern-Ca(11)	rLMO-11
pLenti	Ubiq	NpHR-Nanolantern-Ca(600)	rLMO-600
pLenti	Ubiq	TagRFP-Rluc	Renilla luciferase
pLenti	Ubiq	GFP-Aequorin	Ca-dependent luciferase
pLenti	Ubiq	eNano-lantern	Ca-dependent luciferase
pLenti	Ubiq	sbGluc-SwiChR2.0-EYFP	Inhibitory step function luminopsin
pLenti	Ubiq	sbGluc-SwiChR3.0-EYFP	Inhibitory step function luminopsin

REFERENCES

1. Yoon, D., Frick, K., Carr, D. & Austin, J. Economic impact of epilepsy in the United States. *Epilepsia* **50**, 2186–91 (2009).
2. Strzelczyk, A., Reese, J. P., Dodel, R. & Hamer, H. M. Cost of Epilepsy. *Pharmacoeconomics* **26**, 463–476 (2008).
3. Epilepsy Fact Sheet. *World Health Organization* (2015).
4. Perucca, P. & Gilliam, F. G. Adverse effects of antiepileptic drugs. *Lancet. Neurol.* **11**, 792–802 (2012).
5. Eadie, M. J. Shortcomings in the current treatment of epilepsy. *Expert Rev. Neurother.* **12**, 1419–27 (2012).
6. Duncan, J. S. Epilepsy surgery. *Clin. Med. (Northfield. Il)*. **7**, 137–142 (2007).
7. Gumnit, R., Labiner, D., Fountain, N. & Herman, S. in *Epilepsy Across the Spectrum: Promoting Health and Understanding*. (eds. England, M., Liverman, C. & Schultz, A.) (National Academies Press, 2012).
8. Morris III, G., Meuller, W. & Group, T. V. N. S. S. Long-term treatment with vagus nerve stimulation in patients with refractory epilepsy. *Neurology* **53**, 1731 (1999).
9. Ben-Menachem, E. *et al.* Vagus Nerve Stimulation for Treatment of Partial Seizures: 1. A Controlled Study of Effect on Seizures. *Epilepsia* **35**, 616–626 (1994).
10. Ben-menachem, E. Reviews Vagus-nerve stimulation for the treatment of epilepsy. **1**, 477–482 (2002).
11. Kerrigan, J. F. *et al.* Electrical stimulation of the anterior nucleus of the thalamus for the treatment of intractable epilepsy. *Epilepsia* **45**, 346–54 (2004).
12. Fisher, R. *et al.* Electrical stimulation of the anterior nucleus of thalamus for treatment of refractory epilepsy. *Epilepsia* **51**, 899–908 (2010).
13. Morrell, M. J. Responsive cortical stimulation for the treatment of medically intractable partial epilepsy. *Neurology* **77**, 1295–304 (2011).
14. Sun, F. T. & Morrell, M. J. The RNS System: responsive cortical stimulation for the treatment of refractory partial epilepsy. *Expert Rev. Med. Devices* **11**, 563–72 (2014).
15. Krishna, V., Sammartino, F., King, N. K. K., So, R. Q. Y. & Wennberg, R. Neuromodulation for Epilepsy. *Neurosurg. Clin. N. Am.* **27**, 123–131 (2016).
16. Gradinaru, V. *et al.* Targeting and readout strategies for fast optical neural control in vitro and in vivo. *J. Neurosci.* **27**, 14231–14238 (2007).
17. Zhang, F. *et al.* Multimodal fast optical interrogation of neural circuitry. *Nature* **446**, 633–639 (2007).

18. Zhang, F. *et al.* Optogenetic interrogation of neural circuits: technology for probing mammalian brain structures. *Nat. Protoc.* **5**, 439–56 (2010).
19. Schnütgen, F. *et al.* A directional strategy for monitoring Cre-mediated recombination at the cellular level in the mouse. *Nat. Biotechnol.* **21**, 562–565 (2003).
20. Atasoy, D., Aponte, Y., Su, H. H. & Sternson, S. M. A FLEX Switch Targets Channelrhodopsin-2 to Multiple Cell Types for Imaging and Long-Range Circuit Mapping. *J. Neurosci.* **28**, 7025–7030 (2008).
21. Berglind, F. *et al.* Optogenetic inhibition of chemically induced hypersynchronized bursting in mice. *Neurobiol. Dis.* **65**, 133–41 (2014).
22. Tønnesen, J., Sørensen, A. T., Deisseroth, K., Lundberg, C. & Kokaia, M. Optogenetic control of epileptiform activity. *Proc. Natl. Acad. Sci. U. S. A.* **106**, 12162–7 (2009).
23. Wykes, R. C. *et al.* Optogenetic and Potassium Channel Gene Therapy in a Rodent Model of Focal Neocortical Epilepsy. *Sci. Transl. Med.* (2012). doi:10.1126/scitranslmed.3004190
24. Gradinaru, V. *et al.* Molecular and cellular approaches for diversifying and extending optogenetics. *Cell* **141**, 154–65 (2010).
25. Sukhotinsky, I. *et al.* Optogenetic delay of status epilepticus onset in an in vivo rodent epilepsy model. *PLoS One* **8**, e62013 (2013).
26. Chiang, C.-C., Ladas, T. P., Gonzalez-Reyes, L. E. & Durand, D. M. Seizure Suppression by High Frequency Optogenetic Stimulation Using In Vitro and In Vivo Animal Models of Epilepsy. *Brain Stimul.* 1–10 (2014). doi:10.1016/j.brs.2014.07.034
27. Li, X., Somogyi, P., Ylinen, A. & Buzsáki, G. The Hippocampal CA3 Network : An In Vivo Intracellular Labeling Study. **208**, 181–208 (1994).
28. Sik, A., Penttonen, M., Ylinen, A. & Buzsáki, G. Hippocampal CA1 Interneurons : Labeling Study An in vivo Intracellular. *J. Neurosci.* **75**, (1995).
29. Lasztóczy, B., Nyitrai, G., Héja, L. & Kardos, J. Synchronization of GABAergic inputs to CA3 pyramidal cells precedes seizure-like event onset in juvenile rat hippocampal slices. *J. Neurophysiol.* **102**, 2538–53 (2009).
30. Velazquez, J. L. P. & Carlen, P. L. Synchronization of GABAergic interneuronal networks during seizure-like activity in the rat horizontal hippocampal slice. *Eur. J. Neurosci.* **11**, 4110–4118 (1999).
31. Fujiwara-Tsakamoto, Y. *et al.* Prototypic seizure activity driven by mature hippocampal fast-spiking interneurons. *J. Neurosci.* **30**, 13679–89 (2010).
32. Avanzini, G., Forcelli, P. & Gale, K. Are there really ‘epileptogenic’ mechanisms or only corruptions of ‘normal’ plasticity? *Adv Exp Med Biol.* **813**, 95–107 (2014).
33. J, R., K, D., RL, R. & WT., C. Irving S. Cooper and his role in intracranial

- stimulation for movement disorders and epilepsy. *Stereotact Funct Neurosurg* **78**, 95–112 (2002).
34. IS, C. *et al.* Safety and efficacy of chronic cerebellar stimulation. *Appl Neurophysiol* **40**, 124–34
 35. IS, C. & AR, U. Effects of cerebellar stimulation on epilepsy, the EEG and cerebral palsy in man. *Electroencephalogr Clin Neurophysiol Suppl* **34**, 349–54 (1978).
 36. GL, K. & RS, F. Cerebellar and thalamic stimulation for epilepsy. *Adv Neurol* **63**, 231–45 (1993).
 37. Velasco, F. *et al.* Double-blind, randomized controlled pilot study of bilateral cerebellar stimulation for treatment of intractable motor seizures. *Epilepsia* **46**, 1071–81 (2005).
 38. Fisher, R. S. *et al.* Placebo-controlled pilot study of centromedian thalamic stimulation in treatment of intractable seizures. *Epilepsia* **33**, 841–851 (1992).
 39. Velasco, F. *et al.* Electrical stimulation of the centromedian thalamic nucleus in control of seizures: long-term studies. *Epilepsia* **36**, 63–71 (1995).
 40. Valentin, A. *et al.* Deep brain stimulation of the centromedian thalamic nucleus for the treatment of generalized and frontal epilepsies. *Epilepsia* **54**, 1823–1833 (2013).
 41. Pasnicu, A., Denoyer, Y., Haegelen, C., Pasqualini, E. & Biraben, A. Modulation of paroxysmal activity in focal cortical dysplasia by centromedian thalamic nucleus stimulation. *Epilepsy Res.* **104**, 264–268 (2013).
 42. Graves, N. M. & Fisher, R. S. Neurostimulation for epilepsy, including a pilot study of anterior nucleus stimulation. *Clin. Neurosurg.* **52**, 127–134 (2005).
 43. Lee, K. J., Shon, Y. M. & Cho, C. B. Long-term outcome of anterior thalamic nucleus stimulation for intractable epilepsy. *Stereotact. Funct. Neurosurg.* **90**, 379–385 (2012).
 44. Salanova, V. *et al.* Long-term efficacy and safety of thalamic stimulation for drug-resistant partial epilepsy. *Neurology* **84**, 1017–1025 (2015).
 45. Chabardes, S. *et al.* Deep brain stimulation in epilepsy with particular reference to the subthalamic nucleus. *Epileptic Disord.* **4 Suppl 3**, S83–93 (2002).
 46. Capecchi, M. *et al.* Chronic bilateral subthalamic stimulation after anterior callosotomy in drug-resistant epilepsy: long-term clinical and functional outcome of two cases. *Epilepsy Res.* **98**, 135–139 (2012).
 47. Handforth, A., DeSalles, A. A. F. & Krahl, S. E. Deep brain stimulation of the subthalamic nucleus as adjunct treatment for refractory epilepsy. *Epilepsia* **47**, 1239–1241 (2006).
 48. Sramka, M., Fritz, G., Galanda, M. & Nadvornik, P. Some observations in treatment stimulation of epilepsy. *Acta Neurochir. (Wien).* 257–262 (1976).

49. Sramka, M. & Chkhenkeli, S. A. Clinical experience in intraoperative determination of brain inhibitory structures and application of implanted neurostimulators in epilepsy. *Stereotact. Funct. Neurosurg.* **54-55**, 56–59 (1990).
50. Chkhenkeli, S. A. *et al.* Electrophysiological effects and clinical results of direct brain stimulation for intractable epilepsy. *Clin. Neurol. Neurosurg.* **106**, 318–329 (2004).
51. Paz, J. T. *et al.* Closed-loop optogenetic control of thalamus as a tool for interrupting seizures after cortical injury. *Nat. Neurosci.* 1–10 (2012). doi:10.1038/nn.3269
52. Esther Krook-Magnuson, Gergely G. Szabo, Caren Armstrong, Mikko Oijala, and I. S. Cerebellar Directed Optogenetic Intervention Inhibits Spontaneous Hippocampal Seizures in a Mouse Model of Temporal Lobe Epilepsy. *Eneuro.* **9**, 1–14 (2014).
53. Soper, C., Wicker, E., Kulick, C., N’Gouemo, P. & Forcelli, P. Optogenetic activation of superior colliculus neurons suppresses seizures originating in diverse brain networks. *Neurobiol. Dis.* (2015). doi:10.1016/j.nbd.2015.12.012
54. Krook-Magnuson, E., Armstrong, C., Oijala, M. & Soltesz, I. On-demand optogenetic control of spontaneous seizures in temporal lobe epilepsy. *Nat. Commun.* **4**, 1376 (2013).
55. Krook-Magnuson, E. *et al.* In vivo evaluation of the dentate gate theory in epilepsy. *J. Physiol.* **10**, n/a–n/a (2015).
56. Berglind, F. *et al.* Optogenetic inhibition of chemically induced hypersynchronized bursting in mice. *Neurobiol. Dis.* 1–9 (2014). doi:10.1016/j.nbd.2014.01.015
57. Gradinaru, V., Mogri, M., Thompson, K. R., Henderson, J. M. & Deisseroth, K. Optical deconstruction of parkinsonian neural circuitry. *Science* **324**, 354–9 (2009).
58. Cheng, M. Y. *et al.* Optogenetic neuronal stimulation promotes functional recovery after stroke. *Proc. Natl. Acad. Sci.* 1–6 (2014). doi:10.1073/pnas.1404109111
59. Yizhar, O., Fenno, L. E., Davidson, T. J., Mogri, M. & Deisseroth, K. Optogenetics in neural systems. *Neuron* **71**, 9–34 (2011).
60. Chuong, A. S. *et al.* Noninvasive optical inhibition with a red-shifted microbial rhodopsin. *Nat. Neurosci.* (2014). doi:10.1038/nn.3752
61. Aswendt, M., Adamczak, J., Couillard-Despres, S. & Hoehn, M. Boosting bioluminescence neuroimaging: an optimized protocol for brain studies. *PLoS One* **8**, e55662 (2013).
62. Maguire, C. a *et al.* Triple bioluminescence imaging for in vivo monitoring of cellular processes. *Mol. Ther. Nucleic Acids* **2**, e99 (2013).
63. Evans, M. S. *et al.* A synthetic luciferin improves bioluminescence imaging in live

- mice. *Nat. Methods* 1–4 (2014). doi:10.1038/nmeth.2839
64. Im, H. *et al.* In Vivo Visualization and Monitoring of Viable Neural Stem Cells Using Noninvasive Bioluminescence Imaging in the 6-Hydroxydopamine-Induced Mouse Model of Parkinson Disease. **12**, 224–234 (2013).
 65. Shah, K. *Imaging neural stem cell fate in mouse model of glioma. Current protocols in stem cell biology Chapter 5*, (2009).
 66. Bakhsheshian, J. *et al.* Bioluminescent imaging of drug efflux at the blood-brain barrier mediated by the transporter ABCG2. *Proc. Natl. Acad. Sci. U. S. A.* **110**, 20801–6 (2013).
 67. Zhu, L. *et al.* Non-invasive imaging of GFAP expression after neuronal damage in mice. *Neurosci. Lett.* **367**, 210–2 (2004).
 68. Watts, J. C. *et al.* Bioluminescence imaging of Abeta deposition in bigenic mouse models of Alzheimer's disease. *Proc. Natl. Acad. Sci. U. S. A.* **108**, 2528–33 (2011).
 69. Keller, a F., Gravel, M. & Kriz, J. Live imaging of amyotrophic lateral sclerosis pathogenesis: disease onset is characterized by marked induction of GFAP in Schwann cells. *Glia* **57**, 1130–42 (2009).
 70. Hwang, D. W. *et al.* Noninvasive in vivo monitoring of neuronal differentiation using reporter driven by a neuronal promoter. *Eur. J. Nucl. Med. Mol. Imaging* **35**, 135–145 (2008).
 71. Oh, H. J., Hwang, D. W., Youn, H. & Lee, D. S. In vivo bioluminescence reporter gene imaging for the activation of neuronal differentiation induced by the neuronal activator neurogenin 1 (Ngn1) in neuronal precursor cells. *Eur. J. Nucl. Med. Mol. Imaging* **40**, 1607–1617 (2013).
 72. Saito, K. *et al.* Luminescent proteins for high-speed single-cell and whole-body imaging. *Nat. Commun.* **3**, 1262 (2012).
 73. Tung, J. K., Gutekunst, C.-A. & Gross, R. E. Inhibitory luminopsins: genetically-encoded bioluminescent opsins for versatile, scalable, and hardware-independent optogenetic inhibition. *Sci. Rep.* **5**, 14366 (2015).
 74. Takai, A. *et al.* Expanded palette of Nano-lanterns for real-time multicolor luminescence imaging. 1–5 (2015). doi:10.1073/pnas.1418468112
 75. Tannous, B. a, Kim, D.-E., Fernandez, J. L., Weissleder, R. & Breakefield, X. O. Codon-optimized Gaussia luciferase cDNA for mammalian gene expression in culture and in vivo. *Mol. Ther.* **11**, 435–43 (2005).
 76. Niers, J. M. *et al.* Single Reporter for Targeted Multimodal in Vivo Imaging. (2012).
 77. Bakayan, A., Vaquero, C. F., Picazo, F. & Llopis, J. Red fluorescent protein-aequorin fusions as improved bioluminescent Ca²⁺ reporters in single cells and mice. *PLoS One* **6**, e19520 (2011).

78. Thomas Curie, Kelly L. Rogers, Cesare Colasante, and P. B. Red-Shifted Aequorin-Based Bioluminescent Reporters for. **6**, 30–42 (2007).
79. Baubet, V. *et al.* Chimeric green fluorescent protein-aequorin as bioluminescent Ca²⁺ reporters at the single-cell level. *Proc. Natl. Acad. Sci. U. S. A.* **97**, 7260–5 (2000).
80. Rogers, K. L. *et al.* Visualization of local Ca²⁺ dynamics with genetically encoded bioluminescent reporters. *Eur. J. Neurosci.* **21**, 597–610 (2005).
81. Drobac, E., Tricoire, L., Chaffotte, A.-F., Guiot, E. & Lambolez, B. Calcium imaging in single neurons from brain slices using bioluminescent reporters. *J. Neurosci. Res.* **88**, 695–711 (2010).
82. Choy, G. *et al.* Comparison of noninvasive fluorescent and bioluminescent small animal optical imaging. **35**, 1–7 (2003).
83. Troy, T., Jekic-McMullen, D., Sambucetti, L. & Rice, B. Quantitative comparison of the sensitivity of detection of fluorescent and bioluminescent reporters in animal models. *Mol. Imaging* **3**, 9–23 (2004).
84. Billinton, N. & Knight, a W. Seeing the wood through the trees: a review of techniques for distinguishing green fluorescent protein from endogenous autofluorescence. *Anal. Biochem.* **291**, 175–97 (2001).
85. Dragulescu-andrasi, A., Chan, C. T., De, A., Massoud, T. F. & Gambhir, S. S. Bioluminescence resonance energy transfer (BRET) imaging of protein – protein interactions within deep tissues of living subjects. *PNAS* 2–7 (2011).
doi:10.1073/pnas.1100923108/-
/DCSupplemental.www.pnas.org/cgi/doi/10.1073/pnas.1100923108
86. De, A., Jasani, A., Arora, R. & Gambhir, S. S. Evolution of BRET Biosensors from Live Cell to Tissue-Scale In vivo Imaging. *Front. Endocrinol. (Lausanne)*. **4**, 131 (2013).
87. Xia, Z. & Rao, J. Biosensing and imaging based on bioluminescence resonance energy transfer. *Curr. Opin. Biotechnol.* **20**, 37–44 (2009).
88. Kim, S. B., Suzuki, H., Sato, M. & Tao, H. Superluminescent Variants of Marine Luciferases. 8732–8740 (2011).
89. Branchini, B. R. *et al.* Red-emitting luciferases for bioluminescence reporter and imaging applications. *Anal. Biochem.* **396**, 290–7 (2010).
90. Loening, A. M., Wu, A. M. & Gambhir, S. S. Red-shifted *Renilla reniformis* luciferase variants for imaging in living subjects. *Nat. Methods* **4**, 641–643 (2007).
91. Loening, A. M., Wu, A. M. & Gambhir, S. S. *Renilla* Luciferase Variants with Green-Peaked Emission Spectra for Improved Imaging in Living Subjects.
92. Branchini, B. R., Southworth, T. L., Khattak, N. F., Michelini, E. & Roda, A. Red- and green-emitting firefly luciferase mutants for bioluminescent reporter applications. *Anal. Biochem.* **345**, 140–8 (2005).

93. Teranishi, K. & Shimomura, O. Solubilizing Coelenterazine in Water with Hydroxypropyl cyclodextrin. *Biosci. Biotech. Biochem.* **61**, 1219–1220 (1997).
94. Berglund, K., Birkner, E., Augustine, G. J. & Hochgeschwender, U. Light-Emitting Channelrhodopsins for Combined Optogenetic and Chemical-Genetic Control of Neurons. *PLoS One* **8**, e59759 (2013).
95. Mezzanotte, L. *et al.* Evaluating reporter genes of different luciferases for optimized in vivo bioluminescence imaging of transplanted neural stem cells in the brain. *Contrast Media Mol. Imaging* **8**, 505–513 (2013).
96. Tennstaedt, A., Aswendt, M., Adamczak, J. & Hoehn, M. Noninvasive Multimodal Imaging of Stem Cell Transplants in the Brain Using Bioluminescence Imaging and Magnetic Resonance Imaging. 153–166 (2013). doi:10.1007/7651
97. Hochgräfe, K. & Mandelkow, E.-M. Making the Brain Glow: In Vivo Bioluminescence Imaging to Study Neurodegeneration. *Mol. Neurobiol.* **47**, 868–82 (2013).
98. Fenno, L., Yizhar, O. & Deisseroth, K. The Development and Application of Optogenetics. *Annu. Rev. Neurosci.* **34**, 110301101035033 (2010).
99. AM, A. *et al.* An optical neural interface: in vivo control of rodent motor cortex with integrated fiberoptic and optogenetic technology. *J Neural Eng.* **4**, S143–56 (2007).
100. Al-Juboori, S. *et al.* Light scattering properties vary across different regions of the adult mouse brain. *PLoS One* **8**, (2013).
101. Yizhar, O., Fenno, L. E., Davidson, T. J., Mogri, M. & Deisseroth, K. Optogenetics in neural systems. *Neuron* **71**, 9–34 (2011).
102. Ambrosi, C. & Entcheva, E. Optogenetics' promise: pacing and cardioversion by light? *Futur. Cardiol.* **10**, 1–4 (2014).
103. Towne, C., Montgomery, K. L., Iyer, S. M., Deisseroth, K. & Delp, S. L. Optogenetic Control of Targeted Peripheral Axons in Freely Moving Animals. *PLoS One* **8**, (2013).
104. Jacques, S. L. Optical Properties of Biological Tissues: A Review. *Phys. Med. Biol.* **58**, R37–61 (2013).
105. Lin, J. Y., Knutsen, P. M., Muller, A., Kleinfeld, D. & Tsien, R. Y. ReaChR: a red-shifted variant of channelrhodopsin enables deep transcranial optogenetic excitation. *Nat. Neurosci.* 1–12 (2013). doi:10.1038/nn.3502
106. Zhang, F. *et al.* Red-shifted optogenetic excitation: a tool for fast neural control derived from *Volvox carteri*. *Nat. Neurosci.* **11**, 631–3 (2008).
107. Dragulescu-andrasi, A., Chan, C. T., De, A., Massoud, T. F. & Gambhir, S. S. Bioluminescence resonance energy transfer (BRET) imaging of protein – protein interactions within deep tissues of living subjects. *PNAS* 2–7 (2011). doi:10.1073/pnas.1100923108/-

108. CP, P., Bordeleau, M., Pelletier, J. & Sharp, P. Short RNAs Repress Translation after Initiation in Mammalian Cells. *Mol Cell*. **21**, 533–42 (2006).
109. Bhaumik, S., Lewis, Z. & Gambhir, S. Optical imaging of Renilla luciferase, synthetic Renilla luciferase, and firefly luciferase reporter gene expression in living mice. *J. Biomed. Opt.* **9**, 578–586 (2004).
110. Ward, W. W. & Cormier, M. J. Energy transfer via protein-protein interaction in Renilla bioluminescence. *Photochem. Photobiol.* **27**, 389–396 (1978).
111. Rangaraju, V., Calloway, N. & Ryan, T. a. Activity-driven local ATP synthesis is required for synaptic function. *Cell* **156**, 825–835 (2014).
112. Gradinaru, V., Thompson, K. R. & Deisseroth, K. eNpHR: a Natronomonas halorhodopsin enhanced for optogenetic applications. *Brain Cell Biol.* **36**, 129–39 (2008).
113. Land, B. B., Brayton, C. E., Furman, K. E., LaPalombara, Z. & DiLeone, R. J. Optogenetic inhibition of neurons by internal light production. *Front. Behav. Neurosci.* **8**, 1–6 (2014).
114. Wagenaar, D. a, Pine, J. & Potter, S. M. An extremely rich repertoire of bursting patterns during the development of cortical cultures. *BMC Neurosci.* **7**, 11 (2006).
115. Wagenaar, D. a, Madhavan, R., Pine, J. & Potter, S. M. Controlling bursting in cortical cultures with closed-loop multi-electrode stimulation. *J. Neurosci.* **25**, 680–8 (2005).
116. Zhou, W. *et al.* Homeostatically regulated synchronized oscillations induced by short-term tetrodotoxin treatment in cultured neuronal network. *BioSystems* **95**, 61–66 (2009).
117. Barde, I., Salmon, P. & Trono, D. Production and Titration of Lentiviral Vectors. *Curr. Protoc. Neurosci.* **53**, 4.21.1–4.21.23 (2010).
118. Hales, C. M., Rolston, J. D., Potter, S. M. How to Culture, Record and Stimulate Neuronal Networks on Micro-electrode Arrays (MEAs). *J. Vis. Exp.* **39**, e2056 (2010).
119. Newman, J. P. *et al.* Closed-Loop, Multichannel Experimentation Using the Open-Source NeuroRighter Electrophysiology Platform. *Front. Neural Circuits* **6**, 98 (2012).
120. Quiroga, R. Q., Kreuz, T. & Grassberger, P. Event synchronization: A simple and fast method to measure synchronicity and time delay patterns. *Phys. Rev. E - Stat. Nonlinear, Soft Matter Phys.* **66**, 1–9 (2002).
121. Buzsáki, G. Theta oscillations in the hippocampus. *Neuron* **33**, 325–340 (2002).
122. Rolston, J. D., Gross, R. E. & Potter, S. M. A low-cost multielectrode system for data acquisition enabling real-time closed-loop processing with rapid recovery from stimulation artifacts. *Front. Neuroeng.* **2**, 12 (2009).

123. H. B., Andrews, P., JE, K., S, M. & PP, M. Chronux: a platform for analyzing neural signals. *J Neurosci Methods* **192**, 146–51 (2010).
124. Quiroga, R. Q., Nadasdy, Z. & Ben-Shaul, Y. Unsupervised spike detection and sorting with wavelets and superparamagnetic clustering. *Neural Comput.* **16**, 1661–1687 (2004).
125. Konitsiotis, S., Kafetzopoulos, E., Anastasopoulos, D. & Blanchet, P. J. Opposite rotation induced by dopamine agonists in rats with unilateral lesions of the globus pallidus or substantia nigra. *Behav. Brain Res.* **92**, 77–83 (1998).
126. Gradinaru, V. *et al.* Molecular and cellular approaches for diversifying and extending optogenetics. *Cell* **141**, 154–65 (2010).
127. Predicted irradiance values: model based on direct measurements in mammalian brain tissue. at <<http://web.stanford.edu/group/dlab/cgi-bin/graph/chart.php>>
128. Xu, J., Zhu, Y. & Heinemann, S. Identification of sequence motifs that target neuronal nicotinic receptors to dendrites and axons. *J Neurosci.* **26**, 9780–93 (2006).
129. Becker, K. *et al.* Low dose isoflurane exerts opposing effects on neuronal network excitability in neocortex and hippocampus. *PLoS One* **7**, 3–9 (2012).
130. MacIver, M. B. & Roth, S. H. Inhalation anaesthetics exhibit pathway-specific and differential actions on hippocampal synaptic responses in vitro. *Br. J. Anaesth.* **60**, 680–691 (1988).
131. Raimondo, J. V., Kay, L., Ellender, T. J. & Akerman, C. J. Optogenetic silencing strategies differ in their effects on inhibitory synaptic transmission. *Nat. Neurosci.* **15**, 1102–1104 (2012).
132. Liu, D. *et al.* Medial prefrontal activity during delay period contributes to learning of a working memory task. *Science (80-.).* **346**, 458–463 (2014).
133. Rogan, S. C. & Roth, B. L. Remote Control of Neuronal Signaling. **63**, 291–315 (2011).
134. Dong, S., Allen, J., Farrell, M. & Roth, B. A chemical-genetic approach for precise spatio-temporal control of cellular signaling. *Mol Biosyst.* **6**, 1376–80 (2010).
135. Kimura, T., Hiraoka, K., Kasahara, N. & Logg, C. Optimization of enzyme–substrate pairing for bioluminescence imaging of gene transfer using Renilla and Gaussia luciferases. *J. Gene Med.* **12**, 528–537 (2010).
136. Chang, W. *et al.* Reversible metabolism of clozapine and clozapine N-oxide in schizophrenic patients. *Prog Neuropsychopharmacol Biol Psychiatry* **22**, 723–39 (1998).
137. Naumann, E. a, Kampff, A. R., Prober, D. a, Schier, A. F. & Engert, F. Monitoring neural activity with bioluminescence during natural behavior. *Nat. Neurosci.* **13**, 513–20 (2010).
138. Rolston, J. D., Laxpati, N. G., Gutekunst, C.-A., Potter, S. M. & Gross, R. E.

- Spontaneous and evoked high-frequency oscillations in the tetanus toxin model of epilepsy. *Epilepsia* **51**, 2289–96 (2010).
139. Löscher, W. Critical review of current animal models of seizures and epilepsy used in the discovery and development of new antiepileptic drugs. *Seizure* **20**, 359–368 (2011).
 140. Ansel, D. J., Ortega, E. & Fisher, R. S. Diazepam prophylaxis for bicuculline-induced seizures: A rat dose-response model. *Neurosci. Lett.* **356**, 66–68 (2004).
 141. Rodrigues, M. C. A., Belebani, R. D. O., Coutinho-Netto, J., dos Santos, W. F. & Garcia-Cairasco, N. Behavioral effects of bicuculline microinjection in the dorsal versus ventral hippocampal formation of rats, and control of seizures by nigral muscimol. *Epilepsy Res.* **58**, 155–65 (2004).
 142. Eder, H. G., Jones, D. B. & Fisher, R. S. Local Perfusion of Diazepam Attenuates Interictal and Ictal Events in the Bicuculline Model of Epilepsy in Rats. **38**, 516–521 (1997).
 143. Mandhane, S. N., Aavula, K. & Rajamannar, T. Timed pentylenetetrazol infusion test: A comparative analysis with s.c.PTZ and MES models of anticonvulsant screening in mice. *Seizure* **16**, 636–644 (2007).
 144. Pantoja-Jiménez, C. R., Magdaleno-Madrigal, V. M., Almazán-Alvarado, S. & Fernández-Mas, R. Anti-epileptogenic effect of high-frequency stimulation in the thalamic reticular nucleus on PTZ-induced seizures. *Brain Stimul.* **7**, 587–94 (2014).
 145. Mirski, M. A., Ann, L., Terry, J. B. & Fisher, R. S. Anticonvulsant effect of anterior thalamic high frequency electrical stimulation in the rat Anticonvulsant effect of anterior thalamic high frequency electrical stimulation in the rat. **28**, 89–100 (1997).
 146. Nehlig, A. Mapping of neuronal networks underlying generalized seizures induced by increasing doses of pentylenetetrazol in the immature and adult rat: A c-Fos immunohistochemical study. *Eur. J. Neurosci.* **10**, 2094–2106 (1998).
 147. Brevard, M. E., Kulkarni, P., King, J. a. & Ferris, C. F. Imaging the neural substrates involved in the genesis of pentylenetetrazol-induced seizures. *Epilepsia* **47**, 745–754 (2006).
 148. Armstrong, C., Krook-Magnuson, E., Oijala, M. & Soltesz, I. Closed-loop optogenetic intervention in mice. *Nat. Protoc.* **8**, 1475–1493 (2013).
 149. Grienberger, C. & Konnerth, A. Imaging calcium in neurons. *Neuron* **73**, 862–85 (2012).
 150. Tricoire, L., Drobac, E. & Lambollez, B. Genetically Encoded Functional Indicators. **72**, 10–12 (2012).
 151. Nagai, T., Horikawa, K., Saito, K. & Matsuda, T. Genetically encoded Ca(2+) indicators; expanded affinity range, color hue and compatibility with optogenetics. *Front. Mol. Neurosci.* **7**, 90 (2014).

152. Hires, S. A., Tian, L. & Looger, L. L. Reporting neural activity with genetically encoded calcium indicators. *Brain Cell Biol.* **36**, 69–86 (2008).
153. Tian, L., Akerboom, J., Schreier, E. R. & Looger, L. L. *Neural activity imaging with genetically encoded calcium indicators. Progress in brain research* **196**, (Elsevier B.V., 2012).
154. Granatiero, V., Patron, M., Tosatto, A., Merli, G. & Rizzuto, R. The use of aequorin and its variants for Ca²⁺ measurements. *Cold Spring Harb. Protoc.* **2014**, (2014).
155. Saito, K. *et al.* Auto-luminescent genetically-encoded ratiometric indicator for real-time Ca²⁺ imaging at the single cell level. *PLoS One* **5**, e9935 (2010).
156. Berndt, A. Structure-Guided Transformation of Channelrhodopsin into a Light-activated Chloride Channel. **420**, (2014).
157. Govorunova, E. G., Sineshchekov, O. A., Janz, R., Liu, X. & Spudich, J. L. Natural light-gated anion channels: A family of microbial rhodopsins for advanced optogenetics.
158. Karra, D. & Dahm, R. Transfection techniques for neuronal cells. *J. Neurosci.* **30**, 6171–7 (2010).
159. Nathanson, J. L. *et al.* Short Promoters in Viral Vectors Drive Selective Expression in Mammalian Inhibitory Neurons, but do not Restrict Activity to Specific Inhibitory Cell-Types. *Front. Neural Circuits* **3**, 19 (2009).